Micro – Thruster Development

Propulsion System for the DelFFi Mission

I. Krusharev

AE5810: Master of Science Thesis
Delft University of Technology

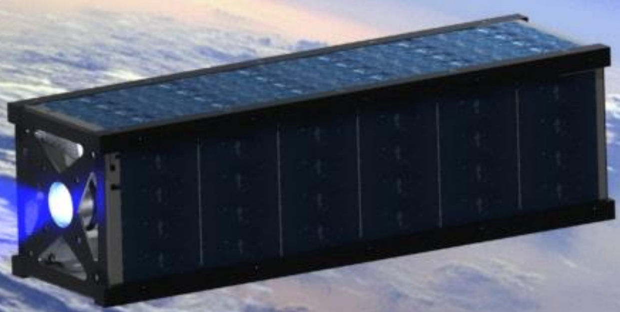

TU Delft Delft University of Technology

Challenge the future

Micro – Thruster Development

Propulsion System for the DelFFi Mission

By

I. Krusharev

AE5810 – Thesis Space

in partial fulfilment of the requirements for the degree of

Master of Science
in Aerospace Engineering

at the Delft University of Technology,
to be defended publicly on August 19, 2015 at 13:00.

Supervisor:	Ir. B. T. C. Zandbergen,	TU Delft
Thesis committee:	Dr. A. Cervone,	TU Delft
	Ir. M.C. Naeije,	TU Delft

An electronic version of this thesis is available at http://repository.tudelft.nl/.

> ***The universe is probably littered with the one-planet graves of cultures which made the sensible economic decision that there's no good reason to go into space—each discovered, studied, and remembered by the ones who made the irrational decision.***

Randall Munroe

Abstract

The format and size specifications of the CubeSat platform require highly miniaturized subsystems, one of the most challenging ones being the propulsion system. Up to date, according to the authors' knowledge, only two CubeSats have successfully operated a propulsion system in space: CanX-2 in 2008 and Defil-n3Xt in 2013. The importance of a miniaturized propulsion system becomes even more apparent when taken into consideration that most, if not all, of the CubeSats launched to date, due to budget constraints, have been piggybacking their launches into space and therefore they may end up in a non-optimal orbit. As a next step, a formation flying technology demonstration mission is planned by the Delft University of Technology (DelFFi), as part of the QB50 project.

This thesis gives an outline of the present development status of micro-propulsion systems at Delft University of Technology. The main design driving criteria are provided by the DelFFi satellites requirements. Keeping in mind the educational environment in which the work is performed, safety drives the requirements: thus, propellants have to be non-toxic and easy to handle. Additionally, present requirements aim at a thrust level in the range of 1 to 10 [mN] and a total ΔV of 15 [m/s] or more. Wet mass, when installed in triple-unit CubeSats, shall be less than 450 [g], and peak power consumption less than 10 [W].

A number of Commercial-Off-The-Shelf (COTS) systems have been investigated to find suitable candidates that fulfil these minimum requirements. However, it has been concluded that all presently available systems have low Technology-Readiness-Level (TRL) or their performance is out of the required range. It was thus necessary to start working at custom designed system. The design process and decisions made will be presented in this thesis. Furthermore for testing purposes also a test setup and an engineering model propulsion system was made. A general test program using LabVIEW was made that can automate the testing process of the thruster. The system was then tested and from the results, recommendations and conclusions were made for the next iteration of the thruster.

We do not see any borders from space. We just see a unique planet with a thin, fragile atmosphere, suspended in a vast and hostile darkness. From up here it is crystal clear that on Earth we are one humanity, we eventually all share the same fate.

Alexander Gerst

List of Publications

- I. Krusharev, R. Poyck, Q. Bellini, B. Zandbergen, A. Cervone, "CubeSat Micro - Propulsion Systems for Extending the Capabilities of Academic Projects" in 65th International Astronautical Congress, Toronto, 2014
- R. Poyck, I. Krusharev, Q. Bellini, B. Zandbergen, A. Cervone, "A Water-Fed Micro-Resistojet for the DelFFi Formation Flying Mission" in 65th International Astronautical Congress, Toronto, 2014

Curious that we spend more time congratulating people who have succeeded than encouraging people who have not.

Neil deGrasse Tyson

Acknowledgments

While this thesis is a personal accomplishment, completing it would not have been possible without the guidance and support of several key individuals. Therefore I would like to acknowledge this help I have received in the past period.

I would like to start by thanking my supervisor ir. Barry Zandbergen. With his comments, questions and input he pushed me to work harder and look deeper in the problems at hand. Next I would like to thank Dr. A. Cervone, my second supervisor for his guidance and providing input where necessary to complete the given task and his extensive input for writing the publications for the IAC conference. Furthermore I would like to thank Marc Naeije for taking the time to review my work and ask the critical questions. Special thanks go to Nuno Baltazar dos Santos for his help and patience during the testing phase. His insight in electronics and the test equipment made my task at hand a lot easier. Immense gratitude also goes to John Stals for his help and guidance during the more turbulent times of my studies and helping me stay at university when others said this was impossible.

Next I would like to thank my fellow students and friends at the Space Engineering chair with whom I have had plenty of discussions and help on the content of this thesis and my friends outside the Aerospace Faculty that have helped me keep my mind off the thesis.

Finally I would like to thank my parents Pavle and Nadica and the rest of my family for their unconditional support both emotional and financial without which completing this journey would be inconceivable.

I love deadlines. I love the whooshing noise they make as they go by.

Douglas Adams

Table of Contents

List of Figures

List of Figures

List of Tables

List of Tables

List of Acronyms

3U	3-Unit
ADC	Analog to Digital Converter
ADCS	Attitude Determination and Control Subsystem
AWG	American Wire Gauge
BFSL	Best Fit Straight Line
BSP	British Standard Pipe
CFD	Computational Fluid Dynamics
CGG	Cool Gas Generator
COM	Communication Port
COTS	Commercial Off The Shelf
DAQ	Data Acquisitioning System
DC	Direct Current
DIY	Do It Yourself
DNS	Direct Numerical Simulations
DOT	Design Option Tree
EBM	Electron-Beam Melting
EDM	Electrical Discharge Machining
EEE	Electrical, Electronic, Electromechanicical
EM	Engineering Model
EPDM	Ethylene Propylene Diene Monomer
EPS	Electric Power System
FDM	Fused Deposition Modeling
FEM	Finite Element Method
FKM	Flurocarbon
FM	Flight Model
H2O	Water
IO	Input Output
IRT	Ideal Rocket Theory
LEO	Low Earth Orbit
LOM	Laminated Object Manufacturing
MEMS	Micro Electro Mechanical Systems
MEOP	Maximum Expected Operating Pressure
N2	Nitrogen

NC	Nickel Chromium
NCAX	Nickel Chromium Aluminium
NI	National Instruments
Ni	Nickel
NPT	National Pipe Thread
NTC	Negative Temperature Coefficient
O.D.	Outer Diameter
OBC	On Board Computer
PC	Personal Computer
PCB	Printed Circuit Board
PEEK	Polyether Ether Ketone
PPT	Pulsed Plasma Thruster
PS	Power Supply
R.O.	Rated Output
RANS	Reynolds-Averaged Navier-Stokes
SLA	Stereolithogrpahy
SLM	Selective Laser Melting
SLS	Selective Laser Sintering
SST	Shear Stress Transport
TBC	To Be Confirmed
TBD	To Be Determined
TC	Thermo-Couple
TRL	Technology Readiness Level
TTL	Transistor – Transistor Logic
UI	User Interface
UNF	Unified Fine Thread
USB	Universal Serial Bus
UV	Ultra Violet
VISA	Virtual Interface Software Architecture
VKI	Van Karman Institute

List of Symbols

p_c	Chamber Pressure

List of Symbols

ΔV	Change of Velocity
c^*	Characteristic Velocity
Ø	Diameter
ε	Dissipation Rate
ΔH	Enthalpy Change
Ae	Exhaust Area
Me	Exhaust Mach Number
pe	Exhaust Pressure
pa	Exhaust Pressure
w	Exhaust Velocity
g_0	Gravitational Acceleration
Q	Heat
cp	Heat Capacity at Constant Pressure
cv	Heat Capacity at Constant Volume
M0	Initial Mass
$\dot{m}$	Mass Flow
λ	Nozzle Efficiency Factor
α	Nozzle Half Angle
P	Power
p	Pressure
Mp	Propellant Mass
γ	Ratio of Specific Heats
ao	Sonic Velocity
ω	Specific Dissipation Rate
R	Specific Gas Constant
Isp	Specific Impulse
T	Temperature
ΔT	Temperature Change
At	Throat Area
Dt	Throat Diameter
F	Thrust Force
t	Time
$\varkappa$	Turbulent Kinetic Energy
Vdc	Voltage DC
V	Volume

1. Introduction

Due to recent trends in miniaturization of electronics and production techniques allowing the creation of smaller components, there has been new trend in the space domain. Instead of designing and building big, monolithic and expensive satellites that have numerous capabilities, scientists and engineers explore the possibility to use smaller, cheaper satellites that are capable to perform some of the more simple functions of traditional satellites by themselves or work together in a formation to perform more complex tasks. This could potentially provide great risk reduction in single point failure and easier and cheaper global coverage due to the ability to launch many satellites at low cost [1] [2] [3].

One of the most promising platforms for small satellites is the CubeSat platform, which represents a set of standardized specifications. Combining this with a lot of Commercial Off The Shelf (COTS) technology allows Nano-Satellites to be designed and built at low cost. Therefore over the last decade, CubeSats have become increasingly popular [4]. While most of the CubeSats launched to date have been university projects aiming to provide valuable learning experience while maintaining the cost at minimum, some large corporations and agencies like NASA and Boeing have also taken part and many more are interested [5] [6].

The format and size specifications of the CubeSat platform require highly integrated and miniaturized subsystems. One of the most challenging subsystems has proved to be the propulsion system. This is proved by the fact that up to date only two CubeSat have been launched with a propulsion system, CanX-2 in 2008 [7] [8] and Delfi-n3Xt in November 2013. The importance of a miniaturized propulsion system becomes even more apparent when taken into consideration that most, if not all, of the CubeSats launched to date, due to budget constraints, have been piggybacking their launches into space and therefore they may end up in a non-optimal orbit. Having a propulsion system onboard the spacecraft would allow the operator to control the satellite velocity which could be used for orbit control and maintenance and attitude control. Finally considering traveling beyond LEO, for a satellite mission like the OLFAR, propulsion system is needed to provide the required ΔV.

1.1. Need Statement

For performing tasks where satellites would need to fly in a formation, a propulsion system is a must. One such planned mission by the Delft University of Technology is the DelFFi mission which is a formation flying demonstration of two 3U CubeSats in LEO. The DelFFi satellites, called 'Delta' and 'Phi', are based on the Delfi-n3Xt bus platform which will be enhanced by an improved propulsion system, relative navigation and onboard algorithms. They will be a part of the QB50 project where 50 CubeSats will be launched together and make in situ measurements in the lower thermosphere (90 – 320 [km]) and study the re-entry process by comparing predicted and actual CubeSat trajectories and orbital lifetimes, a project that is possible only due to the low building cost and fast development time of CubeSats [9]. For this mission there is a need for a CubeSat propulsion system capable of delivering at least 15 [m/s] ΔV to a 3.6 [kg] satellite. [10]

1.2. Research Objective

Currently at the Delft University of Technology several students are committed to research topics related to the propulsion system of the DelFFi satellites. For this mission there is a need for a propulsion system capable of delivering at least 15 [m/s] ΔV to a 3.6 [kg] satellite. The most important requirements are summarized in Table 1 in their up-to-date version at the time of writing this report. The thrust range is given such that at the maximum thrust level, the ADCS system should still be able to compensate the disturbance torques produced due to the thrust vector misalignment. The minimum thrust level is based on the expected drag force on the satellites. The maximum expected operating pressure (MEOP) is limited to 10 [Bar] and this only applies when non energetic fluid is used, such as water or nitrogen otherwise additional testing and waiver from the launch provider / CalPoly may be necessary. Given that the satellite is scheduled for launch in January 2016, the TRL should be higher than 6 since the propulsion system should be ready for integration in less than 2 years (Figure 1). The full list of requirements and their rationales can be found in [10] [11]. It is important to note that no specific requirement was given for cost and the budget for the system ranged at times from € 10.000 – 100.000.

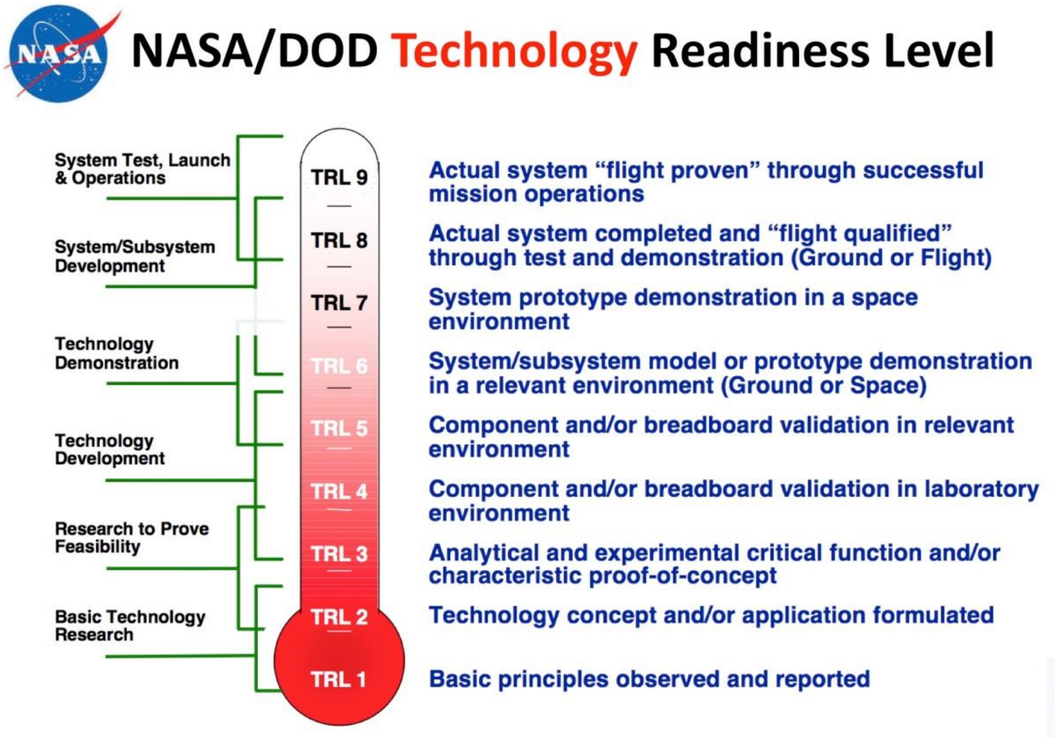

Figure 1: TRL Description [12]

Table 1: Propulsion System Requirements Summary [10]

Parameter	Value	Unit
Thrust	0.5 – 10	mN
ΔV	$\geq$ 15	m/s
MEOP	$\leq$ 10	Bar
Power Usage	$\leq$ 10	W
Mass	$\leq$ 469	g
Volume	$\leq$ 90x90x80	mm
TRL	$\geq$ 6	-

Per earlier definition given in [13], the thruster is defined as the blue part given in Figure 2. The goal of this thesis is to provide a flight model (FM) thruster design and confirm the concept by testing an engineering model (EM) which should be comparable to the FM design functionally wise but preferably at reduced cost.

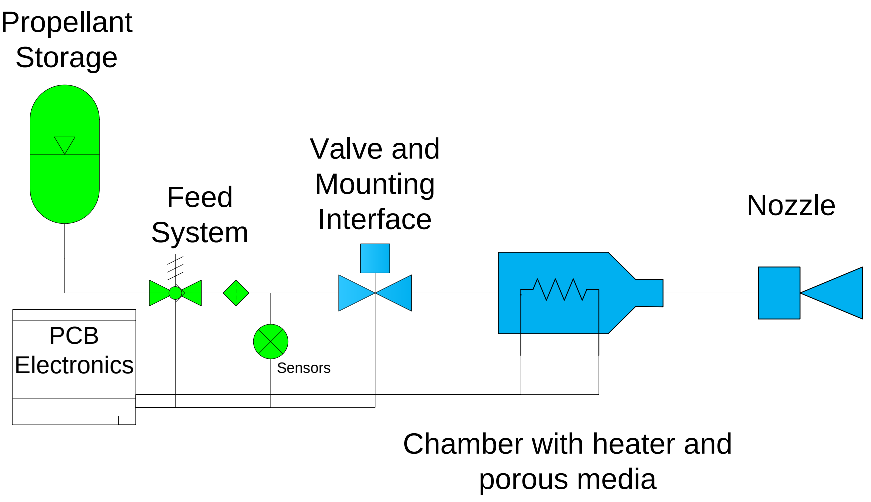

Figure 2: Propulsion System Definition and Task Distribution

1.3. Research Methodology

In order to achieve the goals given in Section 1.2 the following research questions need to be answered:

- Can the fluid be sufficiently heated with less than 10 [W] of power input to achieve the required thrust?
  - What kind of fluid should be used?
  - What is the minimum heating efficiency required?
  - Is there a COTS heater available or custom design is needed?
  - What is the optimal heating time?
  - Can a specific impulse of higher than 100 [s] be achieved?
- What production technique should be used for the thruster?
  - Can the thruster be made using micro – machining?
  - How does it compare against a MEMS thruster both cost and performance wise?
  - What is the optimum cost of production vs. estimated performance of the thruster?
- Can the propulsion system be made within the volume requirements?
  - How much propellant is needed to fulfill the requirements?
  - What kind of packing and level of integration is necessary?
- Can the thruster be characterized with the facilities and equipment available at the chair of Space Engineering?
  - Can the thrust level be measured?

- What is the required resolution and accuracy of the measurements?

To answer the research questions given previously the following task list was generated:

1. Make a Trade – off between different propulsion system design concepts
2. Generate a design of the flight model thruster subsystem
3. Determine production methods and companies capable of producing the different components
    a. Nozzle
    b. Heater
    c. Valve
    d. Support Structure and interfaces
4. Generate a comparable engineering model of the propulsion system
5. Procure all the components
6. Assemble the propulsion system
7. Prepare Test Setup and Test Plan
8. Test the propulsion system as to make sure the requirements are fulfilled
9. Analyze the results and verify that the requirements as given in [10] have been met.

The envisioned timeline of the project is represented by a Gantt Chart given in Appendix A.

1.4. Report Outline

The report follows the events in the thesis in chronological manner. Before starting the thesis a literature study was made. A short recap of this literature study is given in Chapter 2. Next with a good knowledge base about the topic set, different propulsion system concepts where investigated in Chapter 3 and a concept selection was made. With the propulsion system design set, a requirements flow down was made in Chapter 4, starting from the system requirements going down to the thruster requirements including the different components in the thruster. Having the requirements clearly set allowed for the design phase to start. In Chapter 5 component selection based on the previously set requirement was done and components where designed where needed. Emphasis was made on the nozzle design as that component was where the design had the most freedom. For the thruster to be tested a propellant storage and feed system was needed and supporting electronics for sensing and control. Thus an engineering model propulsion system was made which is described in Chapter 6. Having the complete system ready a test setup including both hardware and software was made and it is given in Chapter 7 followed by the test plan and test results given in Chapter 8. Finally the results are analyzed in Chapter 9 and the lessons learn are given including a proposed flight model design. Finally in Chapter 0 the conclusions of the thesis are presented together with the recommendations for the future work on this project.

2. Literature Review

Before the work on the thesis start, students are required to do a literature study on the topic. In this chapter a short recap of the literature study [13] is given which was used as a starting point for this thesis. The first step in the literature study was to make a market research and get insight in the currently available COTS propulsion systems, a short recap of which is given in Section 2.1. Next, the optimal design approach was investigated and the required tools and setting identified, which can also be seen in Section 2.2. With the design tools and approach set, different possible manufacturing methods where considered which are of interested and potential partners for the thruster production where identified. A short summary is given in Section 2.3. Next the current test facilities where investigated and two potential test benches where identified of which a short description is given in Section 0. Finally a summary of the decisions made during the literature study is given in Section 2.5.

2.1. Market Research

In order to avoid unnecessary developments and reduce production time and costs it is wise to look into what is currently available. An overview is given of the current COTS CubeSat propulsion systems, their technology readiness level (TRL) and whether they fulfill the requirements given in [10]. Unfortunately little or no information is available on the thruster component of the COTS propulsion systems and therefore they are evaluated as a whole.

2.1.1. COTS Systems Overview

A good overview of COTS propulsion systems are given in [8] and [14]. These are fairly recent studies made in 2012 and 2010 respectively and give a rather complete overview of the state of the propulsion systems developed specifically with CubeSats in mind, the technology readiness level (TRL) and the specifications of the CubeSats. The most important requirements that the propulsion systems must satisfy are given in Table 1. The TRL should be higher than 6 since the propulsion system should be ready for integration in less than 2 years. All the potential candidates that fulfill most of the requirements given in Table 1, are summarized in Table 2 and updated data is given where available. Since ΔV information for most propulsion systems is not available, total impulse is used instead. For a 3.6 [kg] satellite like the DelFFi satellites a total impulse of at least 54 [Ns] is needed [8]. All the potential systems are pictured in Figure 3.

Table 2: Potential COTS Propulsion Systems [8] [14] [15] [16] [17] [18] [19] [20]

Propulsion System	Propellant	Thrust [mN]	Total Mass [g]	Specific Impulse [s]	Volume [mm^3]	Total Impulse [Ns]	Max Power [W]	TRL	Tank Pressure [Bar]
VACCO	Isobutane	55	456	53	25x100x100	34	1	9	3
T3µPS	Nitrogen	1-100	119	69	94x94x18	0.8	10.5	8	NA
µPPT	Teflon	0.04	210	590	90x90x27	42	0.5	8	NA
MPS - 110	Nitrogen	-	-	-	100x100 x110	36	$<$ 10	6	-
HYDROS	Water	600		300	$<$ 1U	325	10	6	NA
T3µPS+	Nitrogen	9.5	443	69-100	90x90x80	36 - 60	10.5	6	NA

2.1.2. COTS System Trade – Off

From Table 2 it can be seen that no system in the current state fulfills all the requirements as given in Table 1. Therefore it is clear that if any of the propulsion systems are chosen, modification will be necessary. Two subsystems seem the most promising, namely the µPPT from Clyde Space and the T3µPS, which is a development of TU Delft and TNO.

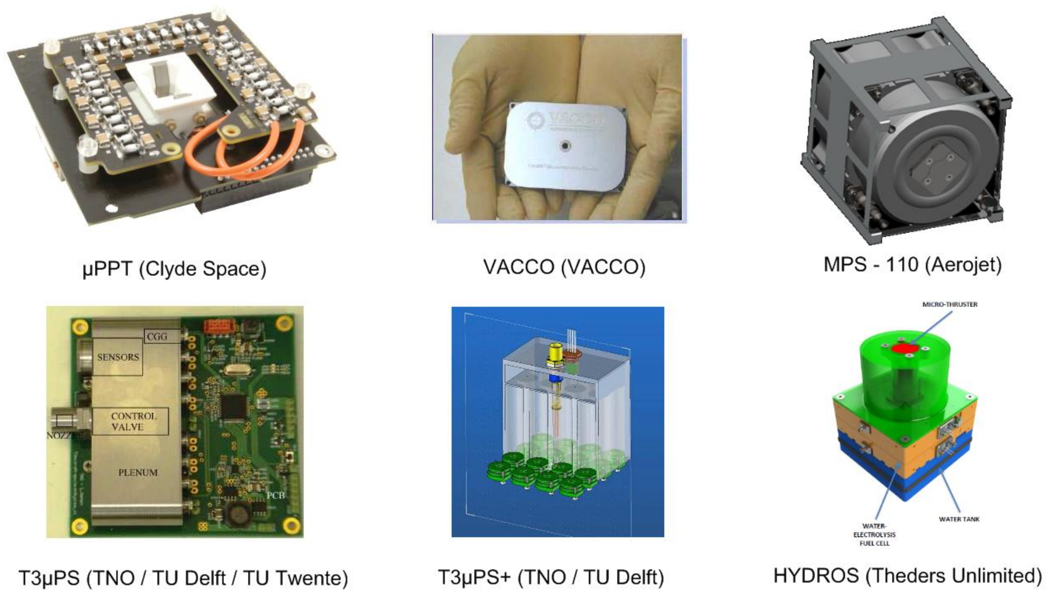

Figure 3: Potential COTS Thrusters [8] [15] [16] [17] [18] [19] [20]

The µPPT from Clyde Space would need about $16*10^5$ pulses to achieve the 15 [m/s] ΔV and since it has a firing frequency in the range of 0.1 -10 [Hz] that means it would need between 2 and 185 days of continuous thrusting [21]. Since the total mission life time is 90 days and the thruster would only operate while the satellite is in the view of the Sun, the µPPT would need to be able to have a continuous firing frequency of at least 0.6 [Hz] which would mean the µPPT would operate continuously for at least a quarter of the mission life time (circa 31 days). However Clyde Space specifies a total impulse of 42 [Ns] which is insufficient to satisfy the requirements given in [10] and it is currently unclear if the amount propellant can be increased. Furthermore there are the typical concerns with PPTs such as non – uniform and late time ablation and electromagnetic interference [8]. Finally the current PPT has been tested of up to 15E5 pulses. If Clyde Space can clear these doubts, this PPT would be a possible option. The quoted price of the µPPT propulsion system is $18,850 [22].

The T3µPS+ is a development of TU Delft and TNO with which there have been numerous collaborations. While the current T3µPS design has very low total impulse, it has a very promising technology for propellant storage that satisfies all the requirements, namely the Cool Gas Generator (CGG). This technology uses nitrogen stored in solid form in cartridges which can be ignited on demand to release nitrogen gas ready to be used as propellant [20]. As it is shown in [8] the main issue with propellant storage in a CubeSat is not the mass but volume budget. A significant improvement needs to be done to the CGGs to be able to store enough propellant to achieve the baseline mission of 15 [m/s]. As an alternative, the specific impulse of the system could be increased. This can be done by integrating a heater in the T3µPS and heating the nitrogen which is the concept of the T3µPS+ [20].

In conclusion two propulsion systems are promising for the DelFFi mission, namely Clyde Space's µPPT and the modified T3µPS+ design. The µPPT from Clyde Space is a ready product which is likely to satisfy all propulsion system requirements with some modifications. However as stated before some doubts remain which need to be clarified with Clyde Space.

2.2. Design Tools and Method

In this chapter the design methodology will be given. The starting point of the design is Ideal Rocket Theory (IRT). This was more in-depth covered in [13]. A short recap will be given in 2.2.1. Since manufacturing of the nozzle is both labor and time expensive, Computational Fluid Dynamics (CFD) is used to provide higher certainty of the design. The theory of CFD is given in Section 2.2.2 and the different models are explained in 2.2.3.

2.2.1. Ideal Rocket Theory

A relatively standard thruster design approach is given in [23]. Using Ideal Rocket Theory (IRT) and assuming no losses in the system and ideal expansion a preliminary sizing of the thruster can be made such that it fits the requirements. The design starts by sizing the nozzle for the desired thrust level and then working back to thru the chamber all the way to the propellant storage tanks. For more realistic results quality coefficients are introduced from statistics and simulations done on similar designs. These quality coefficients cover the loss of performance due to not having ideal expansion, boundary layer effects, manufacturing irregularities etc. and are covered more in depth in [13] and [24]. For big rocket engines, such as the ones used on launchers, the divergence between IRT and test data is in the order of 1 – 10 [%] [25], however for micro – thrusters where boundary layer effects cannot be neglected and manufacturing imperfections play important roles the difference can be 20 – 30 [%] and even more than 50 [%] for non – optimal design [26] [24] [27]. Therefore for greater confidence in the results and final optimization of the design CFD simulations can be used.

However unlike a propulsion system with nitrogen, for a propulsion system with liquid water as propellant, the available power to heat the water is the limiting factor. This determines the maximum mass flow allowable in steady state operation and from that the maximum throat area can be calculated. From the rest the design procedure follows the one as given in [23] and [28].

2.2.2. Computation Fluid Dynamics Theory

CFD is a numerical method of simulating the behavior of systems involving fluid flow, heat transfer, and other related physical processes such as chemical reactions in combusting flows. The physical characteristics of the fluid motion are solved using equations of fluid flow (in a special form) over a region of interest, with specified (known) conditions on the boundary of that region. [29] These equations that govern the process of interest are often called governing equations in CFD. A complete CFD analysis consists of three main elements, namely pre-processor, solver and post-processor which are inter connected as shown in Figure 4 [30].

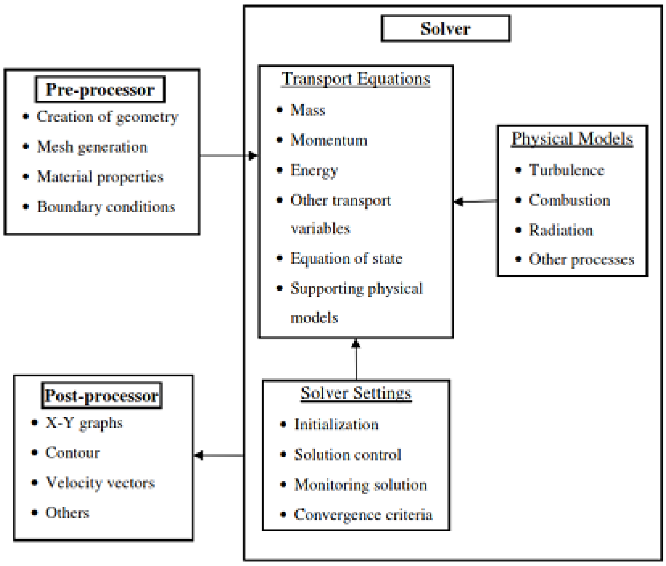

Figure 4: CFD Analysis Main Elements [30]

For all flow types, Fluent solves the equations for conservation of mass and momentum. In addition to those the equation for energy conservation is solved for compressible flows or flows that have heat transfer. Since the whole principle of the thruster is to compress the propellant to achieve Mach 1 in the throat, all these 3 equations will be used throughout the CFD simulation. When the flow is turbulent, additional transport equations are solved as well.

Examples of governing equations being solved by Fluent are the Navier-Stokes equations for compressible flow. The continuity equation which describes the conservation of mass is given, the momentum conservation equation and the energy conservation equation are given by (2.1) [30].

$$\begin{aligned}
&\frac{\partial \rho}{\partial t} + \nabla \cdot \left(\rho \cdot \vec{V} \right) = 0 \\
&\frac{\partial \left(\rho \cdot \vec{V} \right)}{\partial t} + \nabla \cdot \left(\rho \cdot \vec{V} \cdot \vec{V} - \underline{\underline{T}} \right) = \rho \vec{b} \\
&\frac{\partial \left(e_o \cdot \rho \right)}{\partial t} + \nabla \cdot \left(e_o \cdot \rho \cdot \vec{V} - \underline{\underline{T}} \cdot \vec{V} + \vec{\dot{q}}_c + \vec{\dot{q}}_r \right) = \rho \left(\vec{V} \cdot \vec{b} + \vec{\dot{q}} \right)
\end{aligned} \tag{2.1}$$

2.2.3. Computational Fluid Dynamics Models

The majority of all flows of engineering interest are turbulent [31]. Turbulence is the three-dimensional unsteady random motion observed in fluids at moderate to high Reynolds numbers [29].

While turbulence is, in principle, described by the Navier-Stokes equations, using Direct Numerical Simulations (DNS) is not feasible since the computing power required far exceeds what is available today. Therefore the Navier-Stokes equations are averaged which filters out all or part of the turbulent flow. The most widely applied averaging procedure is Reynolds-averaging (which, for all practical purposes is time-averaging) of the equations, resulting in the Reynolds-Averaged Navier-Stokes (RANS) equations [29]. However, by averaging new, additional unknowns are introduced in the system of equations. Choosing the proper turbulence model and meshing grid greatly affects the quality of the simulation

Unfortunately different turbulence models have different applications and a single, universal turbulence model does not exist. The choice of the turbulence model used depends on the problem at hand, the level or accuracy required and the computational power available.

Two equation models are historically the most commonly used RANS models, which solve two transport equations and model the Reynolds Stresses using the Eddy Viscosity approach [32]. They provide relatively high accuracy while significantly reducing the computation time. The models available in Fluent are the k-ε and the k–ω. The k-ε models solves for the k equation and dissipation rate equation ε. The k-ω models and its variants solve for ω instead, which is the specific dissipation rate. In this literature study the standard k-ε model and the standard k-ω model will be covered and their variants briefly mentioned.

2.2.3.1. *κ – ε Model*

The standard k – ε model in Fluent is considered the workhorse of practical engineering flow calculations. It is a semi-empirical model based on model transport equations for the turbulence kinetic energy (k) and its dissipation rate (ε). The model transport equation for k is derived from the exact equation, while the model transport equation for ε is obtained using physical reasoning. In the derivation of the k – ε model, the assumption is that the flow is fully turbulent, and the effects of molecular viscosity are negligible. The standard k – ε model is therefore valid only for fully turbulent flows [29].

The advantages of the k – ε is that it is simple and affordable computation wise and it is reasonably accurate for a wide variety of flows that do not have flow separation. The cons of the k – ε is that it is overly diffusive, it lacks universality and it is not accurate in the region close to the wall. To overcome these problems few variants of the k – ε model have been introduced. In Fluent in addition to the standard k – ε model the RNG k – ε model and the realizable k – ε model are also available. When opting for a k – ε model in Fluent it is always recommended to use the realizable k – ε model in combination with Enhanced Wall Treatment. However for situation where flow separation occurs k – ε model are not recommended.

2.2.3.2. *κ – ω Model*

The k – ω model has been developed from when it became apparent that most of the drawbacks of the k – ε models are due to the modeling of the ε equation which is neither accurate nor easy to solve (ε has a local extreme close to the wall) [33]. The standard k – ω model in Fluent is based on the Wilcox k – ω model which incorporates modifications for low-Reynolds number effects, compressibility and shear flow spreading [29].

By using the ω-equation, this model offers several advantages when compared to the k – ε models with the most prominent being better boundary layer modeling and more robust Enhanced Wall Treatment. The disadvantage of the standard k – ω model is that the solution is sensitive to the free stream conditions. Therefore the Shear – Stress Transport (SST) k – ω was developed by Menter [29]. It basically blends the robustness and accuracy of the k – ω model in the near wall region with the free stream independence of the k – ε. Therefore for the CFD results it was decided this model to be used.

2.3. Production Methods

In this section a summary of the different production methods is given. The processes of interest for producing the thruster are Micro – Machining, Additive Fabrication (3D Printing) and Electroforming. More in-depth information and additional manufacturing techniques are available in [34].

2.3.1. Micro – Machining

Machining is defined as the process in which material is removed with a cutting tool in from a work piece in a controlled manner such that a desired final shape is achieved. There are many different processes that have this common trait which are collectively known as subtractive manufacturing processes. Micro – Machining is the same process done on a very small scale. The processes that are of interest for producing the thruster components are the traditional single point (Turning) and multi-point cutting processes (Milling and Drilling) and also non-conventional thermal machining like EDM (Electrical Discharge Machining).

Turning is a machining process in which the cutting tool is fixed and the work piece is rotating and lathes are the principal machine tools used in turning. They are used to produce rotational, typically axi - symmetrical parts which can have various futures such as holes, grooves, threads etc. A typical turning machine and turning product are given in Figure 5 and typical tolerances and surface finish values are given in Table 3. Advantages of turning operations are very good tolerances and relatively short lead times while disadvantages are that products are limited to rotational parts (axi – symmetric), tool wear is significant and several operations may be required to achieve the desired shape. This process would be interesting if axi – symmetric chamber is used, and for the nozzle as well if the small diameters are achievable.

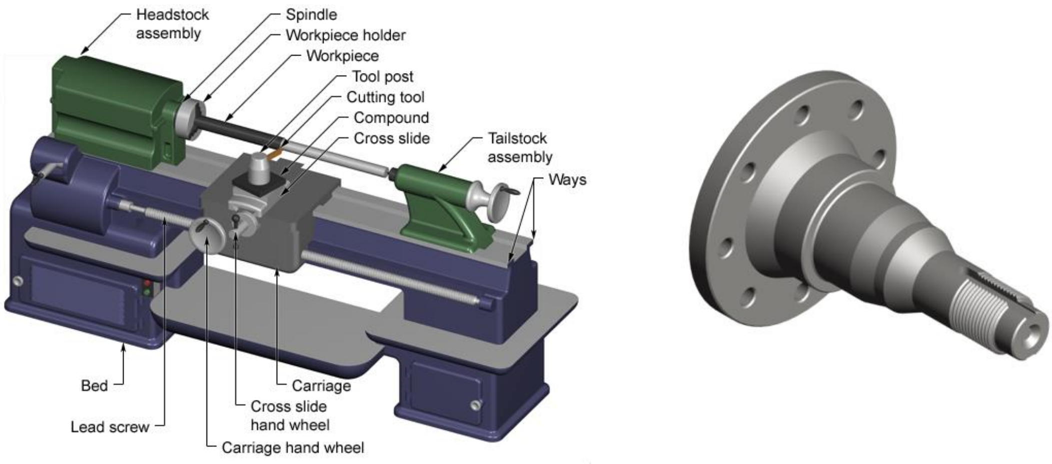

Figure 5: Turning Machine (Lathe) and Turning Product [35]

Table 3: Machining Process Comparison [35]

	Turning		Milling		EDM	
	Typical	Feasible	Typical	Feasible	Typical	Feasible
Part Size [mm]	Ø 0.5 - 2E3		1 – 1.8E3 [L,W]		-	
Surface Finish Ra [µm]	0.4 – 3.2	0.05 – 6.3	0.8 – 3.2	0.2 – 12.5	1.2 – 3.8	0.2 – 6.3
Tolerance [µm]	± 25	± 5	± 25	± 12	± 12	± 4

In contrast to turning, in milling the work piece is fixed and the cutting tool is rotating and the principal machines are called milling machines or mills. Milling is typically used to produce parts that are not axi – symmetrical and may have many different features including 3D surface contours. A typical milling machine and milled product are given in Figure 6 and typical tolerances and surface finish values are given in Table 3. Advantages of milling operations are very good tolerances and relatively short lead times while disadvantages are that products complexity is limited, tool wear is significant and several operations may be required to achieve the desired shape. Milling would be used if non axi – symmetric chamber is used and potentially also for interface brackets used to attach the thruster to the thrust bench or the structure of the satellite.

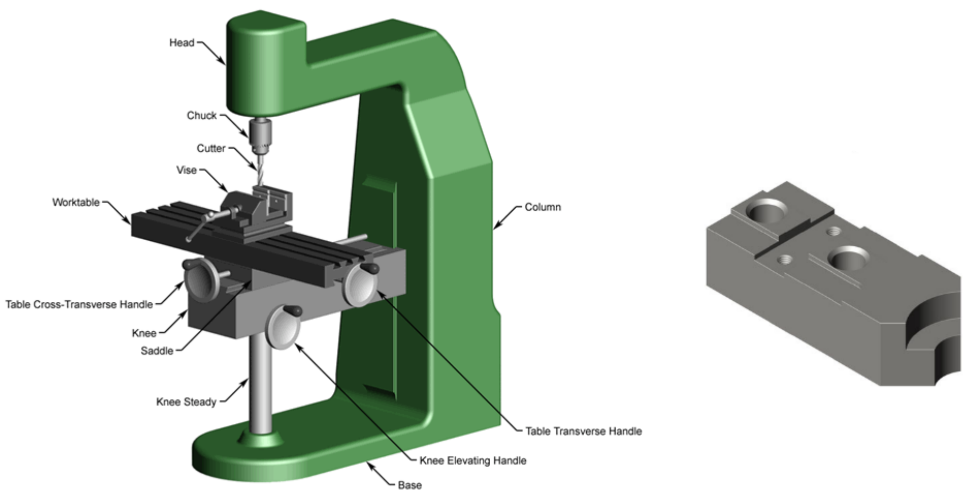

Figure 6: Milling Machine and Milling Product [35]

Drilling is machining operation in which holes are cut into a work piece. Drilling operations are done primarily in drill presses but sometimes also on lathes or mills. Hole diameters can be as small as 50 [µm] with a ± 2 [µm] tolerance. This method would be useful for simpler, primitive nozzle production.

EDM is the process of machining electrically conductive materials by using precisely controlled sparks that occur between an electrode and a work piece in the presence of a dielectric fluid [36]. The electrode may be considered the cutting tool.. The advantages of EDM is that I can form complex shapes and fine details, it have excellent tolerances and low labor cost. The disadvantages are that the material has to be electrically conductive, it has very low production rate and high tooling and equipment cost. EDM is typically applied for production of dies and honeycomb structures. Typical tolerances and surface finish values are given in Table 3. With micro machining both critical components such as the nozzle and bulkier components like the structure can be produced. Companies capable of doing all conventional machining processes on the small scale as needed for the DelFFi thruster is “MICRO PRECISION PARTS MANUFACTURING LTD.” from the USA and the internal workshop “DEMO” from Delft University of Technology.

2.3.2. Additive Fabrication (3D Printing)

Additive fabrication or more commonly referred as 3D printing is a process in which a part is produced by adding layers of material upon one another. These fabrication processes are inherently different from both machining processes which are a subtractive in nature and consolidation processes such as injection molding since no product specific tooling or molding is required.

There are different additive fabrication methods available, which differ both in the method of layer deposition and the type of materials used. These can be split in 3 main groups, namely liquid-based processes, powder-based processes and solid-based processes. Liquid-based additive fabrication typically uses photo-curable polymer resins and Stereolithography (SLA) is the most common process. These photo-curable polymers however have poor mechanical properties that degrade over time and therefore are not of interest for the manufacturing of the DelFFi thruster but can be useful for interface testing.

As the name suggest, in powder-based additive fabrication, powdered material is melted or sintered to form each part layer. This allow not only polymers but also metals and ceramics to be used and the mechanical properties of powder-based processes are more attractive and stable when compared to liquid-based processes. The processes that are of interest for producing the thruster components are Selective Laser Melting (SLM), Direct Metal Laser Sintering (DMLS), Selective Laser Sintering (SLS) and Electron-Beam Melting (EBM).

Solid-based processes use a variety of solid, non-powder, materials and each process differs in how it builds the layers of a part. Most solid-based processes use sheet-stacking methods, in which very thin sheets of material are layered on top of one another and the shape of the layer is cut out. The processes that are of interest for producing the thruster components are Laminated Object Manufacturing (LOM) and Fused Deposition Modeling (FDM).

Each of the previously mentioned methods has its own advantages and drawbacks, and the design of the part and the desired characteristics need to be taken into account when choosing the best production method for each thruster component. Typical characteristics for different additive fabrication processes are given in Table 5. More information can be found in [37]

Table 4: Additive Fabrication Process Comparison [37]

	FDM	SLS	DMLS	LOM
Part Size [cm]	91x61x91	56x56x76	25x25x22	81x56x51
Min Feature Size [mm]	0.13	0.13	0.13	0.20
Min Layer Thickness [mm]	0.13	0.10	0.03	0.05
Surface Finish	Rough	Average	Average	Rough
Tolerance [mm]	±0.13	±0.25	±0.25	±0.10
Applications	Form/fit testing, Functional testing, Rapid tooling patterns, Small detailed parts, Presentation models, Patient and food applications, High heat applications	Form/fit testing, Functional testing, Rapid tooling patterns, Less detailed parts, Parts with snap-fits & living hinges, High heat applications	Form/fit testing, Functional testing, Rapid tooling, High heat applications, Medical implants, Aerospace parts	Form/fit testing, Less detailed parts, Rapid tooling patterns

Numerous companies are available where you can send you CAD drawing and they will produce a prototype. While current 3D printing technology lacks the precision and surface finish quality to produce the nozzle, it is a viable production method for the structure of the thruster, reducing the number of components and making assembly easier.

2.4. Testing Facilities

In this chapter the currently available thruster test benches at the chair of Space System Engineering are presented. In Section 2.4.1 a 50 [mN] called AE-TB-50M is presented, with its characteristics, current state and modifications necessary to be used for testing the DelFFi thruster are given. A test bench currently under development called AE-TB-5M is presented in Section 2.4.2, with its predicted performance, current development status and modifications necessary to be used for testing the DelFFi thruster are given. Finally a decision is made, which test bench is going to be used in the testing campaign of the DelFFi thruster. The information in this chapter is extracted from [38], [39] and [40].

2.4.1. AE-TB-50M Test Bench

The name of this test bench, AE-TB-50M, stands for Aerospace Engineering Thrust Balance 50 [mN]. Originally designed and built in 2009 by Stef Janssens, in its default configuration it can measure forces of up to 50 [mN] and it has been used for the development and testing of the T3μPS micro propulsion system. The design is shown in Figure 7 with the T3μPS mounted on the test bench.

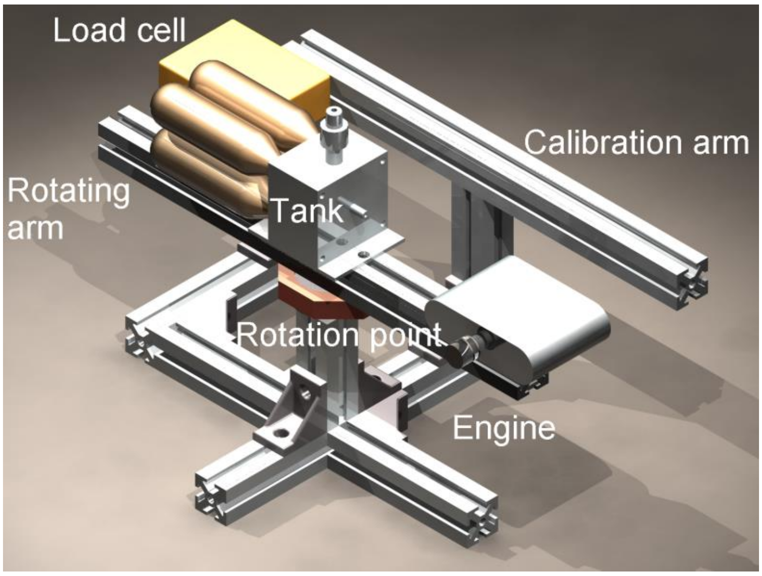

Figure 7: AE-TB-50M Test Bench [39]

In principle the TB-50M is a horizontal balance with direct force measurement where the detector provides the restoring force and measures force instead of displacements. The construction is made out of BOIKON 20x20 mm aluminum profiles which allow simple assembly of the stand and easy mounting of the detector, thrusters and feed system. It uses low-friction ball bearing in the pivot. The maximum mass of the thruster (including the mounting bracket) that the TB-50M supports is 360 [g]. The measurement range is 0.5 – 50 [mN] with and accuracy of 0.5 [mN] and the force is measured by a FUTEK LRF400 load cell. Furthermore the thrust stand has mounting spots for both the feed system and propellant tank. To reduce the influence of the changing mass in the propellant tank on the dynamics and balance of the stand, the tank should be mounted above the pivot. Parasitic forces caused by the power feed lines are reduced by using thin copper wires that are protected by a thin film and suspended above the engine, minimizing their influence on the measured thrust.

In 2009 Krister de Ridder has undertaken the task to make the test stand operational again and modify the design such that the signal noise is reduced, however no documentation is available of this effort.

2.4.2. AE-TB-5M Test Bench

In 2010 Daniel Pérez Grande designed a test bench named AE-TB-2M which can measure thrust in range of 10 - 2000 [μN] for engines with a total mass of less than 300 [g] with an accuracy of less than 2 [μN]. The AE-TB-2M design in principle was a direct displacement measurement pendulum which is supported on two stands using a blade and spike support to minimize friction. The configuration of the thrust stand is shown in Figure 8. The counter mass is used to amplify the moment caused by the weight of the engine, while the torsion spring provides the restoring force required in the pendulum. To damp environmental vibrations, a heavy aluminum baseplate is used on which the test stand is mounted and parasitic forces are reduced by having the propellant tanks mounted on the test stand itself. Additional advantage of this thrust bench is that it can be calibrated remotely using electromagnet thus calibration can be done in vacuum instead of ambient conditions.

In 2013 Roy Bijster took over the task from Daniel Perez Grande thereby incorporating a number of improvements. The goal was set to enable trust measurements in the 1 [μN] to 5 [mN] and impulse bits in the 1 [μNs] to 1 [mNs] range. The test bench was accordingly renamed to AE-TB-5M. However, recent results have shown that the range can be extended to 10 [mN] with no or small modifications to the test stand such as changing the torsion spring.

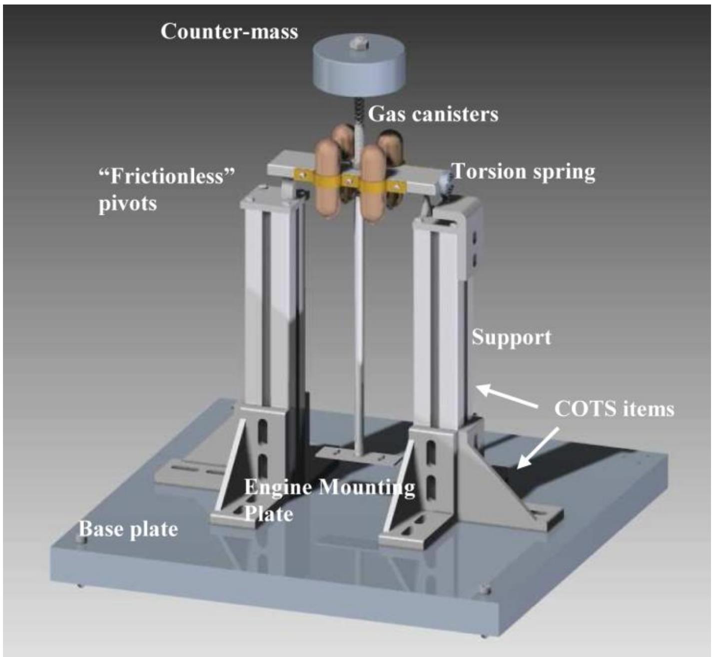

Figure 8: AE-TB-5M Test Bench [40]

2.5. Literature Study Conclusion

At the beginning of this literature study a large number of CubeSat propulsion systems were investigated. It has been concluded that most of the COTS propulsion systems are either too immature or their performance is too low / high to be considered for the DelFFi mission. Two systems however are able to fulfill all the requirements. The first is a µPPT from Clyde Space and the second one is the T3µPS+ from TNO and TU Delft. The µPPT quite possibly can be just integrated in the satellite and fulfill the mission requirements of 15 [m/s] ΔV. However some doubts exist about the thruster pulse rate, non – uniform and late time ablation and possible electromagnetic interference with the rest of the DelFFi systems. It can be ordered from Clyde Space for $17,250. This option however has not been investigated further due to lack of funds, manpower and interest of the project manager.

The T3µPS+ would need a heater capable of heating the Nitrogen gas to 1000 [K] to fulfill the requirements of 15 [m/s] ΔV. It will however require further development from TNO on the CGG side and from TU Delft on the thruster side. The advantage of a resistojet is that in a case the CGGs from TNO underperform, alternative propellants such as water or butane can also be used.

To manufacture the nozzle and the thruster structure a number of production methods alternative to MEMS have been investigated. Injection molding, electroforming and micro –

machining look like promising, cheaper alternative to MEMS, while providing equivalent or better tolerances and surface quality. To produce the chamber and mechanical interfaces an additive fabrication technique such as injection molding or 3D printing instead of machining is expected to simplify the assembly and reduce the number of parts of the thruster.

3. Conceptual System Design and Concept Selection

In this chapter the preliminary design process and sizing of the propulsion system is done. This design process focuses on fulfilling the performance requirements as set in [10] and obtaining initial size information. First an initial design is made using ideal expansion and then iteration is made such that the thruster would be able to fulfill the requirements working both in cold gas and in resistojet mode.

For the initial sizing the following assumptions are made:

- No losses in the feed system
- No pressure and mass losses in the nozzle and boundary layer effects are neglected
- Isentropic flow from the tank to the heater inlet in resistojet mode or nozzle exit in the cold gas mode
- Intermittent operation of the propulsion system which allows the propellant in the tank and feed system to be isothermal at the midpoint of the operational temperature range – 300 [K]
- Operation in vacuum, meaning ambient pressure is 0 [Bar]
- Blow down system with the propellant stored as gas
- No chamber filling effects. Steady state conditions at all time.

3.1. $T^3\mu PS+$

In this section the performance of the propulsion system is calculated taking into consideration the concept given in [20]. First of all the limit conditions are defined. It has been stated in Chapter 1 that the thrust range of the thruster should be between 0.5 [mN] and 9.5 [mN]. The propulsion system should provide at least 15 [m/s] ΔV. The maximum expected propellant pressure is 10 [bar] and the wet mass of the DelFFi satellites is estimated to be 3.6 [kg]. Finally the operating temperature range of the propulsion system is from − 20 to 80 [°C] and the power consumption limited to 10 [W]. These values are summarized in Table 5.

Table 5: Propulsion System Limit Conditions

Limit Conditions	
Minimum Thrust	0.5 [mN]
Maximum Thrust	9.5 [mN]
Minimum ΔV	15 [m/s]
Maximum Propellant Pressure	10 [Bar]
Satellite Wet Mass	3.6 [kg]
Maximum Power Consumption	10 [W]
Maximum Operating Temperature	353.15 [K]
Minimum Operating Temperature	253.15 [K]

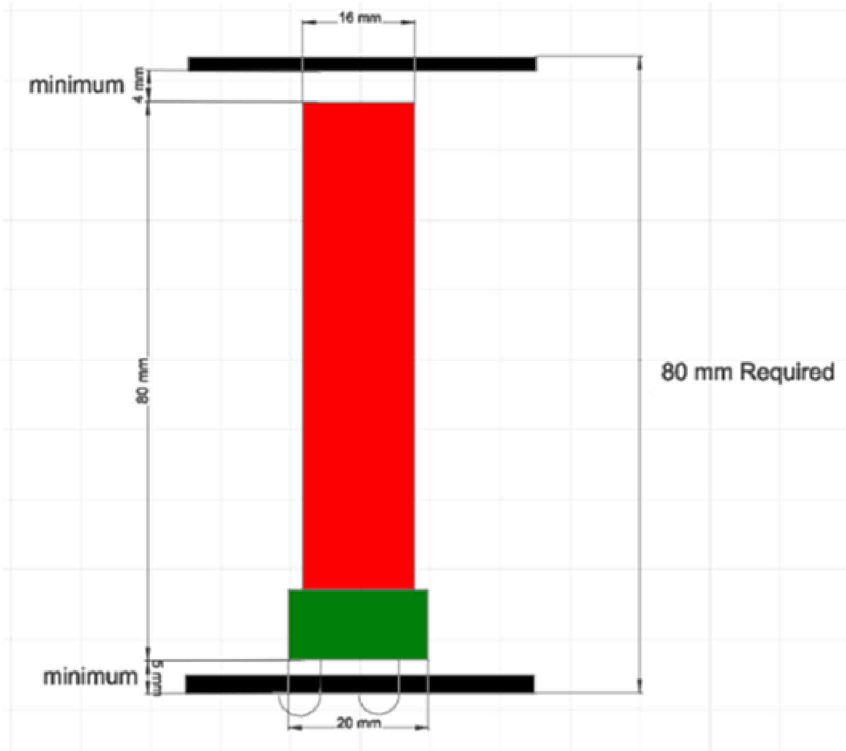

Figure 9: Cool Gas Generator New Design

As it was mentioned earlier in Section 2.1 a significant improvement needs to be made to CGGs for them to be significant. TNO has proposed a new design of the CGGs shown in Figure 9. It has a diameter of 16 [mm], height of 80 [mm] and produced 4.2 [g] of N2 gas. Furthermore it requires a minimum clearing of about 4 [mm] above the CGG and 5 [mm] below the CGG. It immediately becomes clear that using this CGG design will result in a propulsion system with a height of at least 90 [mm]. The project manager accepted the possibility to have the volume budget extended but asked for an alternative design as well. Therefore TNO proposed a smaller 60 [mm] high CGG that would produce 30 [%] less gas or 2.9 [g]. Taking this into account and the fact that the maximum number of CGGs that can be placed in the given volume is 14 due to clearance for mounting rods and other components, a graph was made showing the attainable ΔV budget for nitrogen heated at different temperatures (Figure 10).

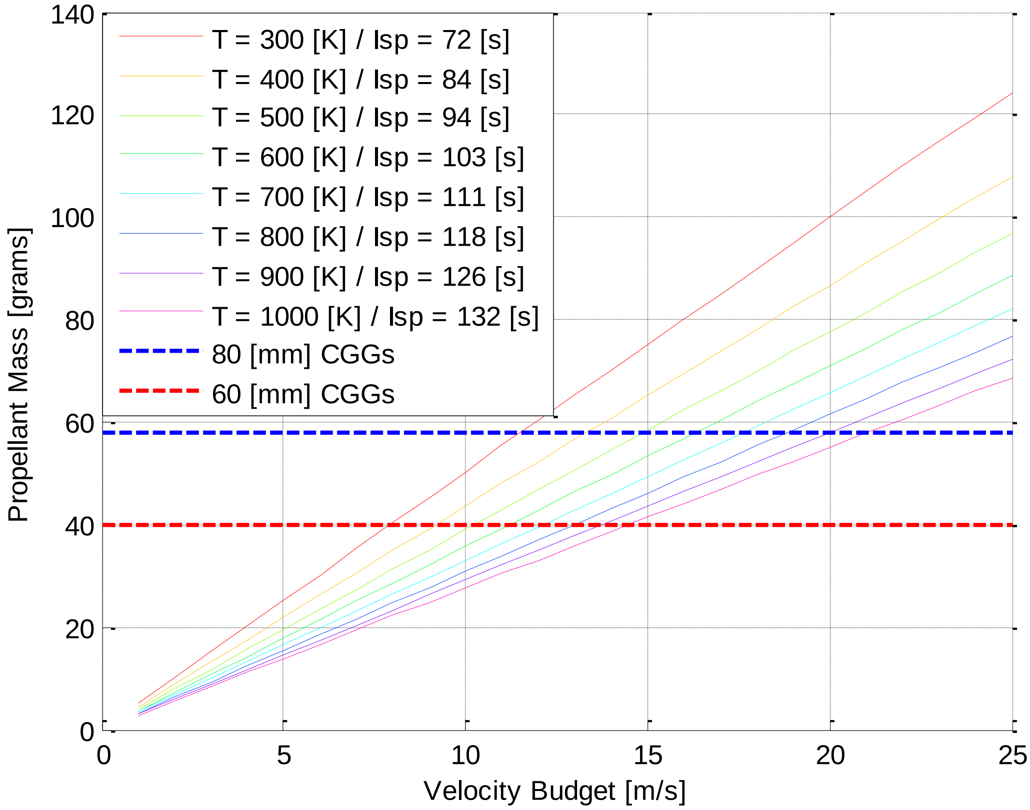

Figure 10: Velocity Budget Attainable with CGGs

As it can be seen, 15 [m/s] is not attainable with the 60 [mm] CGGs even with a heater capable of heating the gas to 1000 [K] and a gas temperature of at least 600 [K] is needed to achieve this goal when using the 80 [mm] CGGs. Taking into account that losses are not taken into account and that a previous MEMS thruster has been able to achieve a specific impulse of 110 [s] and an operational temperature of 700 [K] [41] in this calculation 700 [K] was taken as the gas temperature of the Nitrogen. The nominal storage pressure for the nitrogen was taken from the preliminary study in [20] to be 7 [Bar]. For simplicity single phase, gaseous flow is assumed with uniform temperature. The gas properties for Nitrogen at both temperatures are given in Table 6. As it can be seen the ratio of specific heats and the specific gas constant both are mostly dependent on temperature and not pressure.

Therefore an intermediate value for both of them is taken, namely the average of the maximum and minimum.

Table 6: Nitrogen Gas Properties [42]

P [Bar]	T [K]	c_v [J/g*K]	c_p [J/g*K]	γ [-]	R [J/kg*K]
7	300	0.74	1.05	1.41	306.4
7	700	0.80	1.10	1.37	298.0
5	300	0.74	1.05	1.41	303.7
5	700	0.80	1.10	1.37	297.7
1	300	0.74	1.04	1.40	298.1
1	700	0.80	1.10	1.37	297.0

3.1.1. Thruster Design

The sonic velocity of both gases is given by (3.1) and the characteristic velocity by (3.2) The specific impulse is given by (3.3) and assuming ideal expansion in vacuum ($p_e / p_c = 0$) it reduces to (3.4). It should be noted that ideal expansion would require infinitely long nozzle in vacuum and this is physically impossible, however the following relations are only used as a starting point for the design and later iteration is made taking into consideration the actual expansion ration and specific impulse.

$$a_0 = \sqrt{\gamma \cdot R \cdot T} \tag{3.1}$$

$$c^* = \frac{a_0}{\gamma \cdot \left(\frac{2}{\gamma+1}\right)^{\frac{\gamma+1}{2\gamma-2}}} \tag{3.2}$$

$$I_{sp} = \frac{c^*}{g_0}\gamma \left\{ \left(\frac{2}{\gamma-1}\right)\left(\frac{2}{\gamma+1}\right)^{\frac{\gamma+1}{\gamma-1}} \left[1-\left(\frac{p_e}{p_c}\right)^{\frac{\gamma-1}{\gamma}}\right]\right\}^{\frac{1}{2}} \tag{3.3}$$

$$I_{sp} = \frac{c^*}{g_0}\gamma \left\{ \left(\frac{2}{\gamma-1}\right)\left(\frac{2}{\gamma+1}\right)^{\frac{\gamma+1}{\gamma-1}} \right\}^{\frac{1}{2}} \tag{3.4}$$

From the specific impulse and the maximum thrust, the maximum mass flow can be calculated using (3.5). Logically the mass flow will vary with the tank pressure in a blow down system. The maximum mass flow is interesting to see if with the current power budget the propellant can be heated up to the desired temperature in the resistojet working mode. This is done using (3.6). For initial sizing it is assumed that 50 [%] of the heater power is transferred to the fluid. Finally the total propellant mass required is calculated using (3.7)

$$\dot{m} = \frac{F}{g_0 \cdot I_{sp}} \tag{3.5}$$

$$Q = \dot{m} \cdot C_p \cdot \Delta T \tag{3.6}$$

$$M_{P_{total}} = M_0 \cdot \left(1 - e^{\frac{-\Delta V}{I_{sp} \cdot g_0}} \right) \tag{3.7}$$

The results are summarized Table 12. Furthermore even with 50 [%] heater efficiency the power requirement is within the limit. How the performance differs with a finite expansion ratio is given in the next section.

Table 7: Ideal Propellant Performance

	Cold Gas	Resistojet
	Nitrogen	Nitrogen 700 [K]
γ [-]	1.41	1.37
R [J/kg*K]	303.6	297.7
a_0 [m/s]	358	534
c^* [m/s]	439	672
I_{sp} [s]	80.6	126.6
P_{Cp} [W]	-	6.73
M_p [g]	45.3	28.9

For the preliminary design ideal expansion is not anymore considered. As has been shown in [13] the critical point is not the mass of the propulsion system but the volume. Therefore low propellant mass and thus high specific impulse is crucial. To start the design first a design point needs to be chosen. This is done by plotting the specific impulse for different expansion ratios and comparing it to the ideal specific impulse. The exhaust Mach number as function of the expansion ratio is given in (3.8). With the Mach number know the pressure ratio over the nozzle can be calculated using (3.9) and finally the specific impulse is calculated using (3.3).

$$\frac{A_e}{A_t}=\frac{1}{M_e}\left[\left(\frac{2}{\gamma+1}\right)\left(1+\frac{\gamma-1}{2}M_e^{\ 2}\right)\right]^{\frac{\gamma+1}{2\gamma-2}} \tag{3.8}$$

$$\frac{p_e}{p_c}=\left(1+\frac{\gamma-1}{2}M_e^{\ 2}\right)^{\frac{\gamma}{1-\gamma}} \tag{3.9}$$

The specific impulse vs. the expansion ratio for Nitrogen in the cold gas case is given in Figure 11. A nozzle efficiency of 100 [%] is assumed. It can be seen that 90 [%] of maximum theoretical value is achieved already at expansion ration of 18 and 95 [%] at expansion ratio of 92. Due to the small scale of the nozzle, an area ratio of 92 should be easily achievable and therefore this was chosen as the design point. This would result in Isp of about 76.9 [s]. For the resistojet case 90 [%] of maximum theoretical value of Isp is achieved at expansion ratio of 30 and 95 [%] at expansion ratio of 145 (Figure 12). At an expansion ratio of 92 as in the cold gas case the Isp of the thruster would be around 119 [s]. At this point the actual expansion ratio is taken into account but quality factors are not.

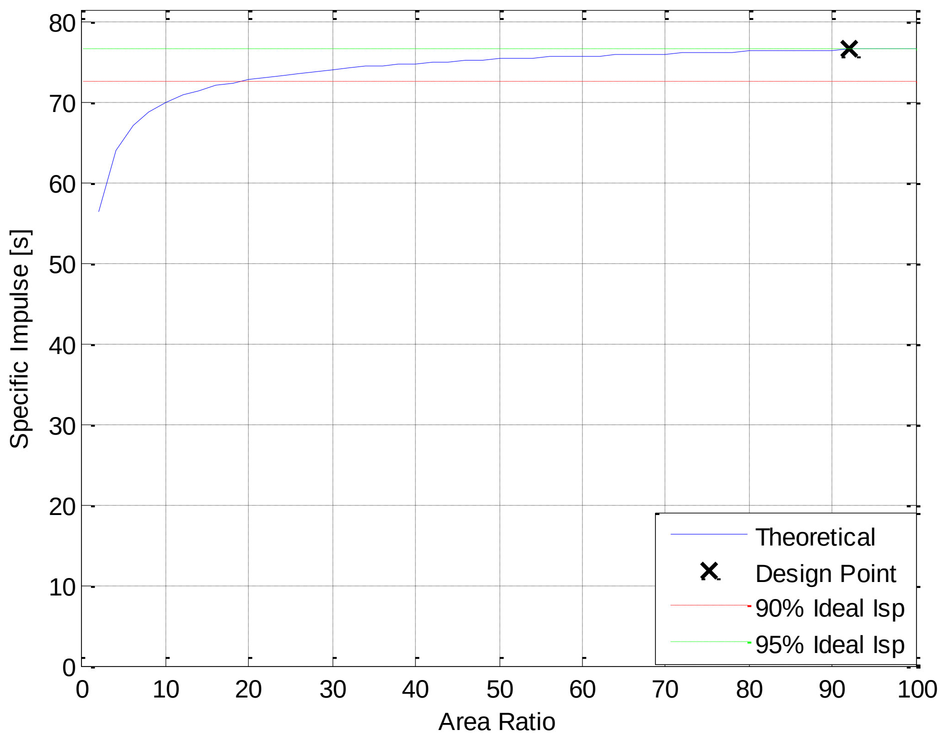

Figure 11: Expansion Ratio vs. Specific Impulse for Nitrogen at 300 [K]

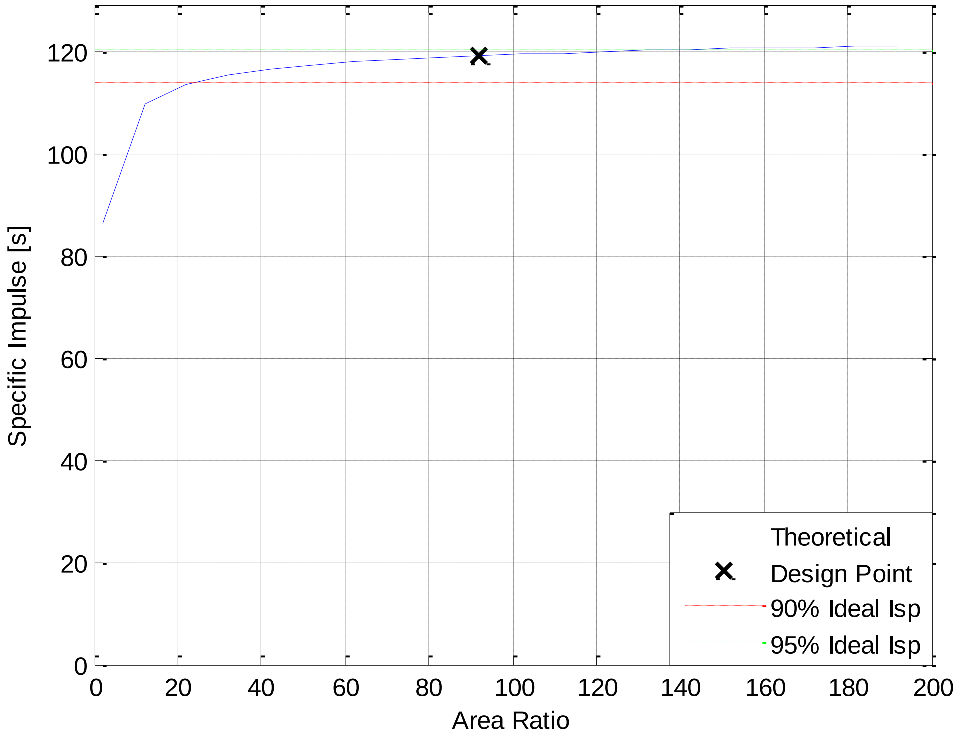

Figure 12: Expansion Ratio vs. Specific Impulse for Nitrogen at 700 [K]

With the area ratio of the nozzle set for both cases, the next step is to define the throat area such that the maximum thrust is in compliance with the requirements as given in Table 5. With the newly calculated Isp values the maximum mass flow is once again calculated with (3.5). Next the throat area is calculated using (3.10). Assuming an axisymmetric nozzle the diameter is calculated using basic algebra.

$$A_t = \frac{\dot{m} \cdot c^*}{p_c} \tag{3.10}$$

The chamber pressure p_c in (3.10) is same as the tank pressure for both the cold gas and the resistojet case. For simplicity reasons, the gas is assumed to behave as ideal gasses. Since the heating is isobaric the throat area will remain unchanged from the cold gas case and only the mass flow will differ. The results are given in Table 8, where the value for the throat diameter in the resistojet case is for isobaric heating. With the geometry defined, in the next section the thruster performance over time is investigated.

Table 8: Preliminary Thruster Geometry

	Cold Gas	Resistojet
A_e/A_t [-]	92	92
I_{sp} [s]	76.9	119.2
D_t [µm]	100	100

3.1.2. Performance Analysis

To calculate the performance of the propulsion system, a basic feed and tank storage system is modeled. As previously mentioned it is assumed that the Nitrogen is stored at 7 [Bar]. The tank temperature is assumed to be constant at 300 [K]. In both the cold gas case and the resistojet case the camber pressure is assumed to be same as the tank pressure ($p_{tank} = p_{chamber}$). Seeing as the feed system has to be compact and the feed system will be made as short as possible it is expected that pressure losses will be negligible. Furthermore the thermal mass of the tank is much larger than the rest of the system thus it is expected that the temperature variations will be much smaller than the rest of the satellite.

Next a nozzle efficiency factor λ is introduced. Federico La Torre in his research has come to the conclusion that in the 1 – 10 [mN] range a nozzle efficiency of 88 - 92 [%] is achievable with optimal design choices [24]. These are explained in more detail later in the report. Assuming that the nozzle is in the middle of this range, a nozzle efficiency of 90 [%] is assumed. The thrust is then given by (3.11) [43].

$$F = \lambda \left\{ A_t \cdot p_c \cdot \gamma \left[\left(\frac{2}{\gamma - 1} \right) \left(\frac{2}{\gamma + 1} \right)^{\frac{\gamma+1}{\gamma-1}} \left\{ 1 - \left(\frac{p_e}{p_c} \right)^{\frac{\gamma-1}{\gamma}} \right\} \right]^{\frac{1}{2}} + \left(p_e - p_a \right) A_e \right\} \tag{3.11}$$

The pressure ratio is calculated from (3.9) and since vacuum is assumed p_a is 0 [Pa]. The throat diameter is sized such that at MEOP the thrust is 9.5 [mN]. From the previously calculated area ratio given in Table 8 the throat area and exit area can be calculated. With the thrust known and the mass flow calculated with (3.12), the specific impulse of the thruster accounting for the efficiency of the nozzle can be calculated using (3.13). Since the specific impulse is constant throughout the thrust and pressure range the propellant mass required can once again be calculated using (3.7). The volume of the tank is sized such that the propellant storage pressure is in compliance with the previously mentioned assumptions.

$$\dot{m} = \frac{A_t \cdot p_c}{c^*} \tag{3.12}$$

$$I_{sp} = \frac{F}{g_0 \cdot \dot{m}} \tag{3.13}$$

With the thruster at $t = 0$ characterized equations (3.14) are calculated over time until the thrust is below the required 0.5 [mN] or there is no propellant left in the tank. As previously mentioned isothermal expansion is assumed due to the intermittent operation of the propulsion system which allows the propellant in the tank and feed system to be isothermal at the midpoint of the operational temperature range. The results are given in Figure 13 for the resistojet case and in Figure 14 for the cold gas case. All the data is summarized in Table 9 and Table 10. As it can be seen the results are different than the ones in Table 7 mainly due to the introduction of the nozzle quality factors.

Table 9: Thruster Performance Summary

	Cold Gas	Resistojet 700 [K]
F_{max} [mN]	8.6	8.8
Total ΔV [m/s]	10.5	16.4
I_{sp} [s]	70.2	109.6
T_{gas} [K]	300	700
M_p [g]	58.8	58.8

Table 10: Thruster Design Summary

A_e/A_t [-]	92
D_t [µm]	100
λ	0.9
p_{tank} [Bar]	7

As it was previously mentioned since exact part production at this scale is rather difficult a sensitivity analysis has been made w.r.t. the throat diameter because it is the driving parameter in the thruster performance. The exit diameter just changes the expansion ratio and with it the specific impulse however as it can be seen in Figure 11 and Figure 12 the design point is far on the right side where the trend becomes nearly horizontal. This means that the thruster performance is almost unaffected by inaccuracy of the exit diameter. Finally the convergent and divergent angle and the surface quality will affect the nozzle efficiency but the effect cannot be calculated using IRT and CFD analysis is needed to investigate these effects.

It should be noted that Figure 11 and Figure 12 are modelled under the assumption that all the propellant is available as gas in the beginning and no CGG firing is taken into account. In reality by using CGGs, the tank volume will be much smaller and the change in pressure much faster. If this concept is chosen and once the tank design is finalized the CGG firing sequence will be incorporated into the simulation.

$$
\begin{aligned}
&M_{p_{(i)}} = M_{p_{(i-1)}} - \dot{m}_{(i)} \cdot \Delta t \\
&p_{c_{(i)}} = p_{t_{(i)}} = \frac{M_{p_{(i)}} \cdot R_t \cdot T_t}{V_t} \\
&\dot{m}_{(i)} = \frac{A_t \cdot p_{c_{(i)}}}{c^*} \\
&p_{e_{(i)}} = p_{c_{(i)}} \cdot \frac{p_e}{p_c} \\
&F_{(i)} = \lambda \left\{ A_t \cdot p_{c_{(i)}} \cdot \gamma \left[\left(\frac{2}{\gamma-1}\right) \left(\frac{2}{\gamma+1}\right)^{\frac{\gamma+1}{\gamma-1}} \left\{ 1 - \left(\frac{p_e}{p_c}\right)^{\frac{\gamma-1}{\gamma}} \right\} \right]^{\frac{1}{2}} + p_{e_{(i)}} A_e \right\} \\
&I_{sp_{(i)}} = \frac{F_{(i)}}{g_0 \cdot \dot{m}_{(i)}} \\
&w_i = \frac{F_i - p_{e_i} \cdot A_e}{\dot{m}_i} \\
&\Delta V_{(i)} = w_i \cdot \ln\left(\frac{M_0}{M_0 - \left(M_{p_{total}} - M_{p_{(i)}}\right)} \right)
\end{aligned}
\tag{3.14}
$$

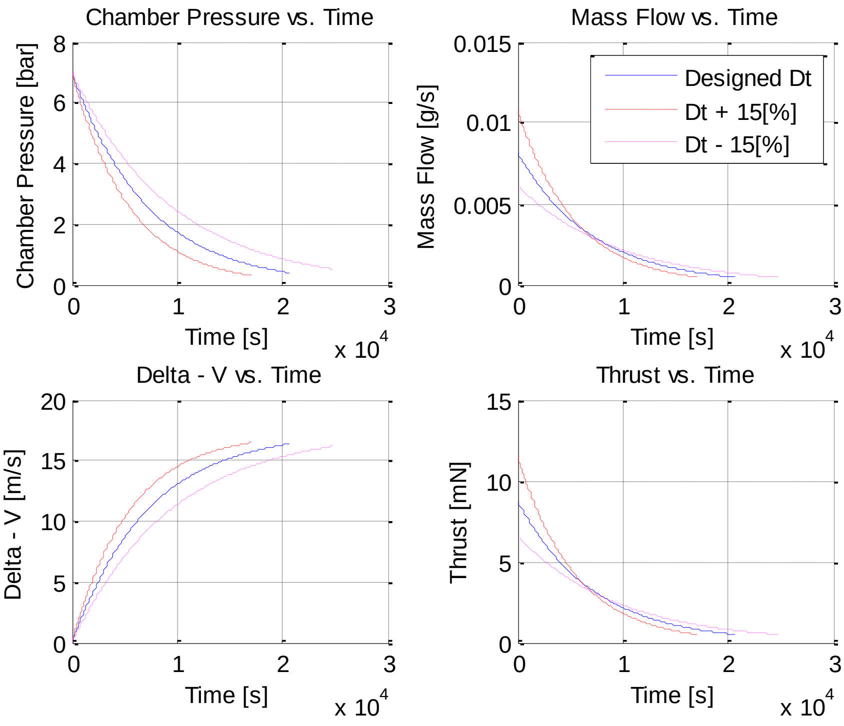

Figure 13: Nitrogen Resistojet Performance vs. Time

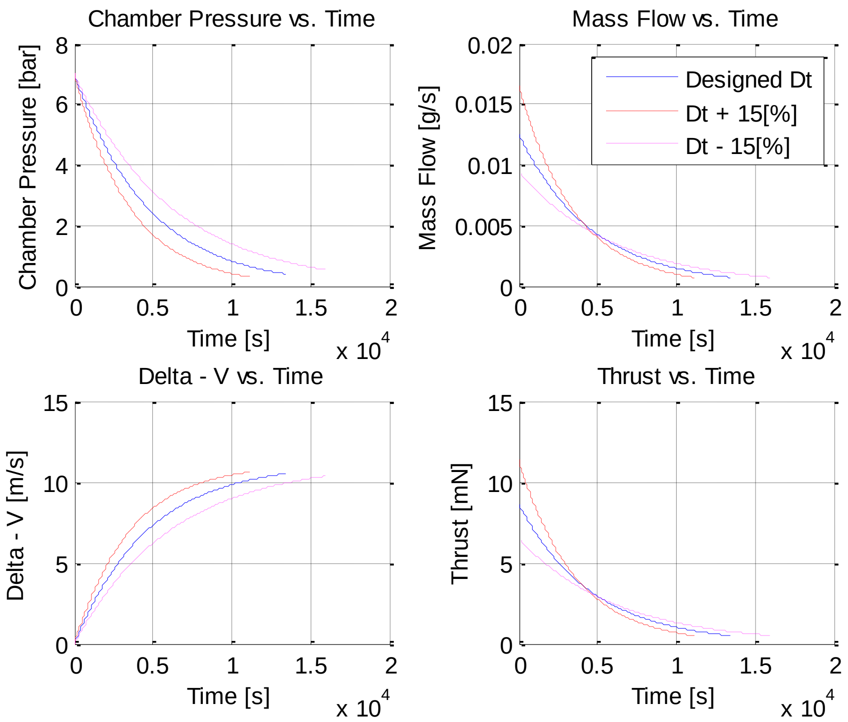

Figure 14: Nitrogen Cold Gas Performance vs. Time

3.1.3. System Design

The pressure in the tank when nitrogen is stored as gas can be calculated using (3.15). If all the propellant is available as gas, as in the previous simulation, this leads to a pressure in the tank of 160 [Bar] for propellant mass of 58 [g]. This is clearly above the requirements as stated in Table 14 and thus it is not a feasible solution.

$$P_{tank} = \frac{R \times T_{tank} \times M_{prop}}{V_{tank}} \tag{3.15}$$

However if CGGs are used, one CGG has a volume of about 16 [cm^3] and produces 4.2 [g] of propellant. Taking 14 CGGs as baseline the total volume used for propellant storage is about 350 [cm^3] which is in compliance with the space available. The design given in [20] actually has 16 CGGs however later it became apparent that 2 CGG diagonally needs to removed such that there is enough space for the mounting roods and supports. The CGG propulsion system concept is shown in Figure 15.

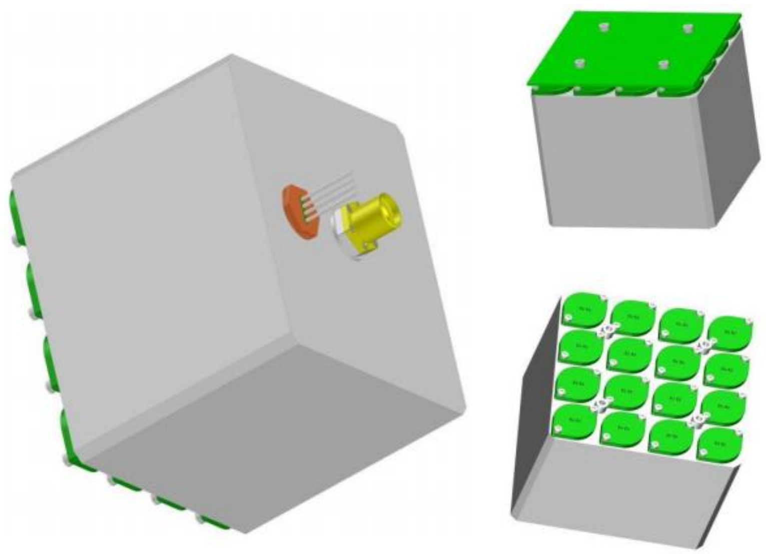

Figure 15: Propulsion System Concept with CGGs [20]

A conceptual design of the thruster in cold gas mode (without heater) is shown in Figure 16.

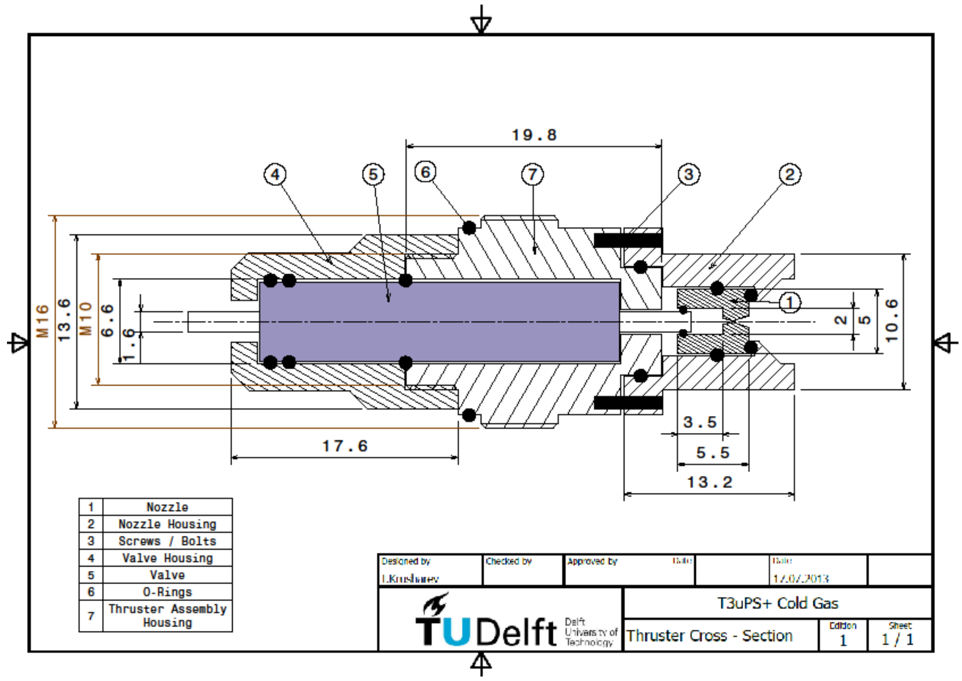

Figure 16: Thruster Concept Design

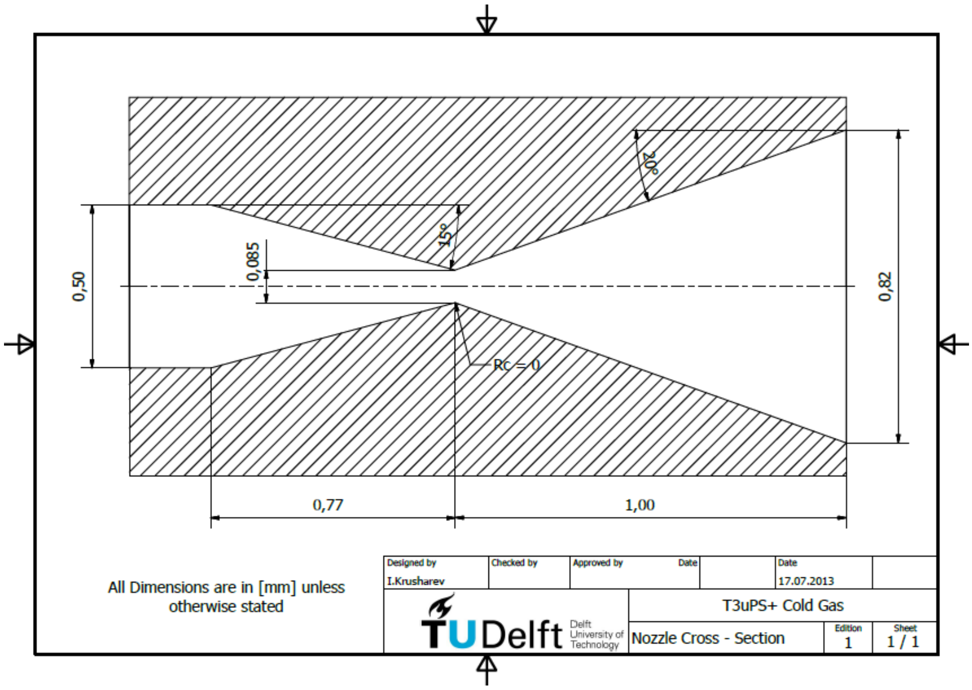

Figure 17: Ideal Nozzle for Nitrogen Fed Thruster

3.2. TU Delft in-house designs

In addition to the design that would be made with TNO, two in-house designs have been considered, both use liquid water as propellant but the pressurization method differs.

One design option uses CGGs for pressurization and another uses N2 gas. The thruster is interchangeable to either concept.

3.2.1. Water Resistojet with Cold Gas Generator

This design option would use the existing CGGs as used in Delfi – n3Xt. While they provide only about 0.1 [g] of N2 gas, this is sufficient for pressurization of the water. This will significantly reduce development costs of the propulsion system, as the CGGs are readily available for purchase. Depending on the tank size 1 – 3 CGGs should be sufficient. The ignition circuit for the CGGs however still comes at a significant cost. The system would work in blow-down mode with pressure ranging between 10 and 1 [Bar]. The conceptual design of the tank is show in Figure 18. The water and the nitrogen gas need to be separated to prevent mixing and to ensure pressurization of the water. This can be done by using piston, membrane or other separation mechanism.

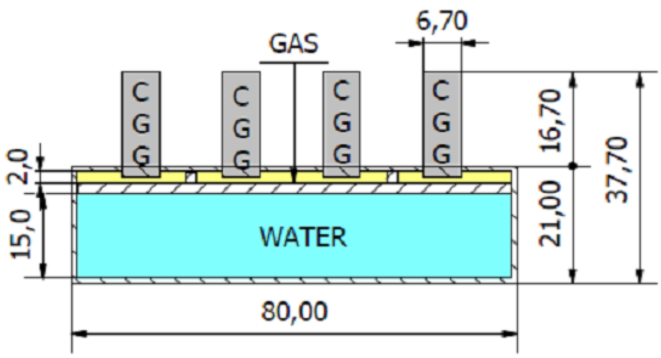

Figure 18: CGG + Water tank design

3.2.2. Water Resistojet with Nitrogen Gas

This design option would use N2 gas to pressure the water, meaning the system will also be pressurized during launch. This simplifies the design significantly, but it introduces additional constraints in terms of regulations and additional testing and safety margins that need to be satisfied such that the propulsion system is allowed on-board the launch vehicle. In terms of performance, they will be the same as the other design option since the performance is driven by the thruster and not the propellant storage and feed system. The conceptual design is shown in Figure 19.

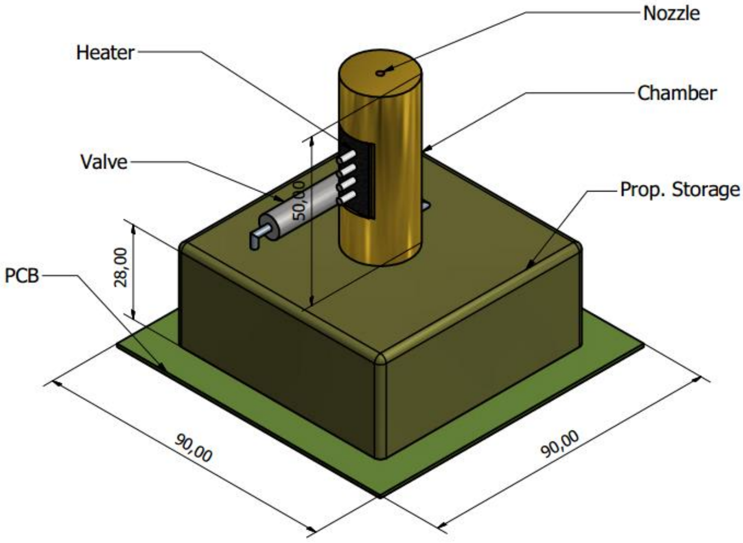

Figure 19: Water Resistojet pressurized with Nitrogen Gas

3.3. Thruster

The maximum input power is 10 [W]. Assuming a maximum heating efficiency of 70%, it follows that 7 [W] is available for heating. Taking into consideration the enthalpy change for heating water from 300 [K] to 550 [K] of 2900 [J/g] [42] the maximum mass flow that can be heated to 550 K can be calculated using (3.16) to be 2.4 [mg/s]. The power required for heating water from 300 [K] to different temperatures and different mass flows is given in Figure 20.

$$\dot{m} = \frac{P}{\Delta H} = 2.4 \ {}^{mg}\!/_{s} \tag{3.16}$$

With this the maximum throat diameter for an axi-symmetrical nozzle can be calculated to be 65 [µm] using (3.17). For the production 60 [µm] was chosen as the next smallest available drill size.

$$\dot{m} = \frac{p_c \times A_t}{c^*} \tag{3.17}$$

To reduce the risk of water droplets condensing in the nozzle exhaust the area ratio should be kept low and thus an area ratio of 25 was selected. Finally the convergence and divergence angle are set to 20° and 30° respectively to make the manufacturing process easier. The whole nozzle has a length of 0.9 [mm] and a diameter of 2 [mm]. It has a M2 thread such that it can easily be screwed in the chamber and the performance of different nozzle geometries can be investigated during the testing phase. The nozzle cross section is shown in Figure 21.

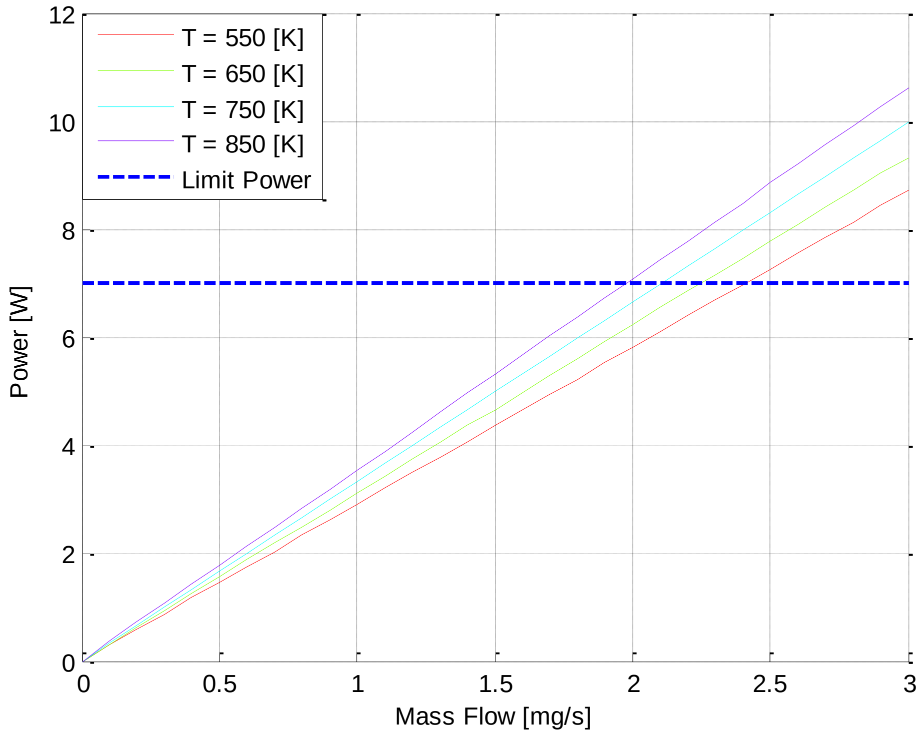

Figure 20: Power required to heat water

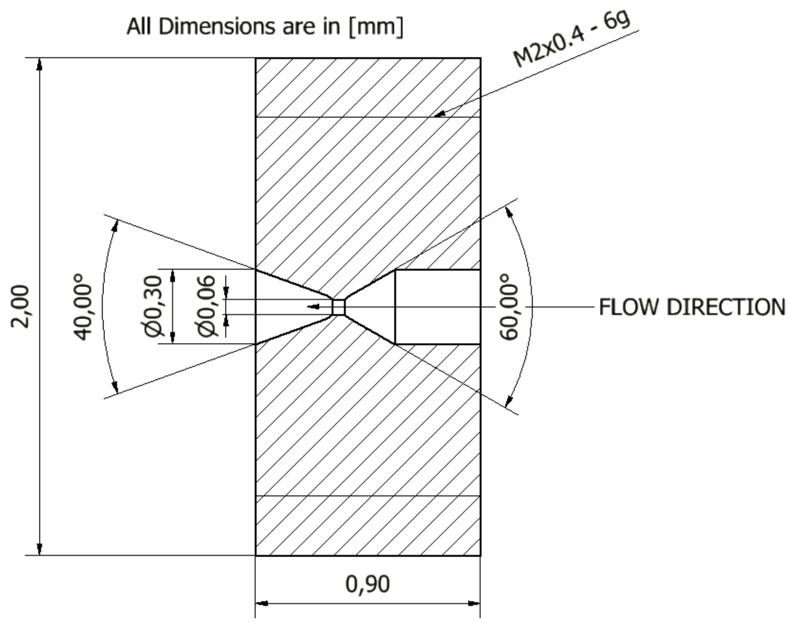

Figure 21: Nozzle Cross Section

From [42] for water at 550 [K] and 7 [Bar] the following properties are valid (Table 11).

Table 11: Water Properties

Parameter	Value	Unit
Cp	2.1056	[J/g*K]
Cv	1.5858	[J/g*K]
R	519.8	[J/kg*K]
γ	1.328	-

With these the results in Table 12 are obtained. Propellant mass was taken to be 50 [g] and ideal nozzle is assumed.

Table 12: Thruster Specifications

Parameter	Value	Unit
Thrust	3.5 – 0.5	[mN]
Pressure	7 – 1	[Bar]
Specific Impulse	141	[s]
Mass flow	2.5 – 0.4	[mg/s]
Power Needed	7.2 – 1.2	[W]
Propellant Mass	50	[g]
ΔV	18.7	[m/s]

3.4. Concept Trade – Off

The trade – off was done on the basis of the criteria given in Table 13. Since this is an academic project the cost and producibility have the highest impact on the project. Next in line is the performance of the thruster since while achieving the requirements is sufficient one should strive for higher performing and more efficient system. Finally the volume and the mass have the lowest weight since their budget is fixed and if a system satisfies it, it should be good enough. Development time is expected to be the same for all systems and therefore was not taken into account.

During the time of the trade – off there were significant updates from both TNO and VKI as the project leader of the QB50 mission. In retrospect the time line of the events are given below:

- First meeting with TNO October 2013: It is estimated by TNO Total cost for the two units is € 100k with a risk level comparable to that for the T3-mps system. Schedule for development is very tight. TNO is unable to contribute funds.

- Second meeting in November 2013 leading to an initial request for proposal to TNO. On request of DelFFi systems engineer the number of systems requested is increased to three.
- January 2014: Third meeting with TNO leading to a new cost estimate of €145k.
- January 23rd: DelFFi systems engineer indicates the cost is simply too high and alternative solutions need to be found
- End January 2014: Confirmation of VKI that water is allowed on board of DelFFi. It is not considered to endanger the launch or others. Decision is made in agreement with systems engineer that the propulsion group will start designing an alternative propulsion system based on the assumption that a maximum pressure of 10 [Bar] is allowed during all mission phases.

Thus due to the fact that the cost estimate provided by TNO is prohibitively high for this project and the relaxation in the constraints in terms of pressurized system onboard it has been decided that Delft University of Technology will continue designing, building and testing the DelFFi propulsion system independently. As it can be seen a propulsion system with water as propellant and gaseous nitrogen as pressurant gas was set as baseline.

Table 13: Propulsion System Concepts Trade - Off

Criteria + Weight		T3µPS+	H_2O + CGG	H_2O + N2
Cost	5	1	3	5
Performance	3	5	4	4
Producibility	4	5	3	3
Volume	1	1	4	5
Mass	1	1	4	5
Pressurization	2	5	5	1
TRL	4	3	1	1
Score		64	61	66

Due to the fact that all the components will be done in-house and no complicated ignition circuit or CGGs are needed the H_2O + N2 scores highest in the Cost category. Performance wise the T3µPS+ can provide the highest thrust and sufficient ΔV while the concepts using water have much lower thrust. Producibility wise the water concepts score lower due to the smaller nozzle needed which complicates the nozzle production. Volume wise the T3µPS+ is outside the initial bounds given by the system engineer while the in-house designs require much smaller tank size. Furthermore the T3µPS+ has much higher mass due to the support needed for the CGGs and the left-over "dead weight" that they have (components such as casing, igniter etc.). Finally since both the T3µPS+ and the H_2O + CGG concept are unpressurized during launch they score the highest in this category while the H_2O + N2 will be at MEOP during launch. TRL wise the for the T3µPS+, smaller CGGs have been proved to work in Space, but these need to be enlarged significantly while a water resistojet at this performance spectrum hasn't been demonstrated in Space.

4. Thruster Requirements Analysis

In this chapter the requirements analysis for the thruster design is given. The thruster has been defined in [13] and Section 1.2 as everything from the valve to the nozzle, including the valve to chamber connection, but excluding the valve to feed system and tank connection

There are 2 groups of requirements. The main requirements (Section 4.1) are the mission specific system requirements coming from the DelFFi and QB50 Mission [10] [11] , from which a flow down is made such that the thruster requirements are obtained in Section 4.1. Furthermore requirements from the interface to the thrust bench (Sections 4.3) are also considered since they will be of importance during the testing phase of the thruster.

4.1. Thruster Requirements

In this section the thruster subsystem requirements are given that flow down from the previously given propulsion system requirements. The rationale for each requirement is given in the sections below. The flow down chart is given in Figure 23 and the summary of the most important requirements are given in Table 14.

Table 14: Thruster Subsystem Requirements

Thruster	
Total Thruster Mass	$<$ 25 [g]
Total Volume	70 x Ø16 [mm]
Propellant Type	Compatible with H_2O (Liquid) and N_2 (Gas)
Specific Impulse	$>$ 100 [s]
Thrust Range	0.5 - 9.5 [mN]
Total Power Consumption	$<$ 8 [W]
Response Time	$<$ 2 [s]
Valve	
Mass	$<$ 10 [g]
Volume	30 x Ø16 [mm]
Leak Rate	$<$ 10E-5 [scc/sec] GN_2
Power Consumption	$<$ 1 [W] Continuous
Lifetime	$>$ 5000 Cycles
MEOP	10 [Bar] (TBC)

Thruster Requirements

Heater	
Mass	< 10 [g]
Volume	50 x Ø16 [mm]
Operating Temperature	550+ [K]
Power Consumption	< 9.5 [W] Continuous
Lifetime	> 5000 Cycles

THR-SYS-101: The total thruster subsystem mass shall be less than 25 [g].

Rationale: Follows from PROP-SYST-100. Estimate given in [20] *taking into as a baseline the old $T^3\mu PS$ and added extra mass for heating element.*

THR-SYS-102: The thruster volume shall be less than 70 x Ø16 [mm].

Rationale: Follows from PROP-SYST-200 and the fact that there is an antenna board infront of the propulsion system. The thruster needs to protrude through the antenna board (about 10 [mm] thick) until the end of the satellite giving about 20 [mm] of extra volume.

THR-SYS-105: The subsystem shall be able to operate in the temperature range 4 [°C] and +80 [°C].

Rationale: Follows from PROP-SYST-710 and the fact liquid water is going to be used plus a thermal margin.

THR-SYS-106: The thruster shall be able to withstand pressure of at least 10 [Bar]

Rationale: Follows from PROP-SYST-600

THR-SYS-107: The thruster shall be able to withstand the operating temperatures of at least 550 [K]

Rationale: Follows from the analysis done in Chapter 3.

THR-SYS-108: The thruster shall be leak tight (<TBD N2/ssc) and resistant to water corrosion

Rationale: Due to the low mass flow rate any leakage will have adverse effect on the produced thrust. Furthermore since water is used as propellant the thruster needs to be water resistant.

4.1.1. Valve Requirements

THR-VLV-100: The maximum leak rate shall be 10E-5 GN_2 (TBC) [scc/s] at maximum operating pressure.

Rationale: From analysis the maximum allowable propellant lost over the designed life time of 1 year (PRO-PERF-400) should be calculated and contamination to other components in the system. Current result from [8]

THR-VLV-101: Minimum Lifetime of 5000 Cycles.

Rationale: Follows from PRO-PERF-400 and PRO-PERF-410.

THR-VLV-102: The valve shall operate at the satellite bus voltage of 12 [VDC]

Rationale: From PROP-SYST-720 and [44] *this is 12 [V].*

THR-VLV-103: The valve response time shall be faster than 2 [ms].

Rationale: Follows from the total reaction time of the system PROP-PERF-300.

THR-VLV-104: The valve shall be able to operate in the pressure range from 0 bars to 10 [Bar].

Rationale: The valve should be able to withstand all operating pressures of the system. 10 [Bar] is the highest expected MEOP with 7 [Bar] MEOP being the more likely [20] [10] [44].

THR-VLV-105: The valve shall have a normally closed configuration.

Rationale: For safety reasons, if there is no power, or there is a sudden cut-off the valve should remain closed or close if it was open to prevent loss of propellant. Furthermore since for the majority of the time the valve will be closed, this operation method is more efficient.

THR-VLV-106: The valve continuous power consumption when open (hold power) shall be less than 1 W.

Rationale: Follows from PROP-SYST-310 and the valve in the current design of $T^3\mu PS$ as given in [45]. *TBC at a later stage.*

THR-VLV-107: The valve mass shall be lower than 10 [g].

Rationale: Follows from PROP-SYST-200 and the $T^3\mu PS+$ estimate as given in [20]. *TBC at a later stage.*

THR-VLV-108: The valve volume shall be smaller than 30 x Ø16 [mm].

Rationale: Follows from PROP-SYST-600 and the valve in the current design of $T^3\mu PS$ as given in [45]. *TBC at a later stage.*

4.1.2. Nozzle Requirements

THR-NZL-100: The nozzle should be designed such that the thruster provides thrust in the 0.5 – 9.5 [mN] range

Rationale: Follows from PRO-PERF-200 and PRO-PERF-205. The throat diameter is defined from this requirement.

THR-NZL-103: The nozzle should be designed such that the thruster has a minimum specific impulse of at least 100 [s].

Rationale: Follows from PRO-PERF-100 and analysis of propellant storage space available. The expansion ratio is defined by this requirement.

THR-NZL-104: The nozzle mass should be less than 1 [g].

Rationale: Follows from PROP-SYST-200 and the $T^3\mu PS+$ estimate as given in [20]. *TBC at a later stage.*

4.1.3. Heater Requirements

THR-HTR-102: The heater shall have an operating temperature of at least 550 [K].

Rationale: Follows from analysis in Chapter 3.

THR-HTR-103: The heater continuous power consumption when active shall be less than 9.5 [W].

Rationale: Follows from PROP-SYST-310 and the power budget left after the power usage is deducted for actuating (≈ 3 [W] for less than 1 [ms] peak / 0.36 [W] average) the *valve and sensing electronics (0.07 [W]) in the current $T^3\mu PS$ design* [46]*. TBC at a later stage.*

THR-HTR-104: The heater mass shall be lower than 10 [g].

Rationale: Follows from PROP-SYST-200 and the $T^3\mu PS+$ estimate as given in [20]*. TBC at a later stage.*

THR-HTR-105: The heater volume shall be smaller than 50 x Ø16 [mm].

Rationale: Follows from PROP-SYST-600. TBC at a later stage.

4.1.4. Mechanical Interface Requirements

THR-STR-100: The structural support should be such that it will allow connection of the thruster to the propellant storage and feed system and integration into DelFFi satellite.

Rationale: Follows from PRO-SYST-400 and PRO-SYST-410. The actual interface design is TBD at a later stage.

THR-STR-101: The structural support should be such that it will withstand the launch loads.

Rationale: Follows from PRO-SYST-500s

THR-STR-103: The tubing from the valve to the thruster will be kept as short as possible and have a diameter of TBD [mm] as to provide the required mass flow to the thruster.

Rationale: Short tubing result in lower pressure drop. Furthermore shorter tubing will result in less residual propellant stuck after the valve is closed.

4.2. PCB and Electrical Interface Requirements

In this section the PCB requirements are given and their rationale. These requirements are made in the early stage of the project development thus may be incomplete and subject to change. The PCB dimensions and profile is given in Figure 22, the important being the total dimensions and the size and positions of the cut outs and mounting holes.

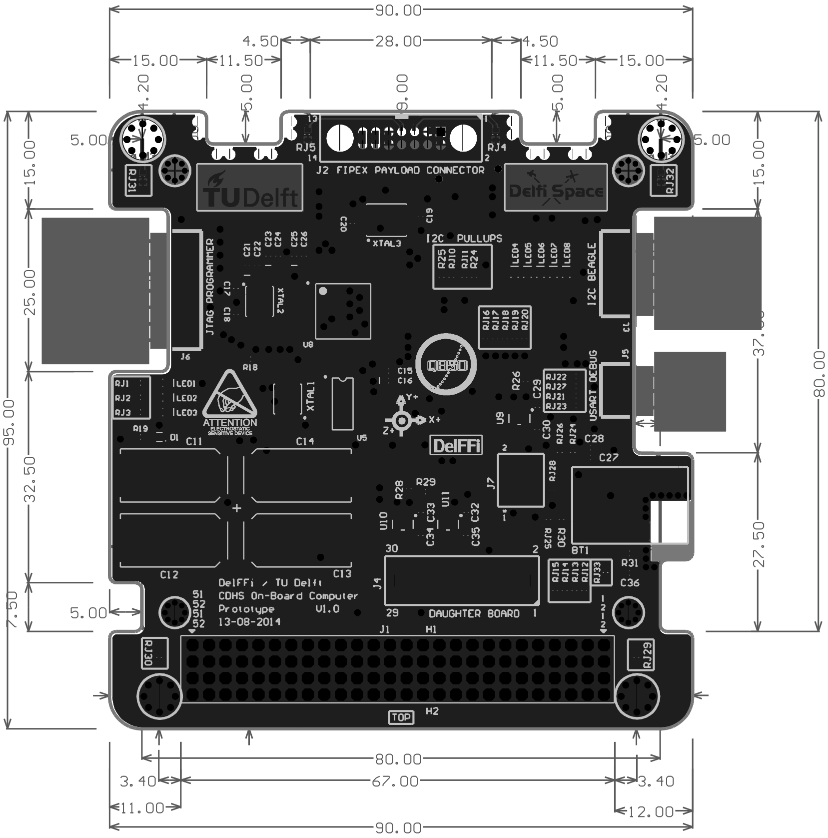

Figure 22: OBC PCB profile

THR-PCB-100: The PCB shall have dimensions of 90 x 90 and will closely follow the layout of the OBC PCB given in Figure 22.

Rationale: Needs to fit in the satellite

THR-PCB-101: The PCB shall have PC104 connector

Rationale: Standard connector used for interfacing in the satellite

THR-PCB-102: The EEE components on the PCB shall have operating temperature range of 4°C to +80°C and non-operating temperature range of -20°C to +80°C

Rationale: The electronic circuitry shall have the same operation and non-operating temperature range as the rest of the propulsion system

THR-PCB-103: The EEE components and the PCB shall have mass lower than 50 [g]

Rationale: This is approximately 10% of the total mass budget

THR-PCB-104: The PCB will be able to convert to 12 [Vdc] locally and the circuit shall be able to provide up to 10 [W] for 600 [s] and 20 [W] for up to 2 [ms]

Rationale: Heater (TBC) and valve work at 12 [V] and the maximum power consumption is 10 [W] for about 600 [s]

THR-PCB-105: The PCB will be able to convert to 1.6 [Vdc] locally and the circuit shall be able to provide up to 20 [W] for up to 2 [ms].

Rationale: The valve spike voltage is 1.6 [Vdc] and the spike duration is up to 2 [ms]. From [47] *a 20[W] power supply is recommended.*

THR-PCB-106: The PCB shall have a Spike and Hold that functions as given in Chapter 7 and [47]

Rationale: Necessary for normal operation of the valve.

THR-PCB-107: The PCB shall have a logic circuit capable of controlling the spike and hold circuit and provide pulsing signals of up to 1000 [Hz] if necessary.

Rationale: TTL signal needed to control the spike and hold circuit and pulsing may be necessary for limiting the mass flow to the chamber. 1000 [Hz] is the maximum pulse rate.

THR-PCB-108: The PCB shall have a control circuit for the heater capable of turning it on and off and pulsing the on / off signal up to 1000 [Hz] if necessary.

Rationale: Control is necessary for turning the heater on and off and pulsing may be necessary for maintain a certain goal temperature.

THR-PCB-109: The PCB shall provide power and sensing leads for a pressure and a temperature sensor in the tank.

Rationale: Necessary for normal operation of the sensors.

THR-PCB-1010: The PCB shall provide a Thermocouple conditioning unit and connection for the integrated TC in the heater.

Rationale: The COTS thruster will have a TC integrated in the heater to monitor the temperature. A TC conditioning unit is necessary for correct read-out of the TC.

THR-PCB-111: The PCB shall be able to provide feedback of the voltage level of the DC/DC convertors, heater and the sensing line of the tank pressure and temperature sensor and the current going through the heater.

Rationale: Necessary for monitoring purposes during EM Testing. This may be omitted for the FM model (TBC)

THR-PCB-112: The PCB shall be able to log and store the values of the voltages and current being monitored either locally or remotely to a different subsystem.

Rationale: Used to simulate FM conditions where data is first stored locally and then transmitted to the Ground Station during a pass.

THR-PCB-113: The PCB shall be able to control all the different components, store and communicate with them either with a local control unit or remotely through the OBC.

Rationale: The PCB needs to be able to be controlled remotely, like when sending a command from the Ground Station, and to be able to communicate with the rest of the satellite.

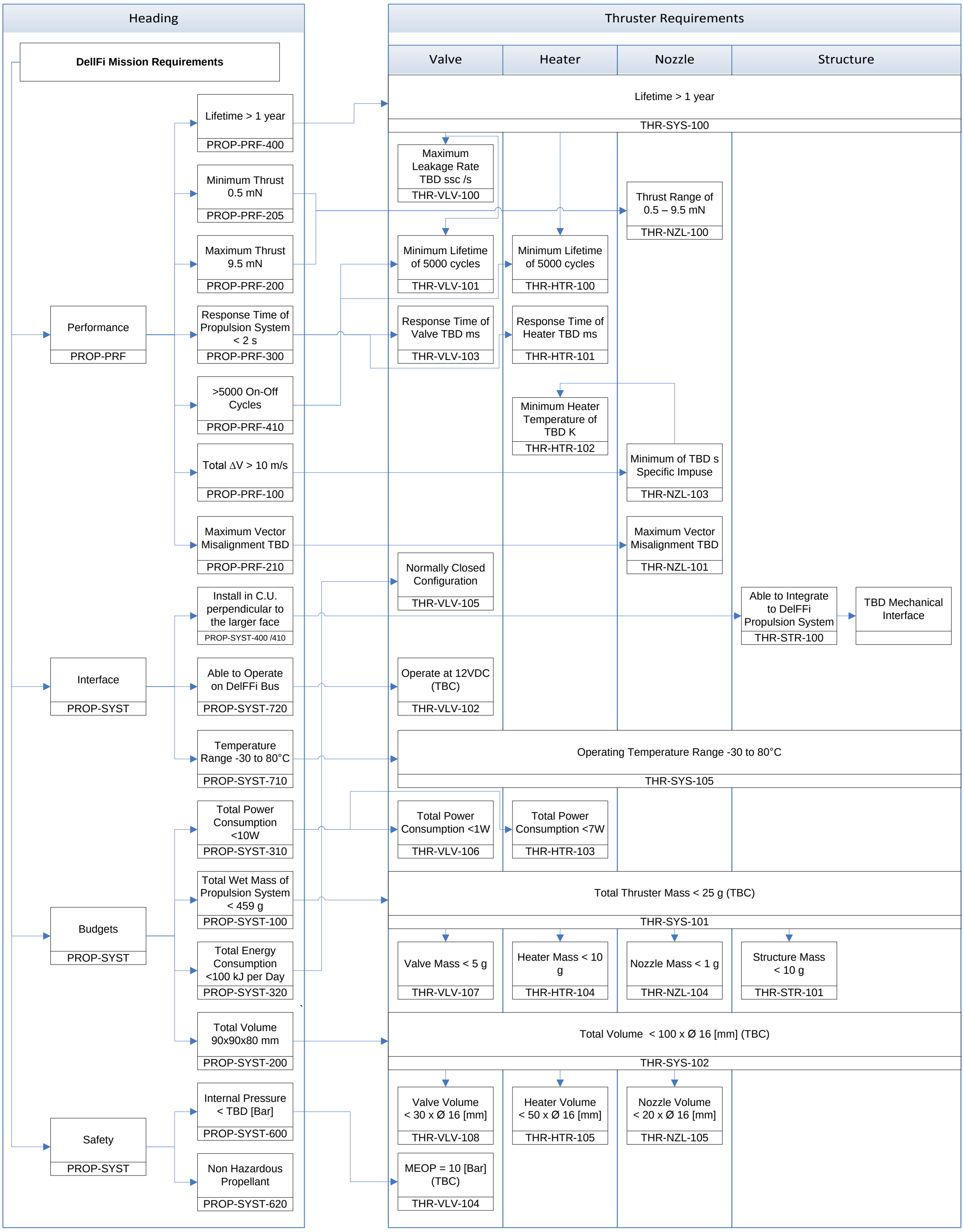

Figure 23: Thruster Requirements Flow Down Chart

4.3. Interface Requirements for Testing

Prior to integrating the thruster in the DelFFi satellites it should be testable at one of the TU Delft's thruster test benches. Currently there are 2 test benches available. Depending on the test bench used, an interface between the thruster and the test bench needs to be made. The requirements imposed by the two test benches are given in the subsequent sections.

4.3.1. Thruster Test Bench AE-TB-5M

The AE-TB-5M that is currently in development imposes the following requirements on the thruster. The rationales behind these requirements are given in [38].

Thrust

PROP-TEST-100: The maximum thrust measureable by the AE-TB-5M test bench in the current set-up is 5 [mN]. With modifications 10 [mN] is possible

PROP-TEST-105: The minimum thrust measureable by the AE-TB-5M test bench in the current set-up is 1 [μN].

Mass

PROP-TEST-200: The maximum mass of the thruster including the mounting bracket is 300 [g].

Volume

PROP-TEST-300: The maximum height of the thruster including the mounting bracket is 40 [mm] and the maximum width is 110 [mm].

Installation

PROP-TEST-400: The thruster shall have a TBD interface such that it can be installed on the AE-TB-5M test bench.

PROP-TEST-405: The mounting bracket shall have TBD dimensions.

4.3.2. Thruster Test Bench AE-TB-50M

The second test bench that is currently in the inventory of the Delft University of Technology Space Engineering department is the AE-TB-50M. It imposes the following requirements on the thruster. Their rationales can be found in [39]

Thrust

PROP-TEST-100: The maximum thrust measureable by the AE-TB-50M test bench is 50 [mN].

PROP-TEST-105: The minimum thrust measureable by the AE-TB-50M test bench is 2 [mN].

Mass

PROP-TEST-200: The maximum mass of the thruster including the mounting bracket is 360 [g].

Volume

PROP-TEST-300: The maximum height of the thruster is TBD [mm] and width is TBD [mm].

Installation

PROP-TEST-400: The thruster shall have a TBD interface such that it can be installed on the AE-TB-50M test bench.

PROP-TEST-405: The mounting bracket shall have TBD dimensions.

5. Thruster Design and Component Selection

In this chapter the thruster is designed and components are selected. As given in Figure 2, the thruster can be separated in 4 components:

- Valve with interface to the feed system
- Heating chamber containing:
    - Heater
    - Porous Media
- Nozzle
- Supporting Electronics and PCB

Since nitrogen is no longer used as propellant the valve cannot be incorporated in the tank as in [20] but will have to be outside of it or incorporated in the thruster module. Two thruster designs are being produced in parallel. The first concept is using an advanced MEMS manufacturing technique, while the second concept concentrates on using traditional manufacturing techniques and components wherever possible. The two thrusters need to be interchangeable with their last common link being the valve. The second thruster is covered in this thesis report.

5.1. Valve Selection

A large number of valves have been investigated during the course of the literature study and the thesis project. The driving requirements for the valve, as given in Chapter 4, are the pressure rating, power consumption, operating temperature and size. After careful consideration the best candidate was chosen to be a valve produced by the Lee Company and coming from their IEP specialty valve series. The Lee Company produces a wide array of miniature solenoid valves and their distributor in the Benelux is Denis de Ploeg BV.

5.1.1. Flight Model Valve

The IEP Series solenoid valves have maximum operating pressure of up to 55 [Bar] and maximum operating temperature of up to 135 [°C] while having mass of less than 6 [g]. This makes them really good candidates for the flight model where wider operating temperature ranges and pressures may be necessary. The valve is shown in Figure 24 and the characteristics are given summarized in Table 15 [48]. This valve is rated to work with gasses as well as fluids and different sealant materials are possible.

Table 15: IEP Valves

MEOP	55 [Bar]
Operating Temperature	Up to 135 [°C]
Operating Voltage	12 [Vdc]
Sealing Materials	EPDM, FKM
Cost	€840 excluding Tax and Shipping
Lead Time	2 - 10 weeks

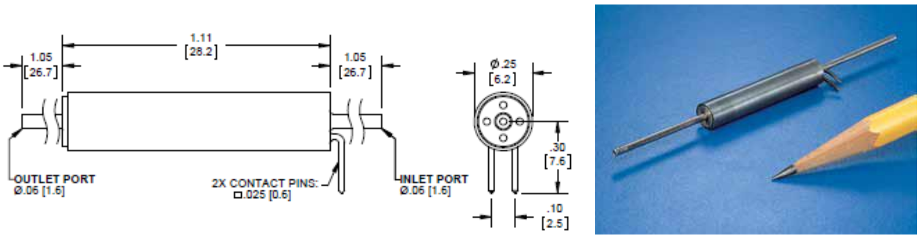

Figure 24: IEP Valve Series (mm in brackets)

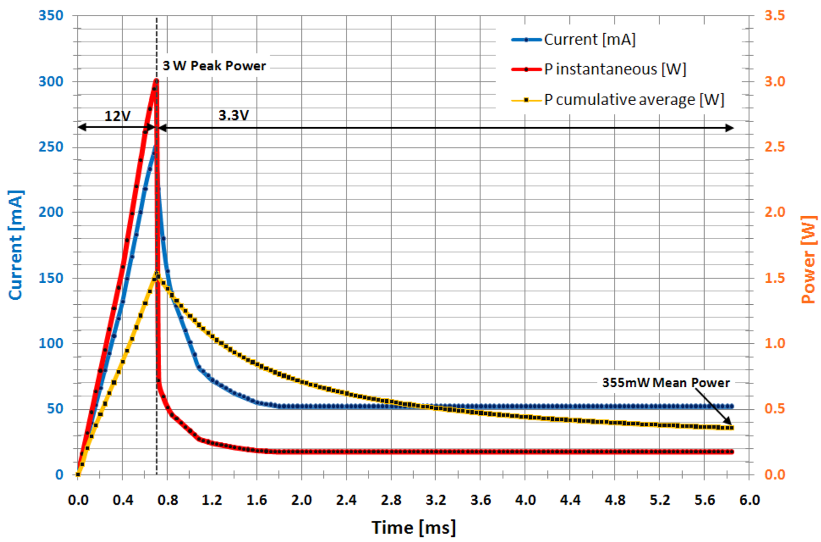

Figure 25: EPSV Valve power consumption [49]

A similar valve has also been used in the T3µPS propulsion system on-board Delfi – n3Xt called EPSV Valve. During testing it had a peak power consumption of 3 [W] and cumulative average power consumption of 0.35 [W] (Figure 25). Seeing as the valve is similar in size and specifications it is safe to assume that the power consumption will be similar. This however needs to be confirmed during the flight model testing. This valve is however expensive and comes with stainless steel pipe that needs to be welded to the rest of the propulsion system. Furthermore due to lack of experience in operating and testing this kind of valves a cheaper alternative is deemed necessary for the engineering model and initial testing.

5.1.2. Engineering Model Valve

More affordable equivalents of the IEP valves described in Section 5.1.1 are the VHS valves. The VHS solenoid valve series are used in both medicine and high-tech industry, they have normally closed configuration and have fast opening times (as fast as 0.25 [ms]), MEOP of up to 120 [PSIG] (circa 7 [Bars] in vacuum) and 250 million cycles as life-time minimum [48]. They are currently one of the smallest on the market, weighting 1.8 [g] and having an internal volume of 35 [µL]. Furthermore they have different inlet and outlet configurations and different orifices can be installed on the valve if necessary.

To guarantee proper functioning of the valves proper filtration is required. System filtration of 12 microns or less is recommended. In addition, last chance PEEK filters are available that can be threaded directly into valves with MINSTAC inlet ports. These are however last chance screens and are not intended to replace system filters. Failing to provide proper filtration can result in damaged valve and leakage due to contamination of the sealing surface.

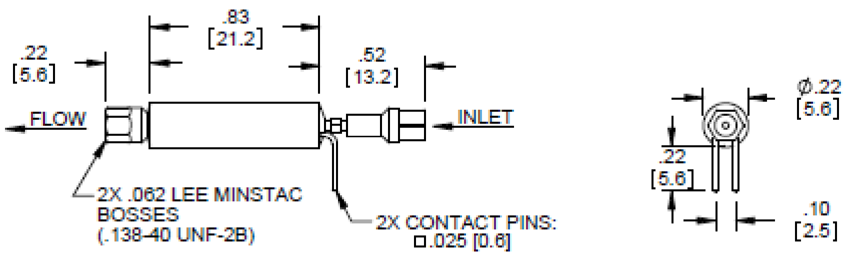

Figure 26: INKX0511400AA5 VHS Solenoid Lee Valve (mm in brackets)

The configuration of interest for the EM, features MINSTAC inlet and outlet and is shown in Figure 26 and the characteristics are given in [48]. The reason why a valve with 2 MINSTAC ports was chosen is that it gives the best flexibility in connecting and positioning the valve. The specifications are also summarized in Table 16 and as it can be seen, different sealing materials are available.

Table 16: VHS Valves

MEOP	120 [PSIG] / 8.3[Bar] in ambient / 7.3 [Bar] in vacuum

Operating Temperature	4 – 49 [°C]
Operating Voltage	12 / 24 [Vdc]
Sealing Materials	EPDM, FKM
Cost	€250 – 270 excluding Tax and Shipping
Lead Time	2 weeks

Ethylene Propylene Diene Monomer (EPDM) is a synthetic rubber that has widespread application on sealing. It has excellent resistance to heat, water, steam, ozone and UV light while still retaining very good low temperature flexibility. Furthermore it has excellent thermal aging and good wear resistance but is not suitable for use mineral oil products. [50] EPDM has minimum service temperature of -50 [°C].

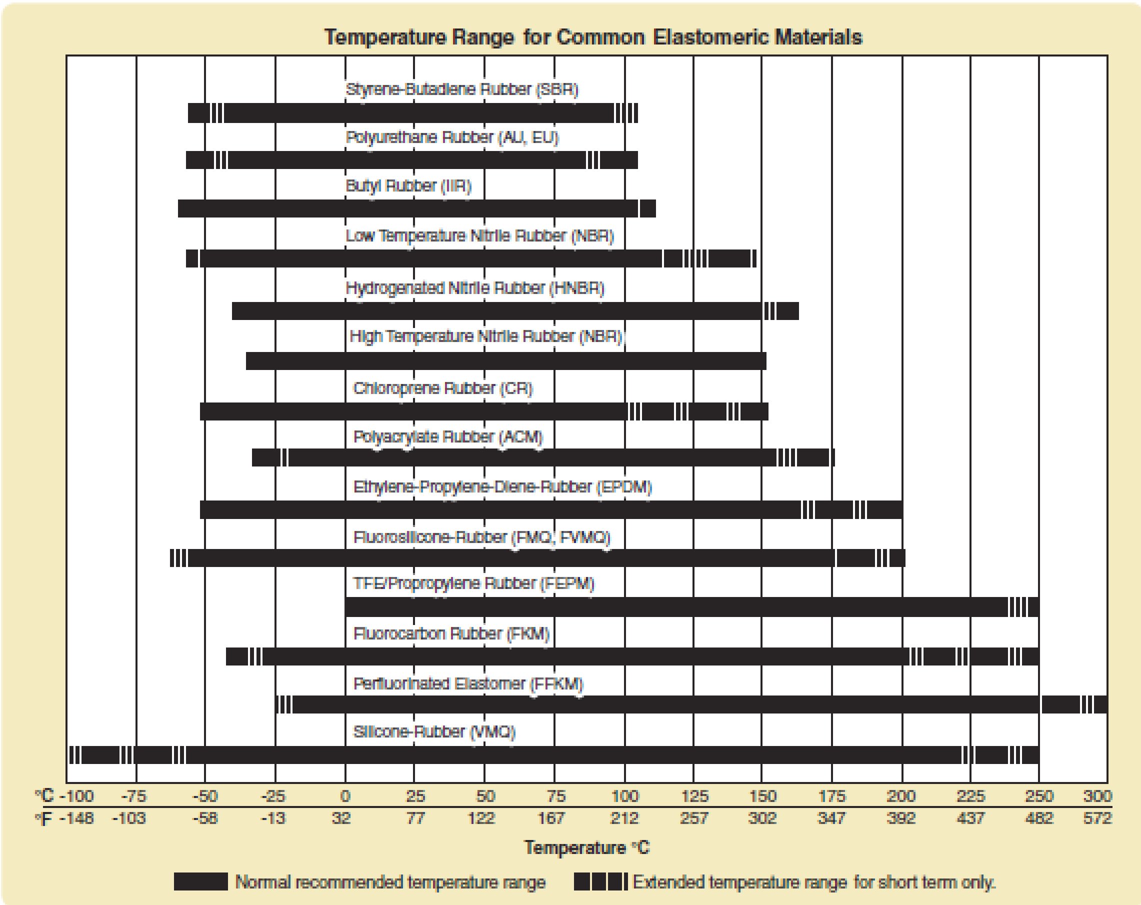

Figure 27: Temperature range for Common Elastomeric Materials [51]

Fluorocarbon (FKM) elastomers are highly fluorinated, carbon backboned polymers used in applications to resist harsh chemical and ozone attack. It has excellent resistance to high temperatures, ozone, oxygen, mineral oil, synthetic hydraulic fluids, fuels, aromatics and many organic solvents and chemicals. Low temperature resistance is normally not favorable and for static applications is limited to approximately -26 [°C] [51]. The applicable temperature ranges of both seals are shown in Figure 27. Since EPDM has lower operating temperature range and it is better suited for water and steam, while FKM is better for oil and hydraulic fluids, EPDM was chosen as the better sealing material for the valve used in water resistojet.

The model numbers of the valves of interest are INKX0511400AA5 and INKX0514300AA4 with the only difference being the operating voltage level of 12 and 24 [Vdc] respectively. Both these valves feature MINSTAC ports on both ends, EPDM sealing, operating temperature range is 4 – 49 [°C].

5.1.3. Valve Control Circuit

Both the IEP and VHS valves require a spike and hold circuit for proper operation. The valve initially requires a 12 or 24 [Vdc] (model dependent spike voltage) pulse for a minimum of 0.3 [ms] to actuate the valve, and then the voltage through the coil needs to be reduced to 1.6 or 3.2 [Vdc] (model dependent hold voltage) to keep the valve open. If the voltage is not reduced to the model dependent hold voltage level, the coil will overheat and the valve will be destroyed.

An example spike and hold driver schematic is shown in Figure 28. The control signal input is 5V TTL control signal, V1 is the valve spike voltage and V2 is the valve hold voltage. Vcc is the input supply voltage for the NE555V which is between 5 and 15 [Vdc] [52]. The spike duration is calculated using equation 5.1. For example with a capacitor of 0.047 [µF] and a 100 [kΩ] variable resistor, the spike duration would be between 0.5 – 5 [ms].

$$t_{pulse} = 1.1 \times R_1 \times C_1 \tag{4.1}$$

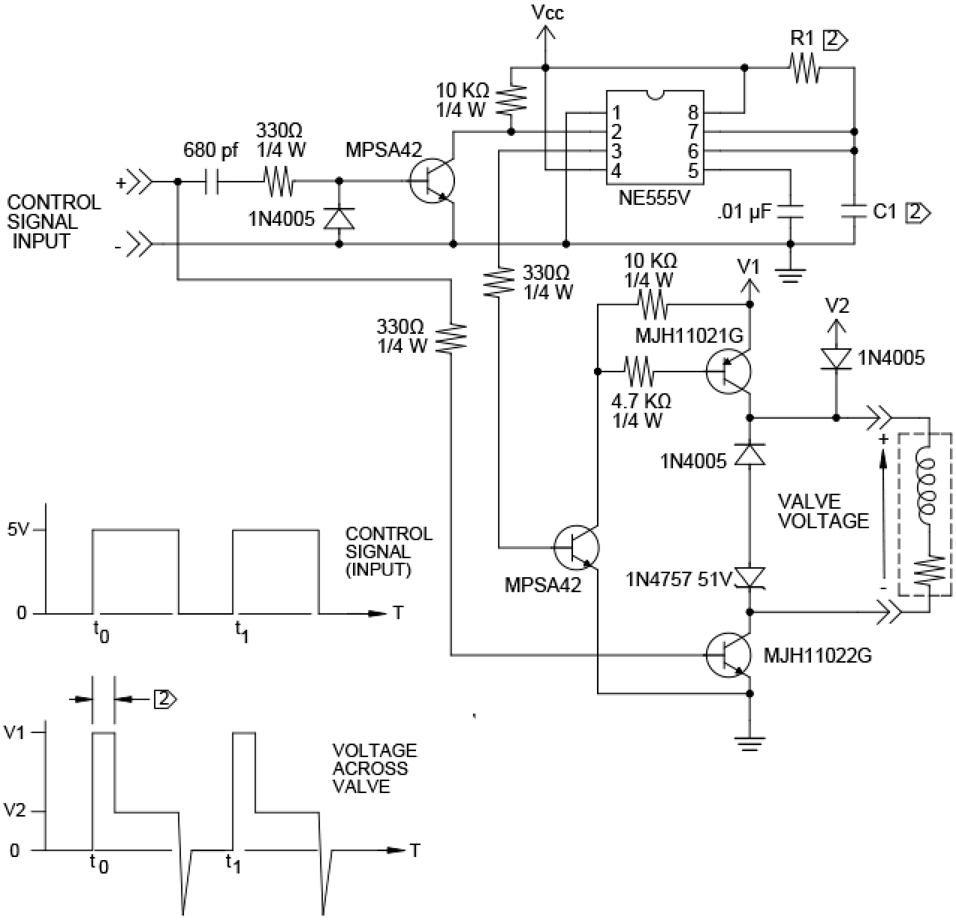

Figure 28: Spike and Hold Driver Schematic

5.2. Porous Media Selection

Common occurrence in water resistojets is spitting of the thruster, namely not vaporized water droplets entering in the nozzle. This was observed in both TU Delft's own DUR [53] thrusters, which resulted in an 80 [%] lower thrust than the theoretical calculations, and also in other thruster designs [54]. This has been attributed to the so called "boiling crisis".

During the boiling of a fluid flowing through a channel, several heat-transfer regimes are encountered. A typical case is illustrated in Figure 29. The liquid water enters the channel and is heated in the liquid phase to the point where bubble nucleation first occurs. Nucleate boiling continues until enough vapor is generated such that the resulting increase in velocity is sufficient to suppress nucleation. Beyond this point, heat is added to a thin liquid film and vaporization occurs at the liquid vapor interface. Throughout these boiling regimes, liquid is being entrained in the vapor core. In spite of any re-deposition of liquid from the core to the film, at some point there is no longer sufficient liquid to wet the wall and the liquid film breaks down. This results in a large reduction in heat transfer coefficient, often more than an order of magnitude. This transition has been termed "boiling crisis". This film breakdown is generally followed by a transitional regime wherein a considerable amount of liquid remains on the wall. Eventually, only a few droplets remain on the wall, and most of the heat added through the wall goes into heating the vapor. It then becomes difficult to vaporize the remaining droplets and when they reach the nozzle, spitting occurs. [54]

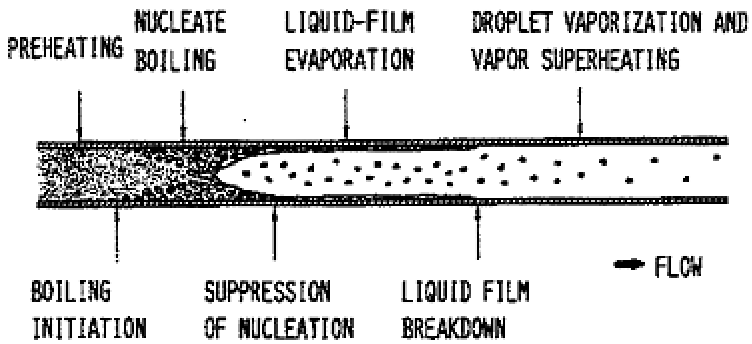

Figure 29: Heat - Transfer phases in channel flow [54]

Prediction of this pattern is complicated due to the wide variety of possible two-phase flow regimes and by the various thermodynamic inequilibria. Therefore it has become apparent that for a coupled system, that needs to both evaporate the water and heat it to high temperature, a turbulent flow is needed so that the liquid is forced to mix with gas, increasing the “stay time” in the heating chamber and increasing the heating efficiency.

In the past numerous methods have been investigated and the most promising options for small satellites are given in Figure 30. Since using heated tubes has been unsuccessful in previous designs (eg. DAR) and option 3 (Figure 30 flow swirling induced by geometry) has shown to work well in engineering models but has had problems in microgravity conditions [53] [54]. Therefore porous media (packed beds) has been chosen to be used for the flight model. However instead of packed beds, metal foam will be used expecting that better heating uniformity will be achieved and no hotspots will be present. Furthermore the metal foam has good thermal properties and it’s resistant to thermal cycling [55]. Since pressure drop and flow instabilities in porous media are rather complicated to calculate accurately even with CFD, the characteristics will be determined experimentally.

System	Advantages	Disadvantages
Tube with helical inserts 	Simple	Low efficiency Pressure drop - UoSAT 12 has low pressure system: ☹
Heated Tube 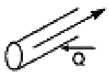	Simple	Very low efficiency - needs high power (kW) or very high volume: ☹
Flow swirling Induced by Geometry 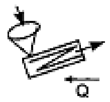	Engineering model systems have been successful	Complex. Have had flow problems under microgravity conditions: ☹
Packed Beds 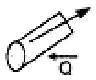	high performance, low complexity, flexibility	hot spots, material problems, thermal cycling, flow instabilities: ☺

Figure 30: Mixing Design Methods [54]

The porous media selected for the thruster is open type metal foam produced by Recemat BV, with a high porosity (up to 95 [%]) and a small pore size, but a rather brittle nature [55]. The Nickel foam (Ni) has excellent properties for battery and electrolysis applications, due to its good electrical and thermal conductivity. Other stronger alloys such as Nickel-Chromium (NC), Nickel-Chromium with extra chromium (NCX) and Nickel-Chromium-Aluminum (NCAX) are also options, with a better corrosion resistance and oxidation resistance but a higher cost. For all these reasons, the foam presently selected for the thruster is made of the Nickel alloy NI-4753. The cost is about €400 per [kg] for the basic Ni foam however with a maximum average density of about 0.6 [g/cm3] the price of the material required for the chamber is expected to be less than €50. Foam with different pore sizes is available and if time allows the difference between different types of foam should be investigated. Recemat provided two different samples for testing for free. Their characteristics are given in Table 17 and one sheet is pictured in Figure 31.

Table 17: Metal Foam Characteristics

Parameter	Ni-2733	Ni-4753
Grade = number of pores/inch	27 . . . 33	47 . . . 53
Estimated average pore (Ø mm)	0.6	0.4
Density average (g/cm3)	0.3 ... 0.6	0.3 ... 0.6
Relative density (foam / solid Ni)	4.8 %	4.8 %
Porosity (100% - rel. density)	95.20%	95.20%
Specific Surface (m2/m3)	2800	5400
Specific Surface Area Density (Kg / m2)	0.152	0.079
Sheet length (mm)	900	900
Sheet width (mm)	600/500	600/500

Figure 31: Recemat Metal Foam

5.3. Heating Element Selection

At TU Delft there have been a number of resistojet designs investigated and produced in the past. The first resistojet design was made by Robert Hoole in 1990 which used a spirally wound tube, made out of stainless steel as a heater [56]. In more recent history Rodrigo Ferreira designed a water resistojet named the DUR − 1 thruster [53]. Another concept is MEMS Heater as done by M. Tittu in [26].

While designing your own heater can provide better results and higher heating efficiency, using COTS heater would reduce the complexity of the design and the workload and would reduce the uncertainty in the design. There are lots of different COTS heaters available but they are mainly 2 types that are of interest for the resistojet, namely coil heaters and cartridge heaters. These can either directly heat up the propellant or indirectly heat up a porous which in turn will heat the propellant.

After a vast amount of heaters investigated [13] and during the course of this thesis, only 3 where identified that are within power, size and budget constraints as given in Chapter 4 and [10] and that have distributors in The Netherlands enabling direct contact and support and faster lead time. For convenience the requirements are given in Table 18.

Table 18: Heater Requirements

Mass	$<$ 10 [g]
Volume	50 x Ø16 [mm]
Operating Temperature	550+ [K]
Power Consumption	$<$ 9.5 [W] Continuous
Lifetime	$>$ 5000 Cycles

5.3.1. Elstein T-MSH/20 [57]

The Elstein T-MSH/20 is a ceramic infrared heater with integrated thermocouple. It is rated up to 860 [°C] operating temperature and surface ratings up to 100 [kW/ m²]. MSH micro system heaters are used in applications, which require partial heating or drying of small goods and areas. It has power rating of 55 [W] at 12 [Vdc] which would translate to 9.5 [W] at 5 [Vdc] (Equation (4.2)) which is what makes this heater particularly attractive. Namely this would allow the heater to work below the rated maximum power consumption of 10 [W] connected directly to the EPS 5 [Vdc] line without the need of a local DC-DC up conversion circuit on the propulsion system PCB. Although ceramics are not commonly susceptible to corrosion, the manufacturer has issued a concern that this might happen if the T-MSH/20 is immersed in water for extended period of time. Furthermore since it's ceramic and not metal there are concerns w.r.t. to the mounting, namely will the ceramic heater and leads be able to connect in a leak-proof manner. The Elstein MSH/20 (same dimensions but without thermocouple and 2 instead of 4 leads) is shown in Figure 32. The price of the Elstein T-MSH/20 is €45 per piece excluding tax and shipping and it has a lead time of 1 week. The distributor in the Netherlands is Wilmod Heating & Systems. The invoice and price quotation is given in Appendix C.

$$P_{actual} = P_{rated} \times \frac{V_{actual}^2}{V_{rated}^2} \tag{4.2}$$

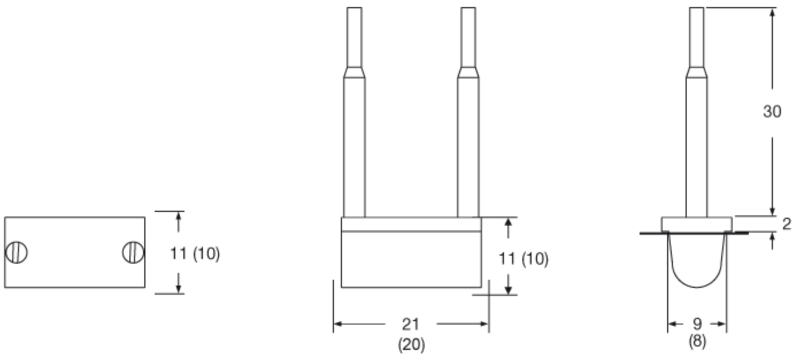

Figure 32: Elstein MSH/20 (dimensions in mm)

5.3.2. HotSet HotRod [58]

HotSet is a water repellent cartridge heater manufacturer from Germany and their distributor in the Netherlands is also Wilmod Heating & Systems. Wilmod has offered a modification of their standard 5210404 heater (Figure 33). The modified version has a diameter of 6.5 [mm] and length of 40 [mm]. At 12 [Vdc] is rated at 7 [W] and has a build in "J" type thermocouple. Furthermore it is offered with a 25 [mm] connection tube + extra 890 [mm] stainless steel protection hose. The minimum order size however is 4 heaters and the price is €170 per piece for a lot of 4 and €129 per piece for a lot of 5 with a lead time of 5 weeks.

Figure 33: HotRod HotSet Cartridge Heater

5.3.3. Watlow Firerod [59]

Watlow is a US electrical heater company with Kurval BV being its local distributor. In their portfolio of heaters they have a water immersion heater with a power rating of 30 [W] at 24 [Vdc] resulting in a power rating of 7.5 [W] at 12 [Vdc] with a model number C1A-

9602. It has a diameter of 1/8 [Inch] and a length of 1 [Inch] without a thermocouple. There is also a thermocouple variant, bearing the part number C1J-9769, which has an integrated K type thermocouple at the tip of the heater and it's 1.5 [Inch] long. The standard heater C1A-9602 has a lead time of 2 weeks and a price of € 36.70, while C1J-9769 is priced at €73.55 and has a lead time of 5 – 6 weeks. The minimum order size for both is 3 units. The heater is shown in Figure 34 and the price quotation and invoice can be found in Appendix C.

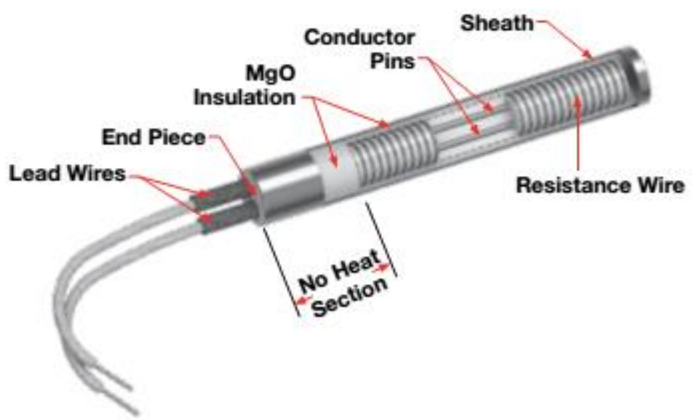

Figure 34: Watlow C1A-9602 Cartridge Heater

5.3.4. Heater Trade – Off

With the different heaters available, a trade-off needs to be made. The trade-off will be made on several criteria, namely cost, lead time, power level, compatibility with water, easy for mounting and the ability to monitor the temperature of the heater. The most important criteria are the power level to be as close as possible to 9.5 [W] and preferably at 3.3 [Vdc] or 5 [Vdc], to be able to be mounted with relative ease in a leak-proof manner and to have thermal monitoring. Furthermore important criteria are cost, since DelFFi has limited budget and compatibility with liquid water. Finally the lead time is the least important criteria that still needs to be taken into account. The trade-off is given in Table 19. In the end it was decided that 2 heaters will be ordered, namely the Elstein T-MSH/20 and the Watlow C1J-9769. The C1J-9769 seems to be the best heater overall, however if the mounting issue can be solved for the T-MSH/20 it has the best technical characteristics. The HotRod was deemed to be too expensive and the Watlow C1A-9602 although the cheapest, it is lacking the ability to have the thermal monitoring.

Table 19: Heater Trade-Off

Criteria	Weight	T-MSH/20	HotRod	C1A-9602	C1J-9769
Cost	3	5	1	5	3
Lead Time	1	5	1	3	1
Power Level	5	5	3	4	4
Water Compatibility	3	3	3	5	5
Mounting	5	1	5	5	5
Thermal Monitoring	5	5	3	0	5
Score		84	68	78	95

5.4. Chamber

The Chamber is used to house the heater and the porous media. It should also have low emissivity coefficients such that the heat is contained inside of it and not radiated in the satellite. Furthermore choosing a material and design that minimizes thermal capacitance will allow the chamber to be quickly heated and cooled and not have power wasted by heating up the whole structure. Finally even though it is out of the scope of this thesis it is important to mention that a crucial parameter to increase the heating efficiency of the design is to keep the thermal conduction between the tank and the thruster as low as possible, otherwise energy and heat is wasted in heating up the whole tank instead of only the propellant in the chamber. For both time and cost efficiency the chamber is to be produced within Delft University of Technology using either the Aerospace Faculty workshop or the central university workshop DEMO. The workshop costs € 400 per day excluding material costs.

As it was shown in Section 5.3, 2 heaters are to be considered for the flight model. For maximum heating efficiency, the chamber should be designed to encapsulate the heater, thus different chamber designs will be needed for the 2 heaters. This however was immediately rejected by the project management for the engineering model due to cost concerns and it was decided to have one design that will incorporate both heaters.

Having to house both heaters would mean that no matter the design, the chamber will be largely oversized. This can potentially result in the chamber not reaching steady state operations until it fills up and furthermore with the excessively large volume and low mass-flow involved the valve opening time will definitely not correspond to the thruster operation time.

Therefore designs where only considered w.r.t. to the mechanical properties. Aluminum was chosen as the material and the chamber should be designed such that it can withstand a pressure difference of 10 [Bar] with a safety factor of 2. Different designs where considered. Once a heater has been chosen, a specific chamber design will be made to that heater for the flight model thruster

5.4.1.1. *Chamber Design 1*

The first chamber design goal is to minimize the volume and mass and provide compact packaging of both heaters. It would have a sliding contact between the two halves and the sliding contact is made such that upon pressurization one half is pushed again the other providing better leak proof contact. To keep the design as compact as possible, soldering or welding of the two halves is recommended. This means that re-assembly is not possible and an inspection post testing will render the chamber useless. The chamber is shown in Figure 35. A plastic 3-D printed version of the chamber was made to check if there would be sufficient clearance for both the heaters and the valve and nozzle connection (Figure 36) which proved that the design was good and there was sufficient clearance for all the components. However upon inspection by the DEMO workshop this design was told to be rather expensive for production with traditional manufacturing techniques and additive manufacturing such as SLS 3D printing was recommended.

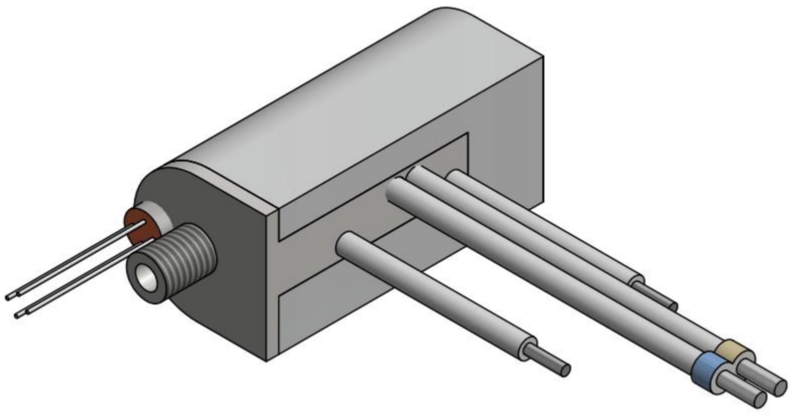

Figure 35: Design Chamber 1

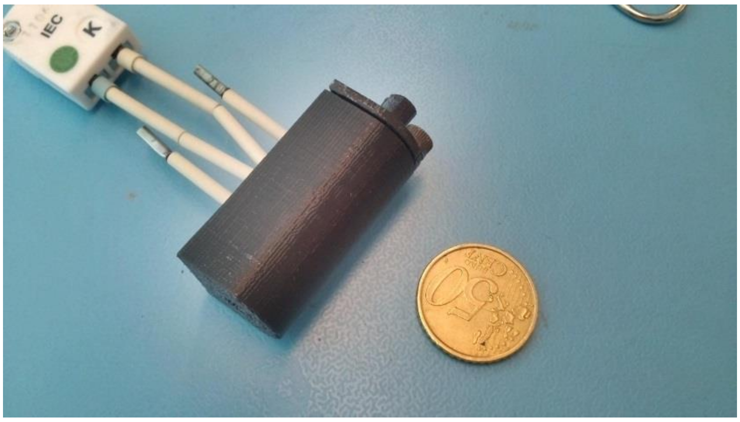

Figure 36: 3D Printed Design

5.4.1.2. *Chamber Design 2*

The second chamber design was made to be easily producible at the DEMO workshop and have easy assembly. It has a simple rectangular shape and a screw-able side. It also features a port for a pressure sensor on the side. Due to the rectangular shape and the thin wall thickness of only 2 [mm] there was a concern if there was enough threaded area for the screws to hold the chamber together and the amount of screws needed to ensure the chamber doesn't fail at 10 [Bar]. Therefore a FEM analysis of the design was made. The load case was 10 [Bar] internal pressure and caution was made that throughout the chamber and the thread included the stress on the material was half of the Aluminum 6061 – T6 yield stress or about 140 [MPa]. A cut out of the FEM analysis is shown in Figure 37 and the results have shown that at least 10 screws are necessary to satisfy this criterion.

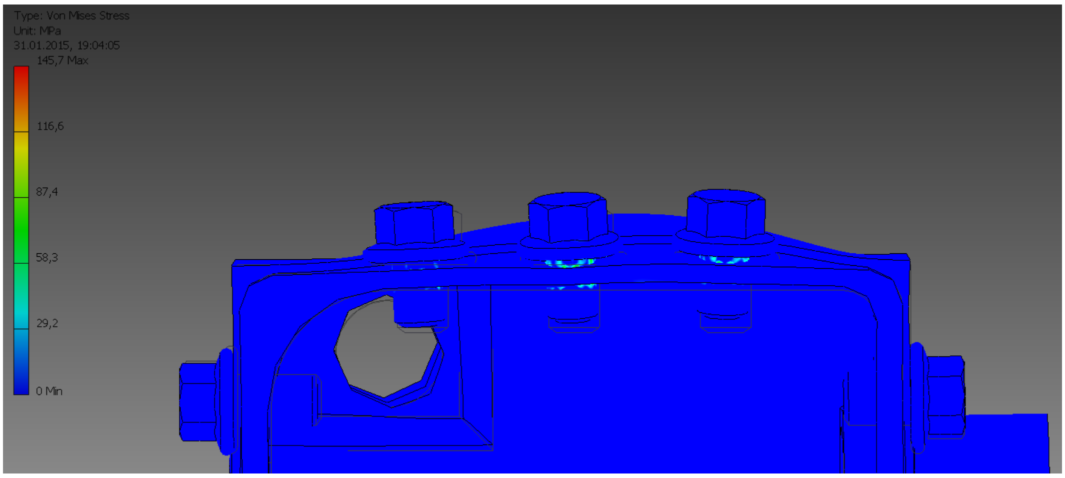

Figure 37: FEM Chamber 2

A concern is how leak proof the connection would be by using just screws. The DEMO workshop is confident that O-Ring would not be necessary for small pressures. The design is shown in Figure 38. Furthermore this is the bulkiest design and would be least efficient when heating.

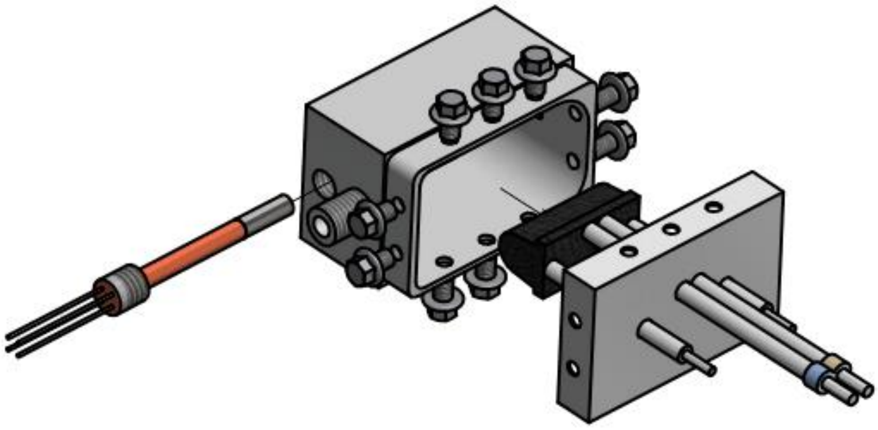

Figure 38: Chamber Design 2

5.4.1.3. *Chamber 3*

The third chamber design is a combination of both the first and the second design. The goal of the design is to minimize volume and mass while maintaining the rectangular design and also to be able to reassemble change the cap if necessary (for example if no leak tight connection can be made with the Elstein heater). The design is shown in. Upon inspection by the DEMO workshop they said however they are not able to produce this design

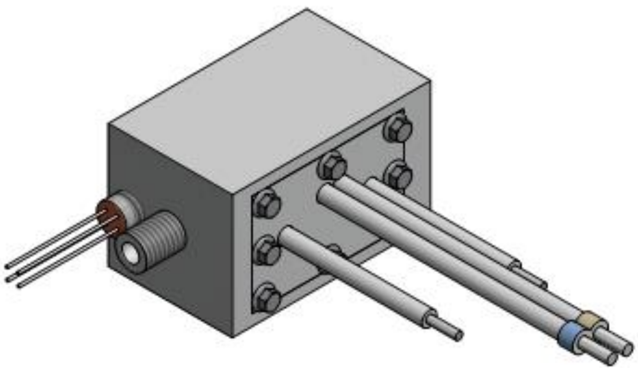

Figure 39: Chamber Design 3

5.4.2. Trade – Off

The trade-off and its criteria are given in Table 20. Since this is an engineering model the cost is the most important criteria. Having the design producible at the DEMO workshop at TU Delft is advantageous due to the short lead time and direct contact. The internal volume while not crucial is advisable to be as small as possible otherwise when filling the chamber with cold water and boiling it with the heater, the pressure from the steam (as in an electric kettle) may rise above the 10 [Bar] MEOP and the chamber may fail structurally. Finally the mass will affect the thermal efficiency only but since there is ample power available in the lab this can be compensated by delivering more than the 10 [W] required during testing. As it can be seen, design 2 is the best design and there-fore it was produced by the DEMO workshop.

Table 20: Chamber Design Trade - Off

Criteria	Weight	Design 1	Design 2	Design 3
Producibility	3	3	5	1
Cost	5	1	5	1
Mass	1	5	1	3
Internal Volume	3	5	1	3
Score		34	44	20

5.5. Nozzle

At the µm scale used in the present micro-propulsion concept, two nozzle shapes are practically possible: axi–symmetrical conical nozzle and a slit nozzle.

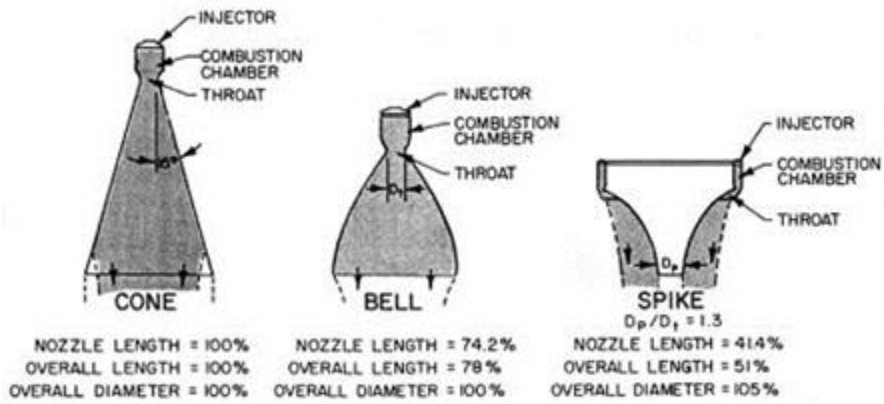

Figure 40: Nozzle Shapes [60]

The conical nozzle is considered the simplest axi – symmetrical nozzle type (Figure 40). It has conical convergent and divergent parts which are characterized by the cone half-angles θ and α respectively (Figure 41). At the scale of DelFFi thruster it would still be difficult to produce and would require advanced micromachining techniques and micro turning machines, however it is by far the simplest traditional nozzle type to produce. A disadvantage is that the flow momentum losses are higher due to flow divergence so generally they have lower efficiency. And while at this scale it is not crucial, conical nozzles tend to be longer and heavier than bell or plug type nozzles [25].

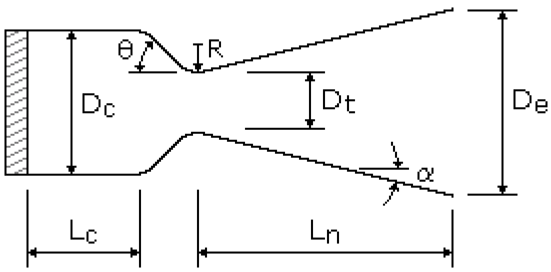

Figure 41: Conical Nozzle Geometry Parameters

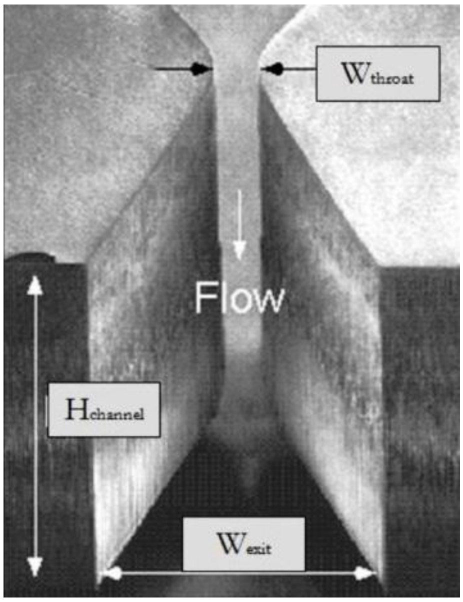

Figure 42: MEMS Nozzle Cross – Section [61]

Another extremely popular nozzle type in micro – propulsion is the slit nozzle. It can be produced using micro – milling or using MEMS technology which can produce miniaturized mechanical and electro-mechanical elements or even fully functional systems and devices such as valves. Since the basic principle of MEMS production is etching in silicone substrate traditional axisymmetric shapes cannot be produced, but instead a rectangular cross – section are made (Figure 42). This means that the width of the channel is additional variable. Due to the fact that the height of the channel is constant, careful designing and optimization is necessary to minimize the boundary layer effects and high aspect ratios are required (Channel Height to Channel Width) [61]. This same nozzle type was used in in the previous version of micro resistojet designed by Mathew Tittu [26]. While using MEMS production techniques, features can be made in the order of [µm], the surface roughness and accuracy of the channel is rather low, with more advanced techniques having an accuracy of ±10 [%] [26] and less advanced as high as ±50 [%] [62] for a throat diameter of 10 [µm].

An extensive research of gas flow in miniaturized nozzles has been done in [24]. It has been concluded that the efficiency of these nozzles is strongly geometry and size dependent. Furthermore, for thrusters in the 1-10 [mN] range, viscous effects cannot be neglected due to the large surface to volume ratio, and viscous boundary layers and surface roughness are the two main contributors to efficiency losses in the nozzle, contributing up to about 10 – 15 [%] each. The thickness of the viscous boundary layer and the resulting decrease of the effective nozzle expansion ratio for nozzles of different thrust levels are shown in Figure 43. It can be seen that for a 10 [mN] nozzle the boundary layer thickness is 10-20[%] of the total local radius, while for the 1 [mN] nozzle it is 20-30[%] of it.

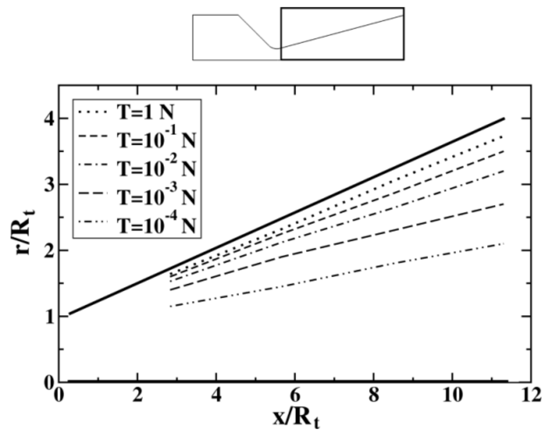

Figure 43: Boundary layer thickness for nozzles of different thrust levels [24]

Furthermore it was found that having a sharp nozzle throat, a converging angle of 15° and a diverging angle of 20° leads to an optimum geometry. The difference however between the most and least optimal solution is about 4 [%]. A much more prominent impact on performance is given by the surface roughness, which can account to losses up to

20 [%]. Therefore to improve the certainty of the design the nozzle will be modeled and designed using CFD.

5.5.1. CFD Analysis Set-Up

The CFD analysis has been done using ANSYS Fluent v14.5. For modelling the flow in the nozzle, the SST k–ω model was used with corrections for Low Reynolds numbers and compressibility effects. This model was chosen because by using the ω-equation, it offers several advantages when compared to the k–ε models. It incorporates modifications for low-Reynolds number effects, compressibility and shear flow spreading [32]. This allows for better boundary layer modelling and more robust Enhanced Wall Treatment. Furthermore, since the flow is compressible, the energy equation was also used but to simplify the simulation heat exchange between the solid and the fluid region has been neglected. Given the small thermal mass of the thruster and the long heating time it is safe to assume that the wall temperature will be the same or close to the flow temperature. Furthermore simulations have shown that for a 3D micro nozzle, thrust output increases as the wall temperature decreases since as heat is removed from the supersonic flow it is further accelerated and performance increases (Rayleigh flow) [63]. Finally single phase flow was used since modeling multi-phase flow in Fluent is rather complex and normally CFX is recommended for these kinds of flows. The choice of the program was made before water propellant was introduced as an option thus it was too late to change it at this time.

Using Ansys Fluent, 3 different nozzle types (2 axi – symmetrical and 1 slit type) producible by 3 different manufacturers will be investigated and compared to the ideal nozzle geometry as proposed by La Torre in [24]. The nozzles geometries are shown in Figure 44. The MEMS nozzle height of the channel is not shown in the figure and it's 100 [μm]. When modelling the fluid region in the nozzle, the straight channel was cut to save computational time. The PM, DEMO and IDEAL nozzles where modelled in 2D using an axi-symmetric space. The MEMS nozzle was modeled in 3D. The fluid properties are given Table 21 and the boundary conditions are given in Table 22.

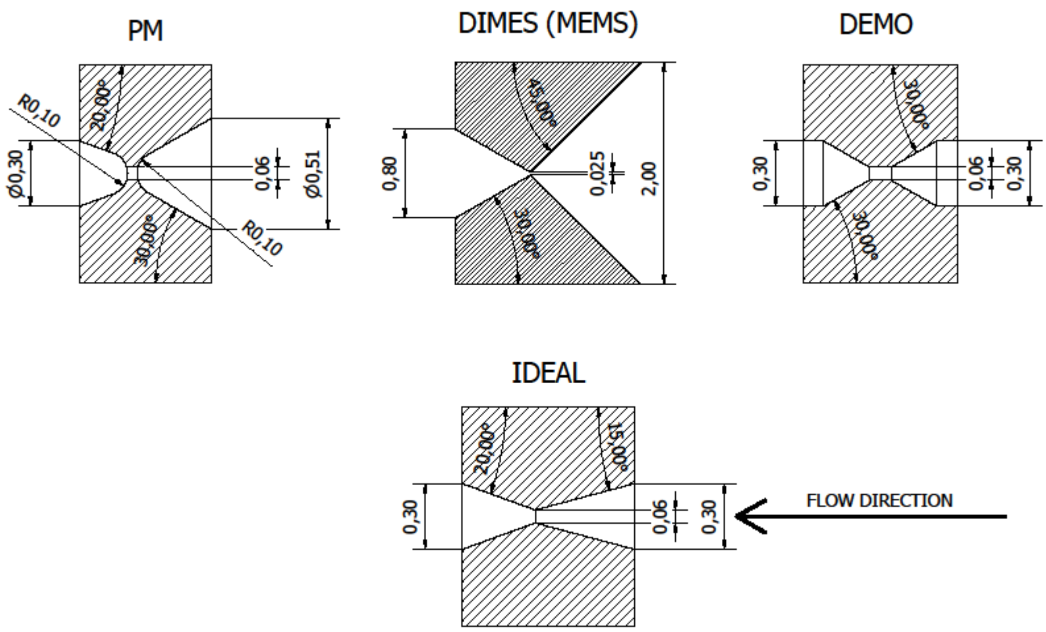

Figure 44: Nozzle Shapes

Table 21: Fluid Properties used in Ansys Fluent

Parameter	Value	Unit
Fluid Material	Water Vapor	-
Density	Real-gas-SRK	-
Cp	Piecewise-polynomial	-
Thermal Conductivity	0.0261	[W/m-s]
Viscosity	1.34E-05	[kg/m-s]
Wall Surface	Smooth	-

Table 22: Boundary conditions used in Ansys Fluent

Parameter	Value	Unit
Ambient Pressure	0	[Pa]
Inlet Pressure	$7x10^5$ - $1x10^5$	[Pa]
Inlet Temperature	550	[K]
Outlet Pressure	4000 – 800	[Pa]
Backflow Total Temperature	300	[K]

For comparison of the different nozzle, 3 points where taken, namely 7 [Bar] which would be the MEOP of the EM, 5 [Bar] which is the pressure mid-point from the requirements and 1 [Bar] which is expected lowest pressure in the system while the temperature of the fluid at the intake was taken to be 550 [K] for all cases. Smooth wall surface was used for the simulation, however once the nozzle is produced, the surface can be scanned using an electronic microscope, and the surface roughness can be incorporated and the flight nozzle design optimized accordingly.

5.5.2. Design Performance and Comparison

The results for the different nozzles are summarized in Table 23. As it can be seen there are significant changes in the mass flow and thus the thrust produced for the different nozzles, while the exhaust velocity and specific impulse are rather similar for the axi–symmetrical nozzles. Still all axi-symmetrical designs are clearly superior to a slit nozzle. Specific impulse is reduced by about 20 [%] and this is mainly due to the much larger boundary layers in the MEMS nozzle in the exhaust and the throat of the nozzles effectively reducing the throat area and expansion ratio. This can be clearly seen in Figure 45 where the boundary layer for the IDEAL and DEMO nozzle design account for about 15 - 20 [%] of the exit diameter, about 30 [%] of the PM nozzle and almost 40 [%] for the MEMS nozzle. It is interesting to note that the velocity profile of the DEMO nozzle looks almost like a bell nozzle. Furthermore looking at the significantly lower specific impulse of the MEMS nozzle, a more optimal height to width ratio could be used than the current design as proposed by DEMO and used for the MEMS thruster in [64].

Table 23: CFD Nozzle Results

Water 7 [Bar]				
Design	Ideal	DEMO	PM	MEMS
Mass Flow [mg]	2.65	2.43	2.18	2.28
Exhaust Velocity [m/s]	1147.73	1107.09	1069.56	970.94
Thrust [mN]	3.04	2.69	2.33	2.22
Isp [s]	117.00	112.85	109.03	98.97
Water 5 [Bar]				
Design	Ideal	DEMO	PM	MEMS
Mass Flow [mg]	1.88	1.72	1.55	1.63
Exhaust Velocity [m/s]	1135.83	1092.81	1065.26	930.44
Thrust [mN]	2.13	1.88	1.65	1.52
Isp [s]	115.78	111.40	108.59	94.85
Water 1 [Bar]				
Design	Ideal	DEMO	PM	MEMS
Mass Flow [mg]	0.37	0.30	0.30	0.32
Exhaust Velocity [m/s]	995.99	935.12	946.03	554.25
Thrust [mN]	0.74	0.57	0.57	0.35
Isp [s]	101.53	95.32	96.44	56.50

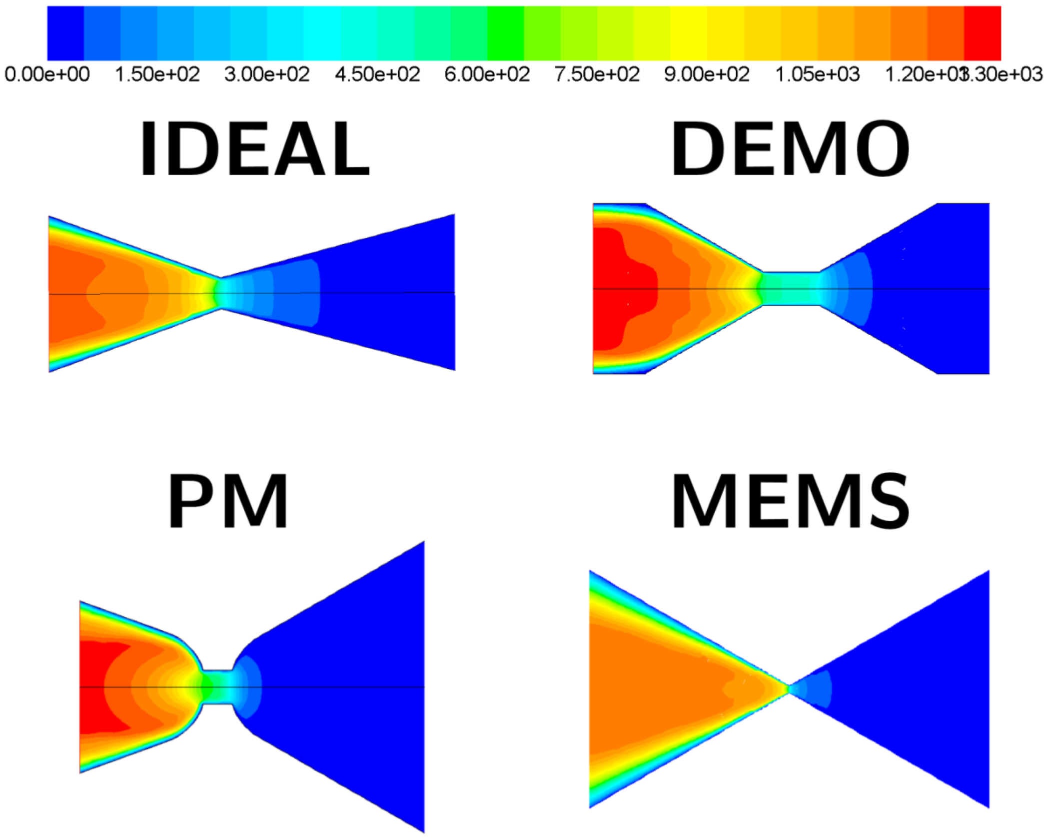

Figure 45: Velocity Magnitude [m/s] Contour

With the performance of the different nozzles available a comparison is made between the designs. Since this is an engineering model the main criteria will be the producibility of the nozzle and the ease of integration within the thruster. Next in the hierarchy are the lead time and the performance since the nozzle should be available when the thruster is ready and the performance should be comparable to what would be used on the flight model. Finally cost is considered the least important criteria since the fraction cost of the nozzle to the whole system is rather small.

Performance wise it is clear that the DEMO offers the best and the MEMS nozzle the worst performance. The cost of the DEMO nozzle was estimated at about € 750, the PM workshop costs $ 400 per day excluding shipping costs and they estimate they would need at least 3 days to produce the design while the MEMS nozzle is already being produced for the MEMS thruster so it will be technically for free.

Producibility wise the DEMO and PM workshops are confident that they can produce the design but cannot guarantee the accuracy of the dimensions and especially the angles while DIMES is confident they can easily produce the MEMS nozzle. However the advantage of the machined nozzles are that they can be machined on a rod which can also have a thread and be easily screw-able in the chamber while the MEMS nozzle needs requires a more complex integration method.

Finally the lead time is the best for the DEMO nozzle with the estimate being 2 weeks and there is no shipping time since the workshop is located on campus. The PM workshop is in the USA and they recon they will need at least 4 weeks before the nozzle is delivered to us. Finally although DIMES is also on campus, their lab will undergo renovation in the near future and they are not certain if they will be able to deliver the MEMS parts before that thus the lead time may be as much as 4 months. This reasoning is reflected in Table 24 where it can be seen that the DEMO nozzle is the clear winner.

Table 24: Nozzle Trade - Off

Design	Weight	DEMO	PM	MEMS
Performance	3	5	3	1
Cost	1	5	3	5
Producibility	5	3	3	5
Integration	5	5	5	1
Lead Time	3	5	3	1
Total		75	61	41

5.5.3. Design Analysis

With the nozzle design chosen a more in-depth analysis can be made of both the design and the model. The velocity vectors are shown in Figure 46. It can be seen that vortices occur after the nozzle throat and at the transition between the expanding and the straight part of the duct. This is due to the sudden large expansion angle which is due to the drill tip. However as it was shown in the previous section this does not affect the performance of the nozzle drastically.

In Figure 47 and Figure 48, the pressure and temperature contours are shown. As it can be seen the temperature of the flow drops down to 100 [K] and the pressure down to 600 [Pa] in the nozzle exhaust. Since multi-phase flow is not taken into consideration, the CFD analysis still treats it as gas, however in reality solid ice particles will likely form (Figure 49), so condensation and even solidification of the water in the exhaust is still a concern to be further analyzed during the test phase

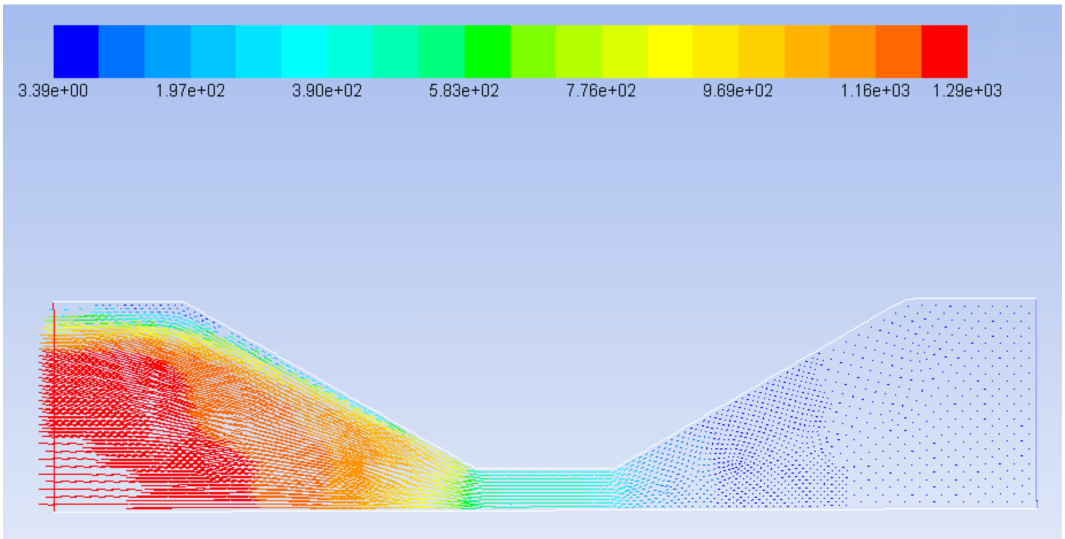

Figure 46: Velocity Vectors obtained by the CFD simulations [m/s].

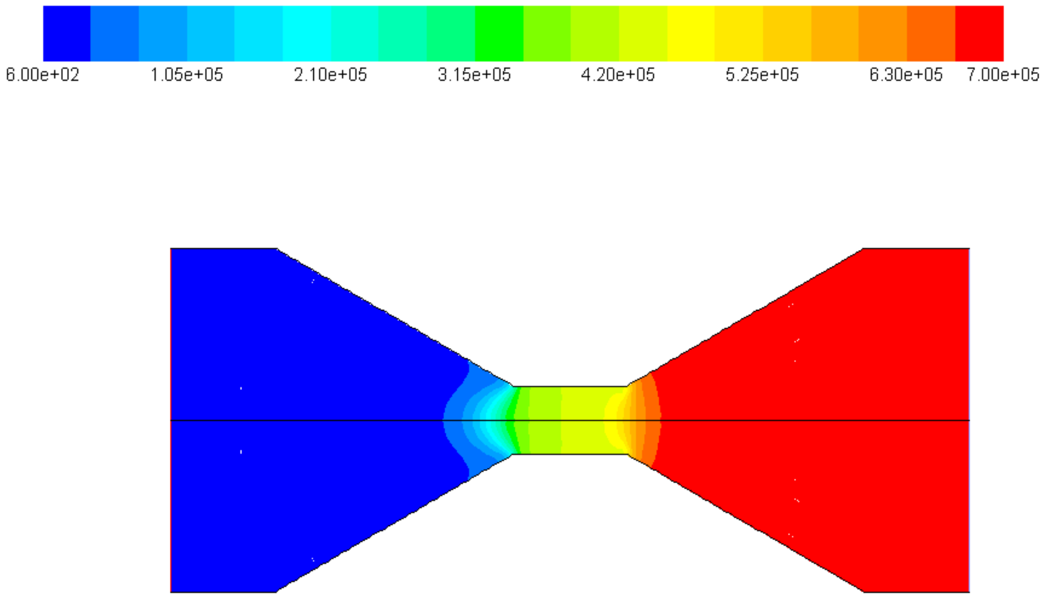

Figure 47: Pressure contour obtained by the CFD simulations [Pa]

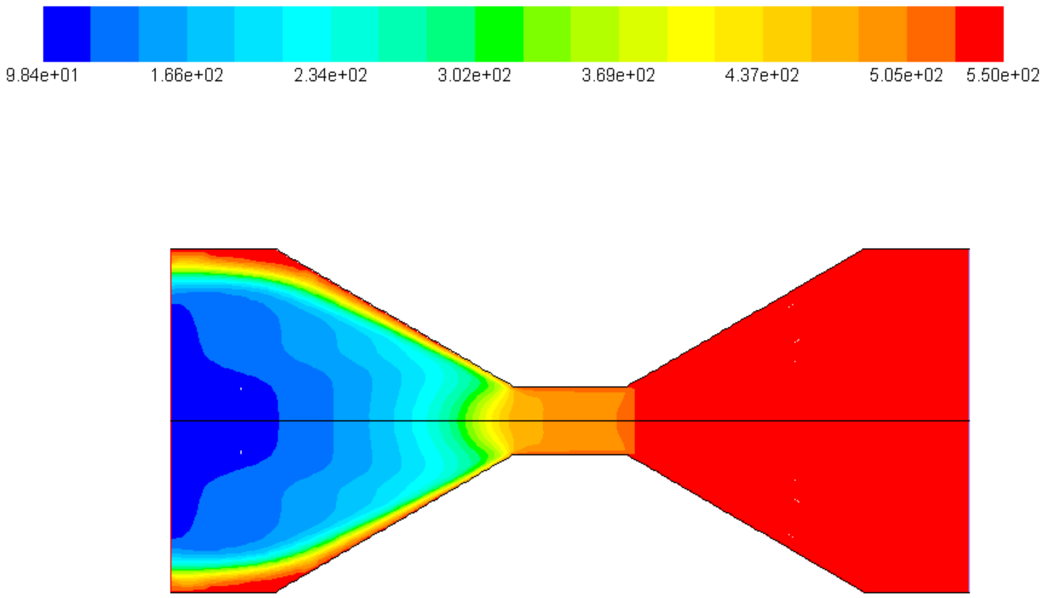

Figure 48: Temperature contour obtained by the CFD simulations [K]

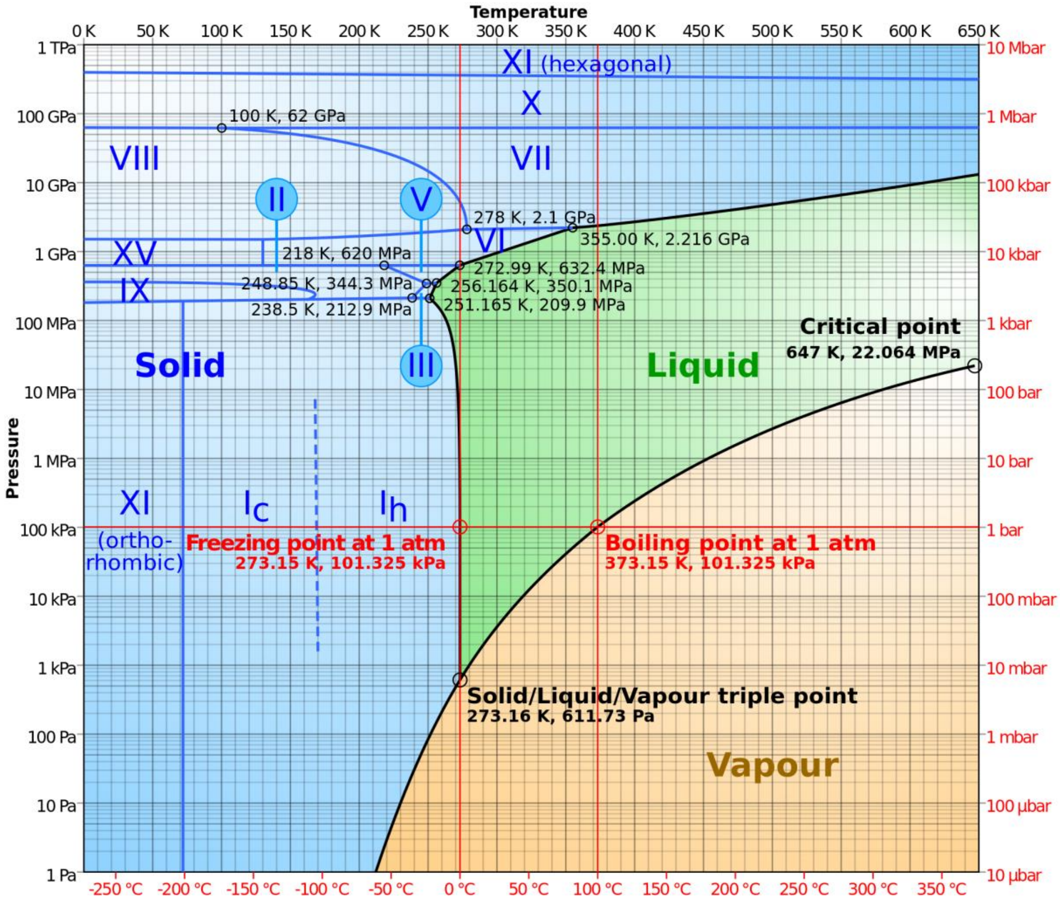

Figure 49: Water 3 - Phase Diagram

5.6. Thruster Performance Summary and Comparison

The thruster performance is summarized in Table 25. As it can be seen, there are quite some differences from the ideal rocket theory results. The reason is mainly the effect of boundary layers and non – optimal geometry.

Table 25: Thruster performance with water as propellant

Parameter	Value	Unit
Thrust	2.7 – 0.6	[mN]
Pressure	7 – 1	[bar]
Target Temperature	550	[K]
Exhaust velocity	1100	[m/s]
Specific Impulse	112	[s]
Propellant Mass	50	[g]
ΔV	15.4	[m/s]
Mass Flow	2.4 – 0.3	[mg/s]

Furthermore since the thruster should still be able to operate with nitrogen as propellant, the performance from the CFD simulation when using nitrogen at 700 [K] are given in Table 26. As it can be seen, the same thruster with the same nozzle and with the heater operating at 700 [K] it would still be able to fulfill the requirements as given in [10]. The power needed to heat up Nitrogen from 300 to 700 [K] is only about 1.2 [W] therefore the power requirement is also within the power budget.

Table 26: Thruster performance with nitrogen as propellant

Parameter	Value	Unit
Thrust	5.3 – 0.6	[mN]
Pressure	7 – 1	[bar]
Target Temperature	700	[K]
Exhaust velocity	970	[m/s]
Specific Impulse	99	[s]
Propellant Mass	58	[g]
ΔV	15.7	[m/s]
Mass Flow	2.7 – 0.4	[mg/s]

In Table 27 a comparison is provided between the results obtained by the ideal rocket theory and the CFD simulations. As it can be seen in the table, the difference in thrust is rather large, namely 30 [%] at a chamber pressure of 7 bar. Furthermore, the specific impulse is also 28 [%] less and the total ΔV is thus also reduced. It should be noted that in the current CFD analysis surface irregularities and phase change have not been taken into account, which are expected to further affect performance with additional losses of up to 20 [%].

Table 27: Comparison between ideal rocket theory (IRT) and CFD results

Parameter	CFD	IRT	Unit	Diff.[%]
Thrust	2.7 – 0.6	3.5 – 0.5	[mN]	up to 30
Pressure	7 – 1	7 – 1	[bar]	-
Specific Impulse	112	141	[s]	28
ΔV	15.4	18.7	[m/s]	23
Mass flow	2.4 – 0.3	2.5 – 0.4	[mg/s]	up to 33

In Table 28 a comparison is made between the COTS and the MEMS thruster at their operating conditions. As it can be the COTS thruster produces more thrust at the same chamber pressure, but for the rest the performance is comparable. What needs to be taken into account though is that the COTS thruster is expected to have much lower heater efficiency when compared to the MEMS heater. The reason for this is because the mass of the heater itself and the surrounding structure is much larger, thus a significant amount of power will be lost in heating up the heater, porous media and chamber. The MEMS thruster, on the other hand, with its suspended heaters and compact structure will lose less heat. However still good packaging and mounting method is needed, as to avoid losing heat from the thruster to the mounting PCB and the rest of the structure.

Table 28: Comparison between COTS and MEMS thruster performance

Parameter	COTS	MEMS	Unit	Diff.[%]
Thrust	2.7 – 0.6	2.1 – 0.3	[mN]	30 - 200
Pressure	7 – 1	7 - 1	[Bar]	-
Temp.	550	773	[K]	-
Specific Impulse	112	111	[s]	-
ΔV	15.4	15.2	[m/s]	-
Mass flow	2.4 – 0.3	1.9 – 0.2	[mg/s]	25 - 50

6. Description of Engineering Model Propulsion System

Before making a flight model thruster, a common practice is to validate the design and proof of concept by making an engineering model thruster. The engineering model should be as representable as possible performance wise but does not have to adhere to the volume and mass budget given in [10]. Furthermore since there was no feed system and tank available at the time, this also needs to be designed and build functionally wise. In this chapter the engineering model will be described and the different components and connections explained.

6.1. Feed System

The feed system is composed of mainly Swagelok parts and custom manufactured components where needed. It can be separated into 4 parts:

- Filling Branch
- Tank
- Hexagon adapter and sensors
- Feed Line to valve

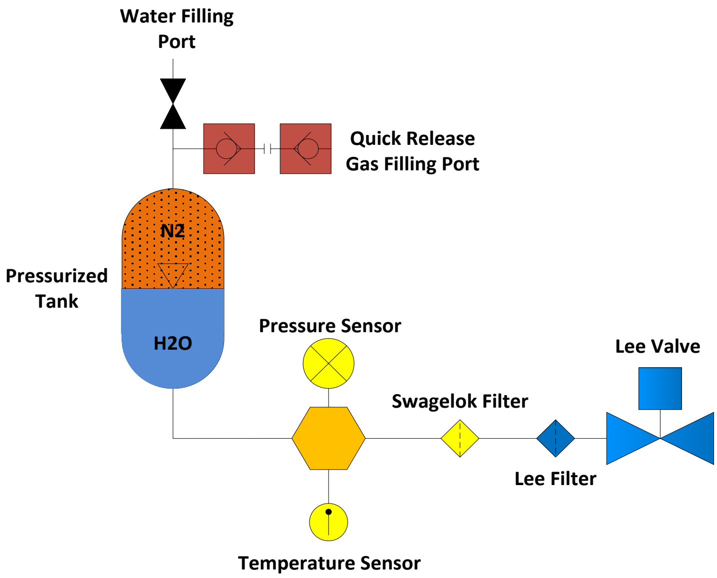

Figure 50: Feed System Schematic

6.1.1. Filling Branch

The filling branch is composed of Swagelok quick release connector used as gas filling port (Figure 51 on the right) and a pneumatic push-in hose connector and valve used as water filling port (Figure 51 on the left). Using the quick release connector allows easy connection of the feed system to the pressurant gas feed. Furthermore disconnection the quick release connector closes that port and allows the system to be used in blow-down mode. The pneumatic push-in hose can connect leak tight to a syringe and precise water quantities can be injected into the tank. Then disconnection the syringe and connecting the push in valve allows for the system to be leak tight.

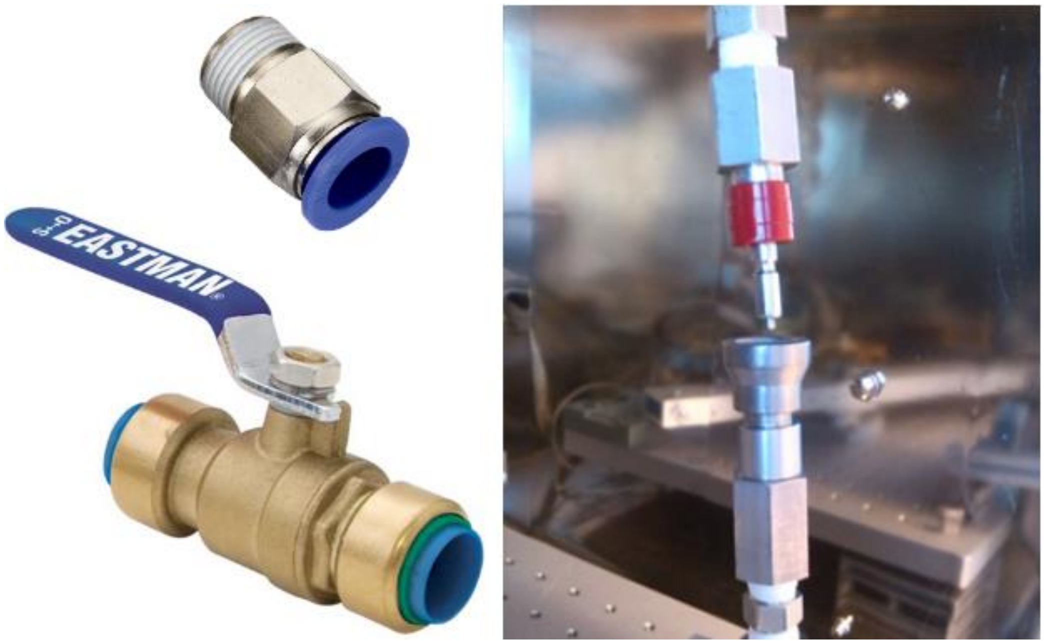

Figure 51: Filling Branch

6.1.2. Tank

The tank used in the engineering model is Swagelok 304L-HDF4-150 (Figure 52). It's double ended cylinder made of stainless steel, has a volume of 150 [cm^3] and it's rated of up to 1800 [psig] or 124 [bar] in atmospheric conditions. On both ends there are female $\frac{1}{4}$ NPT connectors. The tank will be installed in vertical position since in that manner, separation between water and nitrogen is guaranteed due to gravity.

Figure 52: Swagelok Tank 304L-HDF4-150

6.1.3. Hexagon adapter

The hexagon adapter is a custom made brass adapter and its shown in Figure 53. The female connectors are all $\frac{1}{4}$ BSP (number 1), the left male connector (number 2) is 3/8 BSP and the right male connector (number 3) is 1/8 – 27 NPT. The tank is connected to the top using a Swagelok $\frac{1}{4}$ Male NPT to $\frac{1}{4}$ Male BSP connector. The second female hole is used for the temperature sensor and the third is unused and closed-off with a plug. The pressure sensor is connected to the 1/8 – 27 NPT connector using female to female 1/8 – 27 NPT connector and the feed piping to the valve is connected to the 3/8 BSP connector using 3/8 female BSP to $\frac{1}{4}$ Swagelok pipe adapter.

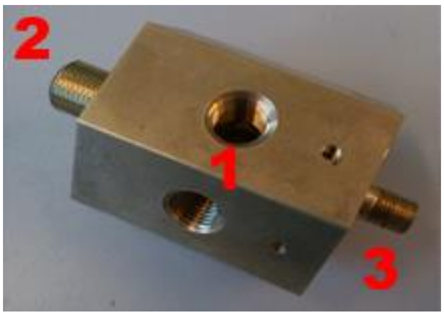

Figure 53: Hexagon adapter

6.1.4. Feed Line to Valve

The feed line to the valve consists of $\frac{1}{4}$ Swagelok pipes, a brass in-line filter of 15µm with part number Swagelok B-4F-15 (Note that 12µm or smaller filter is recommended for VHS Valves but these were unavailable at the time) and conversion pieces that go from $\frac{1}{4}$

Swagelok pipe to 0.250-28 unf-2a thread. This in turn connects to Lee Company boss TMDA3212950Z that goes from 0.250-28 unf-2b to 062 MINSTAC connection and then to 1m Lee Company Teflon tube with part number. TUTC3216910D. Finally a small in-line peek safety screen of 12µm (INMX0350000A) is connected between the Teflon tube and the Lee Valve. The feed system (without the water filling branch and the Teflon tube and valve) is shown in Figure 54.

Figure 54: Feed System

6.2. Valve

The valve used for the EM model was described in Section 5.1. As it was said previously, the VHS solenoid valve series are used in both medicine and high-tech industry, they have normally closed configuration and have fast opening times (as fast as 0.25 [ms]), MEOP of up to 120 [PSIG] (circa 7 [Bars] in vacuum) and 250 million cycles as life-time minimum. To guarantee proper functioning of the valves proper filtration is required. System filtration of 12 microns or less is recommended. In addition, last chance PEEK filters are available that can be threaded directly into valves with MINSTAC inlet ports. The configuration chosen for the EM, features MINSTAC inlet and outlet and has EDPM seal. Two versions where delivered with the difference being one has an operating voltage of 24 [Vdc] and the other of 12 [Vdc]. The valve together with the PEEK filter and the Teflon hose is pictured in Figure 55.

Figure 55: Valve Assembly

6.2.1. MINSTAC

The MINSTAC coupling system is a unique Collet-Lock system developed by the Lee Company, which provides a leak proof connection by threading chamfered Teflon tubing into specially designed boss. The connection is shown in Figure 56. The coupling nut is screwed in the boss and presses the collet which in turn presses the chamfered Teflon tube against an opposite chamfered opening in the boss. Therefore (as it was later realized in this thesis) making a tube with the correct thread will not provide leak proof connection but a specially designed boss is required. Standard tubing assemblies with fittings and bosses are available for order at Lee Company or alternatively for larger number, production kits can be also purchased [48].

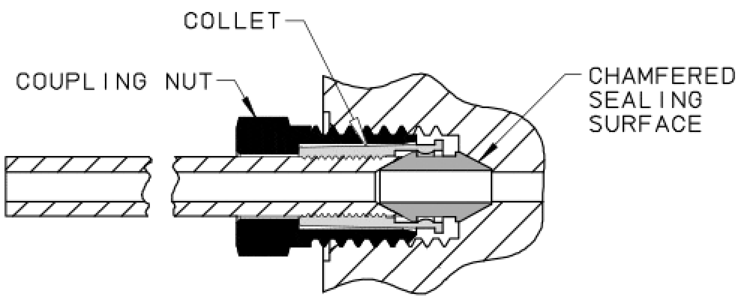

Figure 56: MINSTAC Connection [48]

The 062 MINSTAC fitting system, used on the VHS valves, is shown in Figure 57. It uses 0.062 [Inch] (1.57 [mm]) O.D. Teflon tubing and a 0.138-40 UNF threaded fitting (left in Figure 57) and a special 062 MINSTAC boss. The coupling nut acts like a compression fitting and presses the chamfered end of the tubing against one end of the ferrule. The other end of the Ferrule is pressed against the sealing surface in the boss by the coupling screw. The ferrule is colored blue and the sealing surface red in in Figure 57.

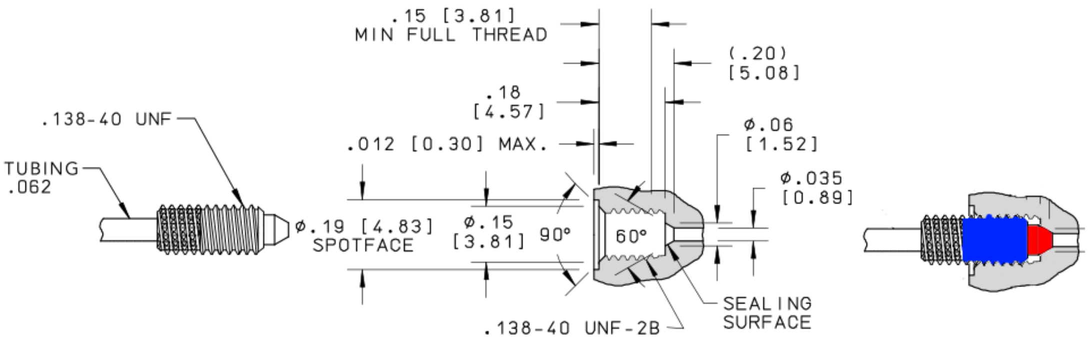

Figure 57: 062 MINSTAC Fitting System [48]

6.2.2. Valve Control Circuit

As it was mentioned earlier the VHS valves require special circuit to operate properly. The valve initially requires a 12 or 24 [Vdc] (model dependent spike voltage) pulse for a minimum of 0.3 [ms] to actuate the valve, and then the voltage through the coil needs to be reduced to 1.6 or 3.2 [Vdc] (model dependent hold voltage) to keep the valve open. If the voltage is not reduced to the model dependent hold voltage level, the coil will overheat and the valve will be destroyed.

Fortunately the Lee Company also offers a readymade Spike and Hold Driver (IECX0501350A) that provides the proper waveform for safe operation of the VHS and IEP valves by using a 5 [Vdc] TTL control signal. The driver (pictured in Figure 58) only requires that the user connect the TTL signal, spike voltage supply, hold voltage supply and the valve itself and set the spike duration using the potentiometer. The duration of the spike can be monitored using a oscilloscope. More details can be found in [47] and later in this report.

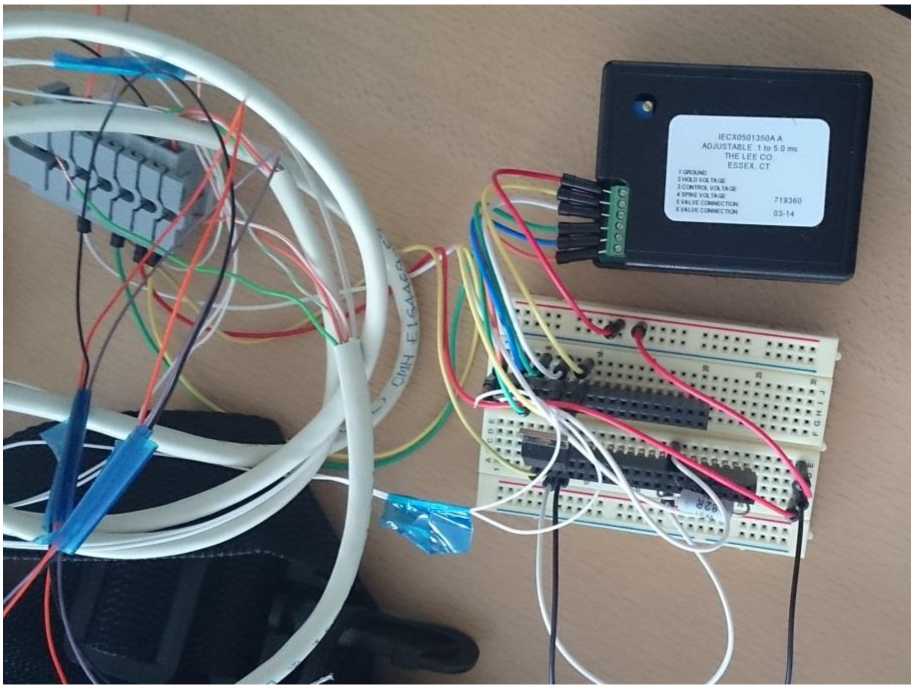

Figure 58: Lee Company Spike and Hold Driver with TTL Signal Circuit

6.2.3. Lee Valve VHS Starter Kit

Considering all the different components needed to support the valve, a good initial investment would be the VHS Starter Kit (Part Number IKTX0322000A). It includes the following components:

- 1 - VHS Dispensing valve
- 1 – Instructional CD
- 3 - MINSTAC Nozzles
- 1 - MINSTAC Atomizing nozzle
- 1 - Spike and hold driver circuit
- 1 - 062 MINSTAC Teflon tubing and fittings
- 1 - Lee 062 MINSTAC 12 micron PEEK Safety Screen
- 1 - 8” Long high retention lead wire assembly with 24 AWG PTFE lead wires
- 1 – MINSTAC Nozzle Torque Wrench
- 1 – Mounting Clip

The kit is shown in Figure 59 and more information about the VHS starter kit can be found in [47]. The price is €685 and it has a lead time of 2 – 4 weeks. In order to have the system connected both to the feed system and the thruster however another set of Teflon tubing with fittings and a boss is needed. Since DIY boss and hose kits are about€700 – 800 and that budget was not considered adequate for the feed system of the EM propulsion system it was decided to purchase just another pre-made Teflon tube and a pair of boss connectors. A 1 [m] 062 MINSTAC Teflon tube with fittings (Part number TUTC3216910D) is €79.5, a 0.250-28 UNF-2B flat bottom boss to 062 MINSTAC (Part number TMDA3212950Z) is €24.54 and will be used to connect to the EM thruster discussed in this report and 0.250-28 UNF-2A flat bottom boss to 062 MINSTAC (Part number TMDA3204950Z) is €17.38 and will be used to connect the VHS valve to the MEMS thruster. All the invoices and price quotations can be found in Appendix C.

Figure 59: VHS Starter Kit

6.3. Heating Elements

The heaters that will be used for the EM model where described in Section 5.3. As it was said the Elstein T-MSH/20 is a ceramic infrared heater with integrated thermocouple. It is rated up to 860 [°C] operating temperature and surface ratings up to 100 [kW/ m^2].

Heating Elements

MSH micro system heaters are used in applications, which require partial heating or drying of small goods and areas. It has power rating of 55 [W] at 12 [Vdc] which would translate to 9.5 [W] at 5 [Vdc] which is what makes this heater particularly attractive. Namely this would allow the heater to work below the rated maximum power consumption of 10 [W] connected directly to the EPS 5 [Vdc] line without the need of a local DC-DC up conversion circuit on the propulsion system PCB. The actual heater is shown in Figure 60.

The second heater is produced by Watlow and it's bearing the model number C1J-9769. It is a water immersion heater with a power rating of 30 [W] at 24 [Vdc] resulting in a power rating of 7.5 [W] at 12 [Vdc]. It has a diameter of 1/8 [Inch] and a length of 1.5 [Inch] without a thermocouple and it's shown in Figure 61.

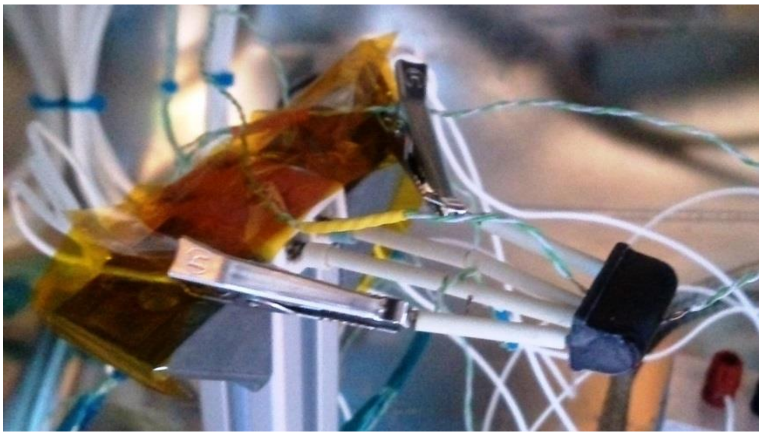

Figure 60: Elstein MSH/20 (dimensions in mm)

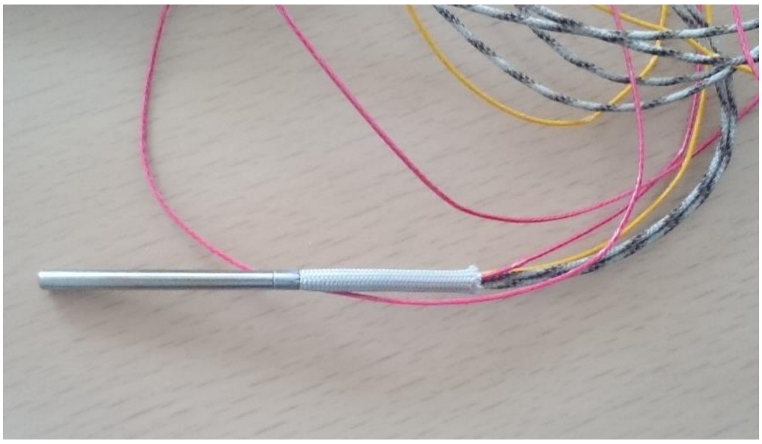

Figure 61: Watlow C1A-9602 Cartridge Heater

6.4. Porous Media

The porous media is used to make sure the flow is turbulent in the heating chamber and that the liquid water is vaporized completely. The porous media selected for the thruster is an open type metal foam produced by Recemat BV, with a high porosity (up to 95 [%]) and a small pore size, but a rather brittle nature [55]. The Nickel foam (Ni) has excellent properties for battery and electrolysis applications, due to its good electrical and thermal conductivity. Foam with different pore sizes is available and if time allows the difference between different types of foam should be investigated. Recemat provided two different samples for testing for free and their properties where given in Section 5.2 and they are shown in Figure 62. The block will be cut in the same footprint as the inside of the chamber and stacked inside.

Figure 62: Recemat Metal Foam

6.5. Chamber

The Chamber is used to house the heater and the porous media. It was produced from aluminum by the DEMO workshop at TU Delft. It consists of two parts, chamber which has a port for the valve connection, cartridge heater, pressure sensor port and the nozzle and a cap that has connection for the ceramic heater. The assembly is shown in Figure 63 and the actual chamber in Figure 64.

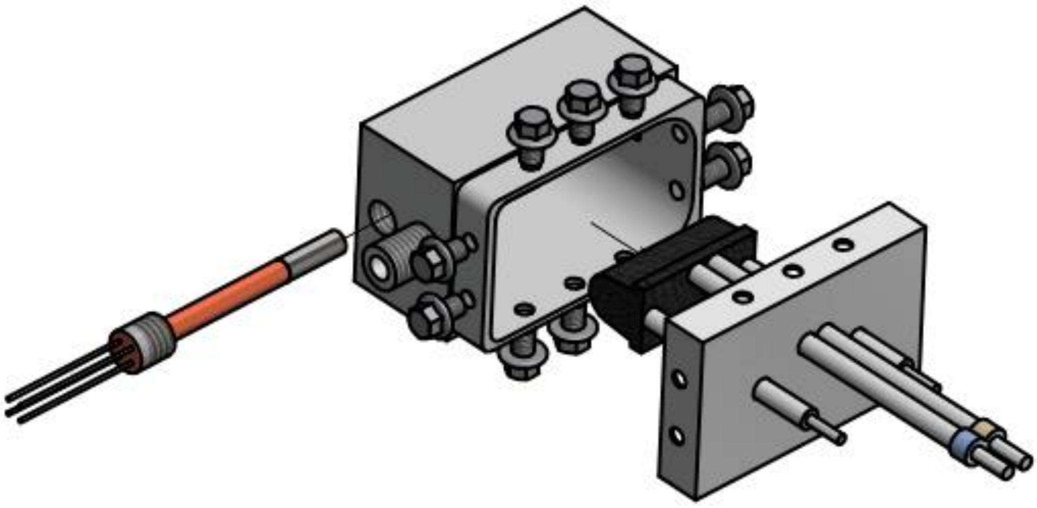

Figure 63: Chamber Assembly

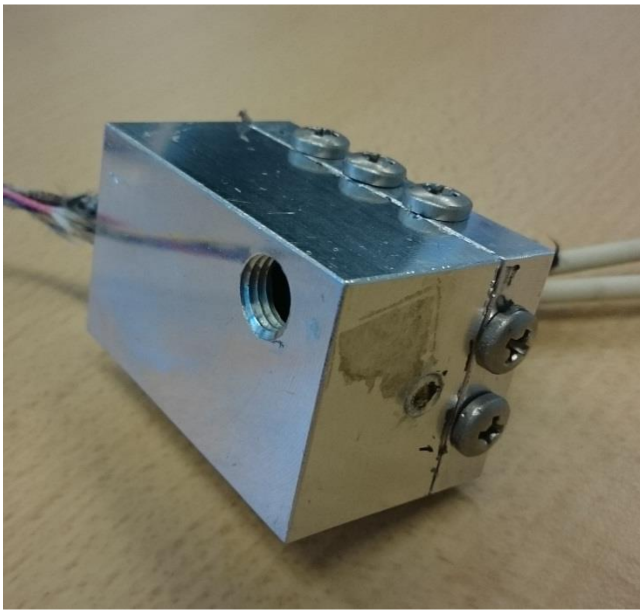

Figure 64: Produced Chamber

6.6. Nozzle

The design process for the nozzle was given in more detail in Section 5.5. The nozzle was to be manufactured using wire EDM by DEMO. However after 4 weeks and many unsuccessful attempts, the design was simplified to being drilled with a 60 [µm] and 300 [µm] drill from one side (the exhaust of the nozzle as to have good alignment), and a 300 [µm] drill from the other side which probably ended up as the nozzle in Figure 65 on right. The produced nozzle is shown in Figure 66. The top is the throat diameter and the bottom is the exit / inlet diameter with the left side being as looked from the nozzle exit and the right side being as looked from the nozzle inlet. The difference in sizes is due to the tapper angle of the drill meaning drilling deeper makes the diameter of the hole larger. The actual size of the nozzle is shown in Figure 67.

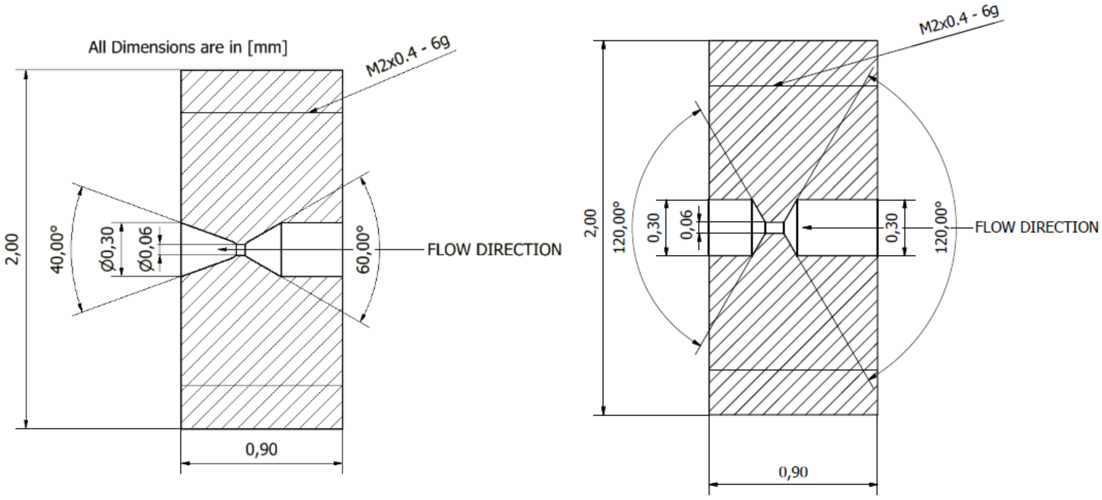

Figure 65: EM Nozzle Design (Left) and Produced (Right)

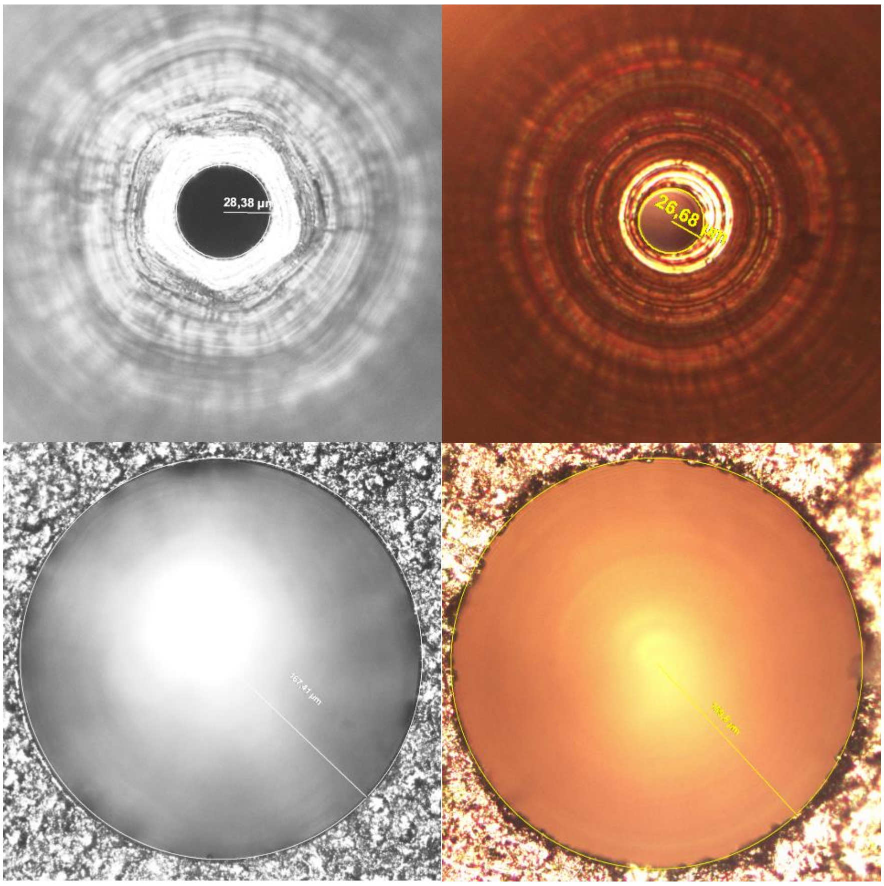

Figure 66: EM Nozzle Produced

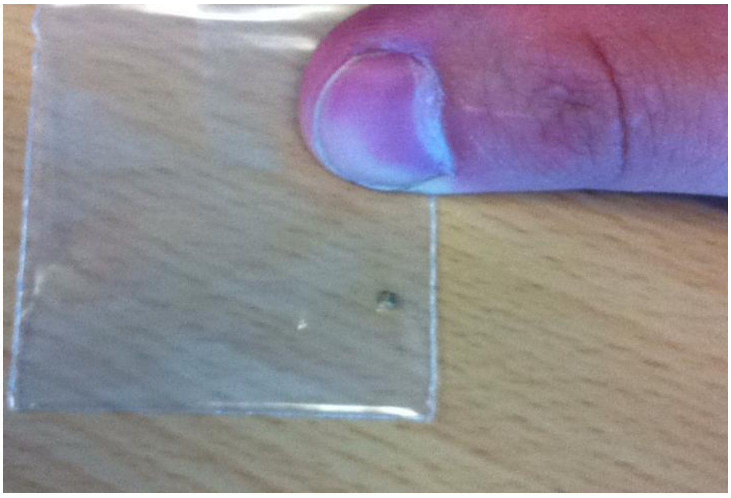

Figure 67: Nozzle Size

6.7. Thrust Bench Interface and Assembly

The thruster also needs to be able to interface with the thrust bench. For this an interface place has been designed and can be seen in Appendix B. The opening on one side is where screws from the chamber need to protrude such that the thruster itself is leveled on the surface. The thruster will be held in place with a bracket that can also house the valve. The whole assembly is pictured in Figure 68. To avoid conducting heat from the chamber to the thrust bench and the rest of the structure, thermal insulator should be placed between the bracket and the thrust bench.

The thruster has a total mass of 48 [g] with the lead wires and the valve and 30 [g] without the heater leads and valve. This is slightly higher than the mass budget as set in Chapter 4, however considering that the chamber is bulky and houses 2 heaters, it is reasonable to assume that a small chamber with only 1 heater will be well within the mass budget.

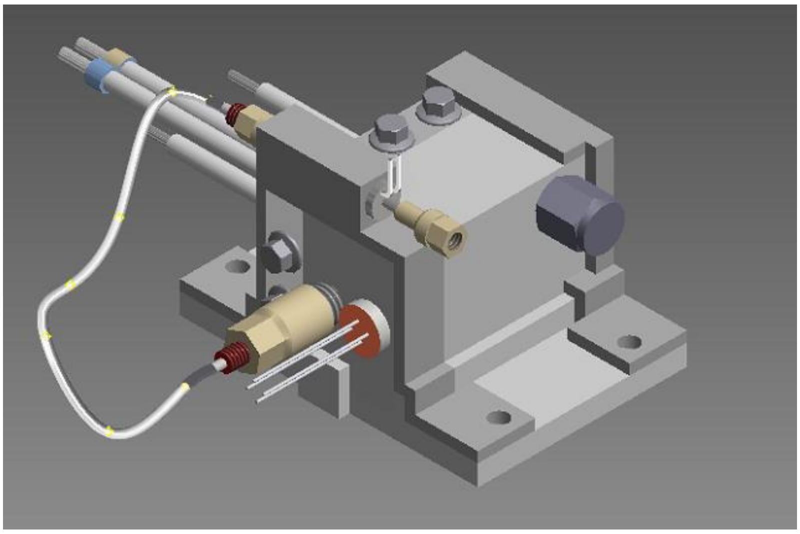

Figure 68: Thruster + Bracket Assembly

7. Test Setup

In this chapter the test setup will be presented including both the hardware and software used. First a choice is made on the thrust test bench to be used. Next the load cell is presented in Section 7.2. The feed system together with the sensing components is given in Section 7.3 and the vacuum chamber in Section 7.4. The different power supplies used are given in Section 7.5 and the control and data acquisitioning electronics are given in Section 7.6. Finally in Section 7.7 the LabView program that controls and logs all other components is described with its different modules.

7.1. Test Bench Trade – Off

The 2 test benches where shown in Section 0, [38] and [13]. In Table 29 the performance and status of both test benches are summarized. Since this thruster is only engineering model and a proof of concept the AE-TB-50M is the better choice. While it has lower accuracy, all the components are readily available and no lead time or funds are necessary to purchase the load cell. Furthermore having experience in testing with this test bench gives advantage in the test setup. For the flight model however the AE-TB-5M is still recommended as it will provide more accurate results.

Table 29: Test Bench Trade - Off

	AE-TB-50M		AE-TB-5M	
	Specifications	Acceptable	Specification	Acceptable
Thruster mass [g]	< 360	Yes	< 300	Yes
Thrust Range [mN]	0.5 – 50	Yes	0.01 – 5 (10)	Yes
Accuracy [mN]	± 0.1	Yes	0.001	Yes
Status	Operable	Yes	Inoperable	No
Documentation Available	Partial	Yes	Yes	Yes
Testing Experience	Yes	Yes	No	No
Cost	0	Yes	1000+	No

7.2. Load Cell

The load cell used in combination with the thrust bench AE-TB-50M is the Futek LRF400 Tension and Compression load cell. It has a capacity of 10 [g] or 100 [mN]. The specifications of the load cell are given in Table 30. The output of the voltage of the load cell depends on both the load and the input voltage due to the Wheatstone Bride. The maximum voltage is 5 [V] resulting in a ± 5 [mV] output for 100 [mN]. Since the expected thrust in the order of 1 – 2 [mN] the actual output voltage would more likely be in the ± 10 [µV] range. The linearity and repeatability of the load cell have been verified by Q. Bellini. For best results the arm and the screw connecting on the load cell need to have 90° angle as shown in Figure 69.

Table 30: Futek LF400 Specifications

Rated Output	$1\ mV/V$ nom.
Zero Balance	$\pm 3\%$ of R.O.
Excitation	$5\ Vdc$ max
Non Linearity	$\pm 0.1\%$ of R.O.
Hysteresis	$\pm 0.1\%$ of R.O.
Non Repeatability	$\pm 0.1\%$ of R.O.
Creep	$\pm 0.2\%$ of Load
Temp. Shift Zero	$\pm 0.1\%$ of R.O./°C
Operating Temp.	-50 $°C$ to 93 $°C$
Capacity	$0.1\ N$
Safe Overload	$22.2\ N$
Weight	$140\ g$

7.3. Propellant storage and feed system

A schematic of the propellant storage and feed system is given in Figure 70. The small tank is pressurized by N2 using manual pressure regulator. The propellant tank is Swagelok 304L-HDF4-150, the pressure sensors are Omega PX181-200G5V and the temperature sensor used to sense the fluid temperature in the feed system is AB Elektronik Sachsen 94-099. The Swagelok filter is 15 [µm] filter with part number B-4F-15 and Lee Company filter is used as a last resort to safe the valve from particles using a finer 12 [µm] mesh. The VHS Lee valve is controlled by a spike and hold circuit which in turn is operated by the workstation using LabVIEW. In the chamber the voltage, current and temperature of the two heaters are constantly monitored and all the data is acquired and stored using NI DAQ USB 6008 and LabVIEW in the workstation. The specifications of all the parts are summarized in Table 31. The Nitrogen tank and pressure regulator used for pressurizing the water are shown in Figure 71 and the feed system together with the water filling port inside the vacuum chamber is shown in Figure 72.

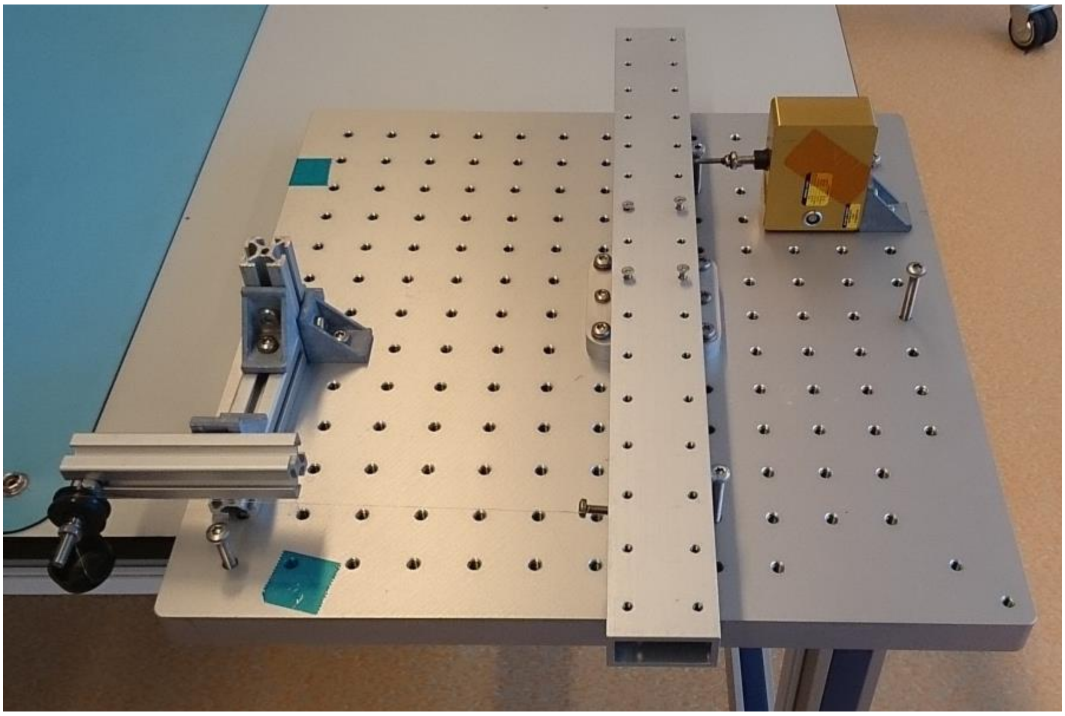

Figure 69: AE-TB-50M Thrust Bench

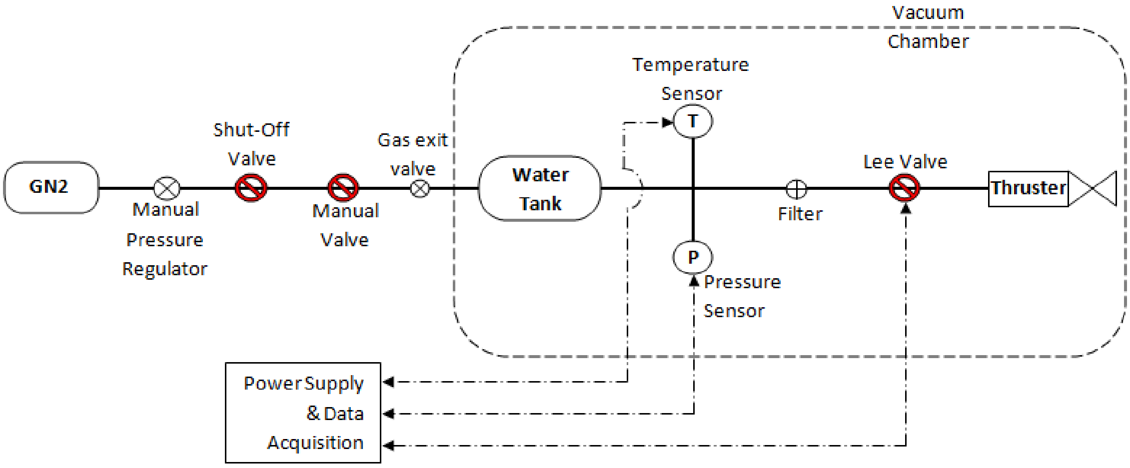

Figure 70: Propellant storage and feed system

Table 31: Feed System Components

COMPONENTS	CHARACTERISTIC
Nitrogen Tank	• High pressure ($\cong 150\ bar$)
Pressure Regulator	• Manual Regulator • (0-15 bar)
Shut-Off Valve	• Manual Valve
Relief Valve	• Rotary valve
Swagelok Water Tank	• Double-Ended Stainless Steel Cylinder • Connection Type : Two $1/4\ in.FNPT$ • Volume : $150\ cm^3$ ($150\ g\ of\ water$) • Max Pressure : $1800\ psig$ ($124\ bar$)
Pressure Sensor *OMEGA PX181-200G5V*	• Excitation : 12-25 Vdc • Accuracy : $\pm 0.3\%\ BFSL$ • Operable T. Range : - 40 to 105°C • Range : 0 to 200 $psig$ (0 -13.8 bar) • Output : 1 to 5 Vdc • Sensitivity : 3.4 bar/V • Port : 1/8-27 NPT stainless steel fitting
Temperature Sensor *AB Elektronik Sachsen GmbH 94 099*	• NTC Sensor • Nominal Resistance : 2251 Ω (25°C), 153 Ω (100°C) • Temperature Range : - 40 to 150°C • Thread : $M12\ x\ 1.5$
Filter	• Brass in-line particulate filter • $1/4\ in.$ Swagelok Tube Fitting • 15 $micron$ pore size
Lee Valve *Lee VHS Micro-Dispensing Valve*	• Input : 12 V • Pressure : 120 psi (8.3 bar) • Ports : 0.062 Lee Minstac Boss • NC valve

Figure 71: Nitrogen Tank and Pressure Regulator

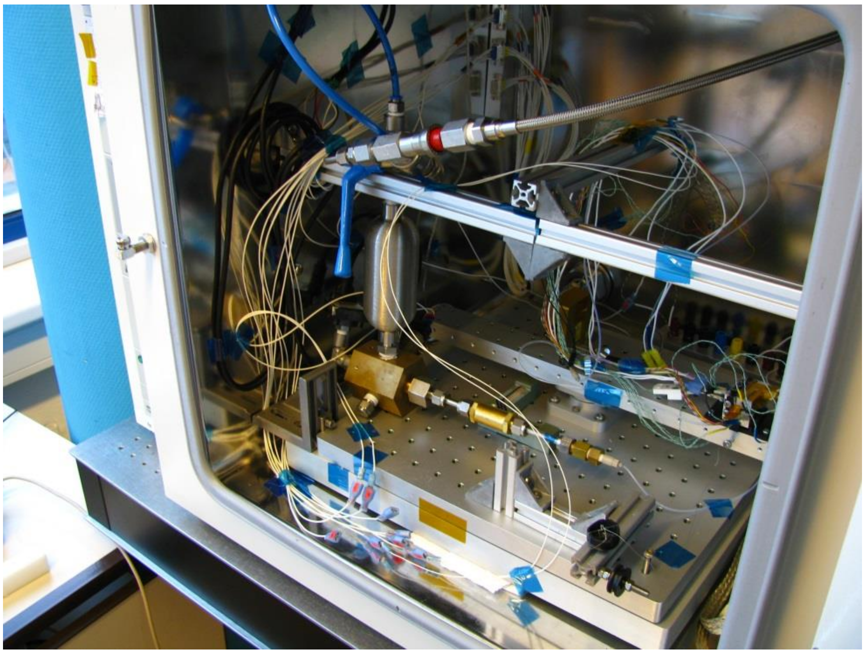

Figure 72: Feed system inside the Vacuum chamber

7.4. Vacuum Chamber

The vacuum chamber used is the Heraeus Vacutherm VT-6060M and the vacuum is created by Vacuubrand MD-1 diaphragm pump. After 30 minutes of operation of the vacuum pump a pressure level of about 10 [mBar] is achieved and after about 1 hour a minimum of 6 [mBar] can be achieved (Figure 73). Once the vacuum pump is switched off the pressure starts increasing by about 0.2 [mBar] per minute. The pressure in the vacuum tank is constantly monitored using an Omega Engineering PXM209-006A10V pressure sensor. The characteristics are given in Table 32. Furthermore in the vacuum chamber 9 K-Type thermocouples, 7 banana plugs and 4 DB9 connectors are available for temperature measurements and signal feed through.

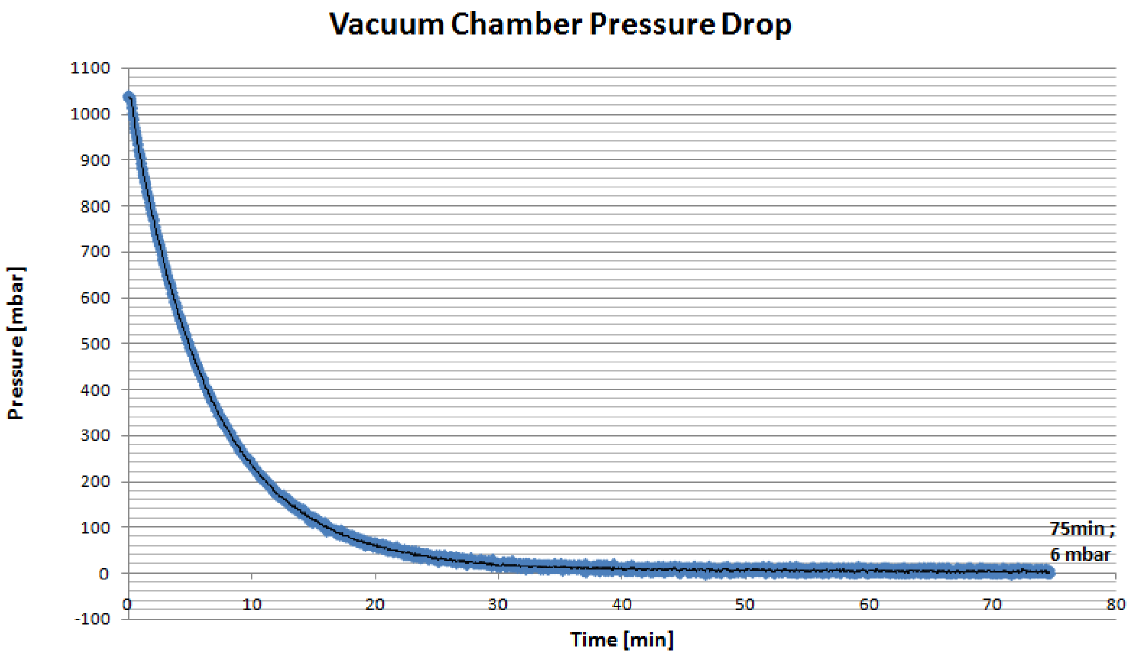

Figure 73: Vacuum Chamber Pressure Drop

Table 32: Vacuum Chamber Characteristics

COMPONENT	CHARACTERISTIC
Vacuum Chamber	• Inside dimensions : $50\ x\ 50\ x50\ cm$ • Volume : $0.125\ m^3$ • Temperature : Up to $200\ °C$ • Ultimate Pressure : $6\ mbar$ in one hour • Leak Rate : $0.2\ mbar/min$
Omega PXM209-006A10V Pressure Sensor	• Accuracy : $0.25\%\ BFSL$ • Excitation : $10\ Vdc$ • Output : $0\ to\ 10\ Vdc$ • Sensitivity : $600\ mbar/V$ • Absolute pressure sensor

7.5. Power Supply

The power is supplied by Delta Electronic power supplies. The test setup uses 4 Delta Elektronika ES030-5 / ES030-10 and 1 Agilent E3631A. The Agilent E3631A is a dual voltage power supply (Figure 74) and it is used for the powering the Lee Valve Spike and Hold Circuit. The 5 Delta Elektronika ES030s (Figure 75) are used for powering the 2 pressure sensors of the propulsion system (chamber + tank pressure), pressure sensor of the vacuum chamber, one for each heater in the thruster and 1 for the load cell. Since the Agilent E3631A is constantly in use at the same voltage levels it is not being controlled by the PC, the DE ES030s on the other hand are controlled using RS-232 connection by the main PC. The specifications are summarized in Table 33.

Figure 74: Agilent E3631A

Table 33: Power Supply Specifications

Characteristics	Agilent ED3631A Output 1	Agilent ED3631A Output 2	ES030-10	ES030-5
Max. Voltage [V]	6	25	30	30
Max. Current [A]	5	1	10	5
Digital IO	RS-232	RS-232	RS-232	RS-232

Figure 75: ES030-5/10 Power Supply

7.6. Control, Data acquisition and Logging

The current interface used during testing is at the functional model level and it is given in Figure 78 where 4 blocks can be identified:

1. Valve control block
2. Heater control block
3. Monitoring block
    a. Temperature Monitoring
    b. Voltage and Current Monitoring
4. Software

The function of each block will be explained in the subsections 7.6.1 through 7.6.4

7.6.1. Valve control block

As the name states this control block is dedicated to the valve. The valve requires 2 voltage levels to operate, a spike and a hold voltage level which differ if a 12 [Vdc] or a 24 [Vdc] version of the valve is being used. The spike and hold circuit is provided by the Lee Company. The connection diagram is shown in Figure 76. It requires 2 power supplies to be connected, one for each voltage level and a TTL control signal which tells the circuit when to open and close the valve. Furthermore on the circuit itself there is a mechanical spike timer set with a potentiometer. In Figure 77 the functional diagram of the valve control block is given. The function of the timer is to change between the spike and hold voltage such that the valve is not damaged from overheating.

The TTL signal is sent using the 5 [Vdc] analog port on the NI USB-6008 DAQ card and the circuit diagram shown in Figure 79 and the circuit itself shown in Figure 80.

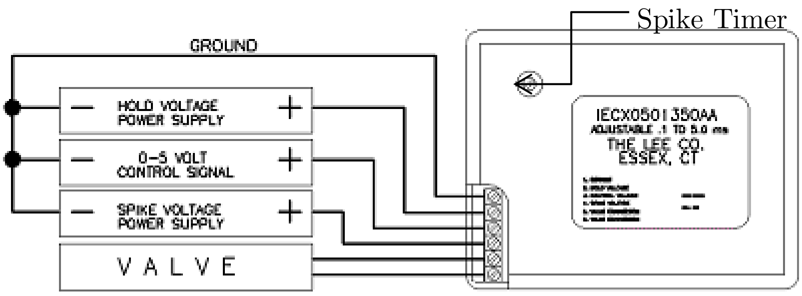

Figure 76: Spike and Hold circuit connection diagram

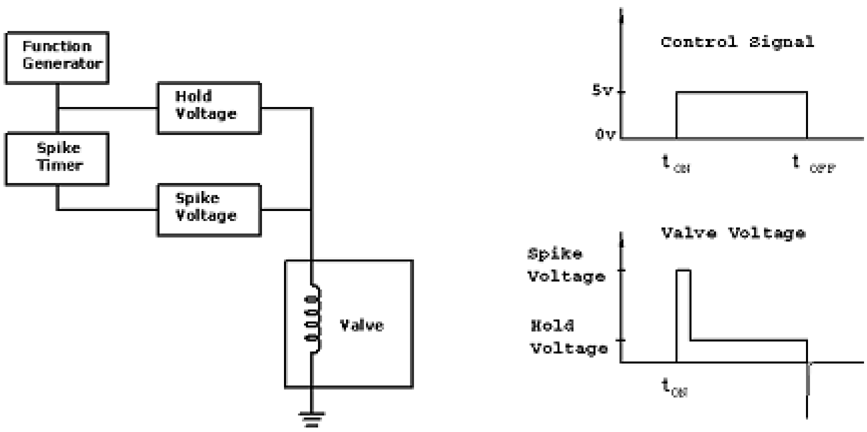

Figure 77: Functional diagram of Valve circuit

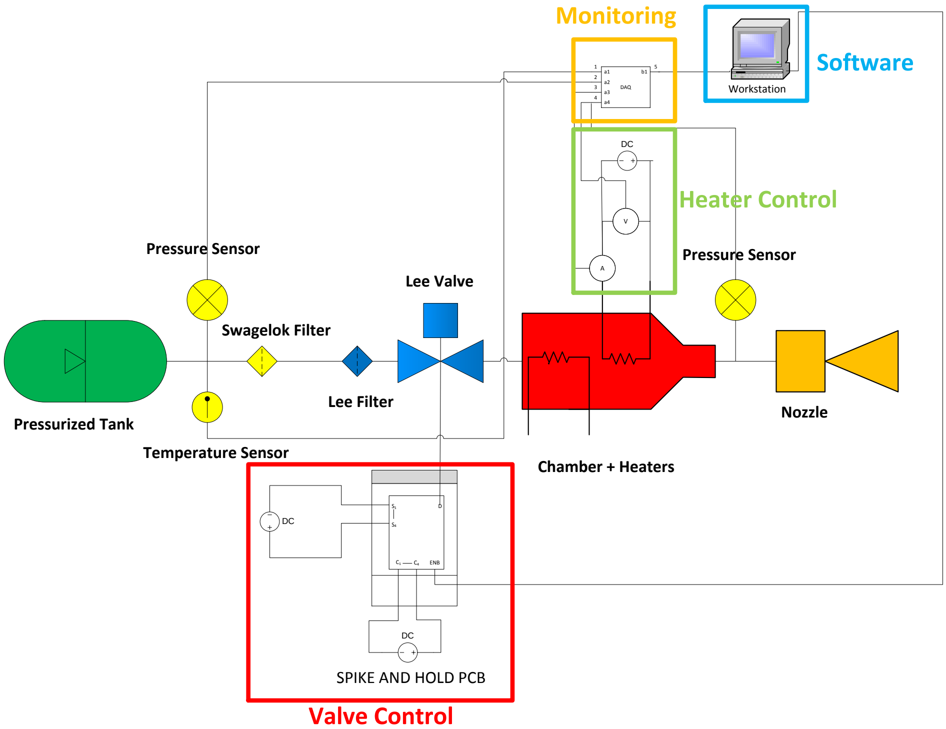

Figure 78: Propulsion System electronic interfaces

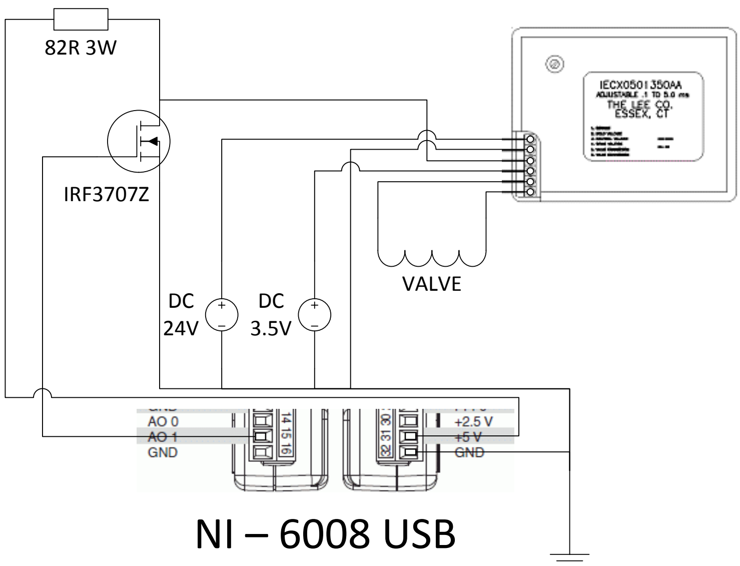

Figure 79: TTL Signal Generator Schematic

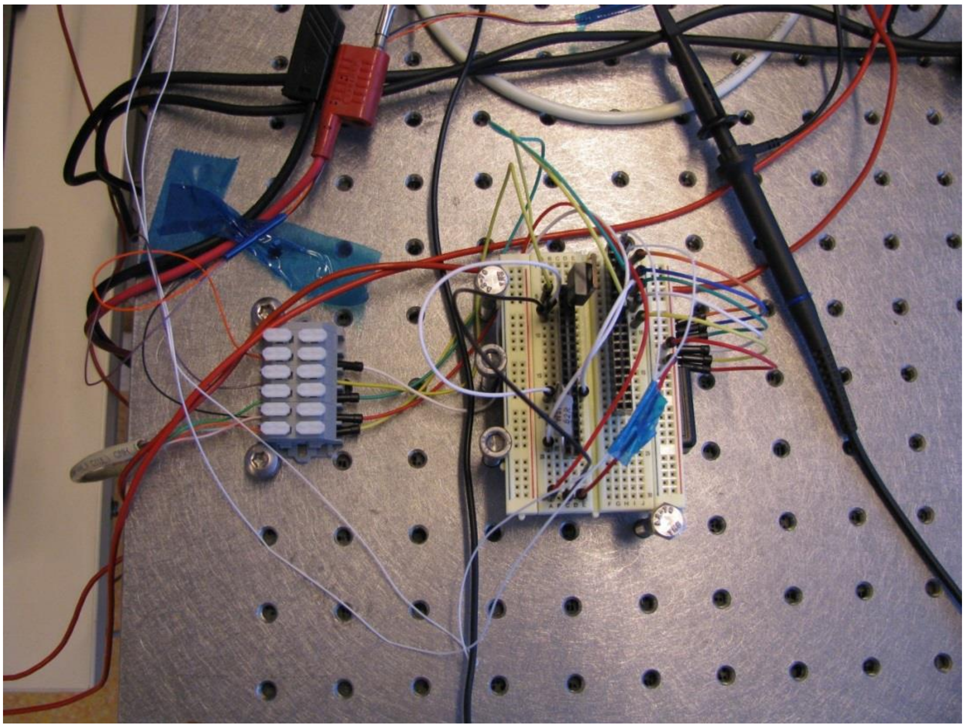

Figure 80: Spike and Hold TTL Signal Generator

7.6.2. Heater control block

The heater control block monitors and control the 2 heaters installed within the chamber. This block can switch both heaters independently on and off, control the voltage level of the two heaters, and monitor the actual (vs. set) voltage level and the current going through the heaters. Furthermore it has a thermocouple conditioning unit that can sense the thermocouple integrated within each heater and thus provide temperature information on the chamber and heaters.

The thermocouples used in the test setup are all K-type thermocouples. They are monitored using a RS-1316 temperature data logger and DHTherm 1.6 for PC interface or NI USB-9211A DAQ Card in combination with LabVIEW. The RS-1316 will be used for standalone temperature tests and it can monitor up 2 thermocouples at the time. All the specifications can be found in [65]. The USB-9211A is 4 channel 24 [Bit] thermocouple input devices, thus 2 are needed for a total of 8 thermocouples. The USB-9211A has wire terminals as input so female thermocouple connectors are needed. Both the RS-1316 and the NI USB-9211A are shown in Figure 81.

Figure 81: RS-1316 (Left) and NI USB-9211A (Right) TC DAQ Card

7.6.3. Monitoring block

The monitoring block currently at this phase consists of 3 NI DAQ Card, namely the NI USB-6008 which has 12-bit ADC and is capable of logging of 10 [kS/s] and two NI USB-9211. The USB-6008 can log single ended voltages from 0 – 10 [Vdc] or differential voltages from -1 – 1 [Vdc] up to -10 to 10 [Vdc]. The DAQ card monitors the voltages of the different sensors, power supplies and heaters. Since the voltage of the load cell is in the order of ± 50 [µV] a more precise multimeter was used for its output, namely a HP 34401a digital multimeter which can also be controlled and monitored with LabVIEW using an RS-232 port.

Figure 82: NI USB-6008 on the left and HP 34401a on the right

Furthermore, as a redundancy, the load cell output is also monitored by the USB-6008 using a Scaime CPJ Rail strain gauge conditioner (Figure 83). This is a signal amplifier that can be adjusted such that the output of the load cell is in a 0 – 5 [Vdc] range which is easily measurable by the DAQ card. Note however the amplifier is both is prone to both drift with time and temperature thus those results are purely there as an extra. To monitor the effect of the spike and hold circuit and the power consumption of the valve an oscilloscope is needed. For this a Tenma 72-8395 was used with a USB interface. Unfortunately it as was not possible to make a driver that will successfully interface with this oscilloscope, however a software was found that can communicate and control the oscilloscope and save graphs directly to the main PC. Finally for monitoring the mass flow or mass change of the system a digital scale was used. The model is Mettler Toledo PB8001-S/FACT and it has RS-232 to communicate with the PC. Unfortunately there were no drivers for this scale in LabVIEW, however using the command list a driver was built from the ground up such that the scale can be controlled and logged using the main PC. The scale is shown in Figure 85 and the complete test setup in Figure 86.

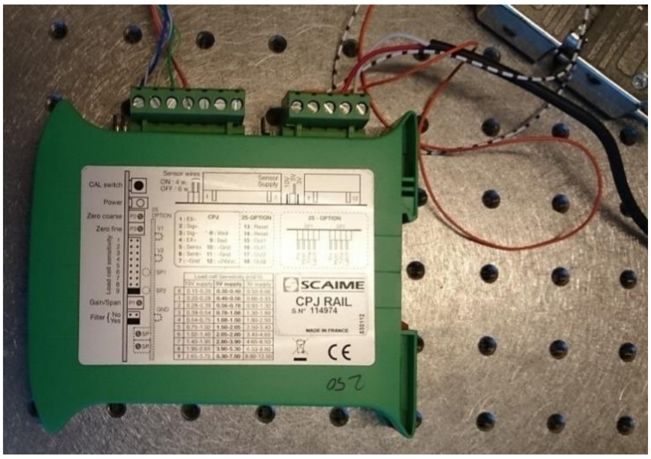

Figure 83: Scaime CPJ Rail Signal Amplifier

Figure 84: Tenma 72-8395 Oscilloscope

7.6.4. Software block

The software block currently consists of LabVIEW program capable of communicating, controlling and monitoring all the different components. It is currently using RS-232 interface to communicate with the different power supplies, valve control block, multimeter and DAQ Cards.

Figure 85: Mettler Toledo PB8001-S/FACT Scale

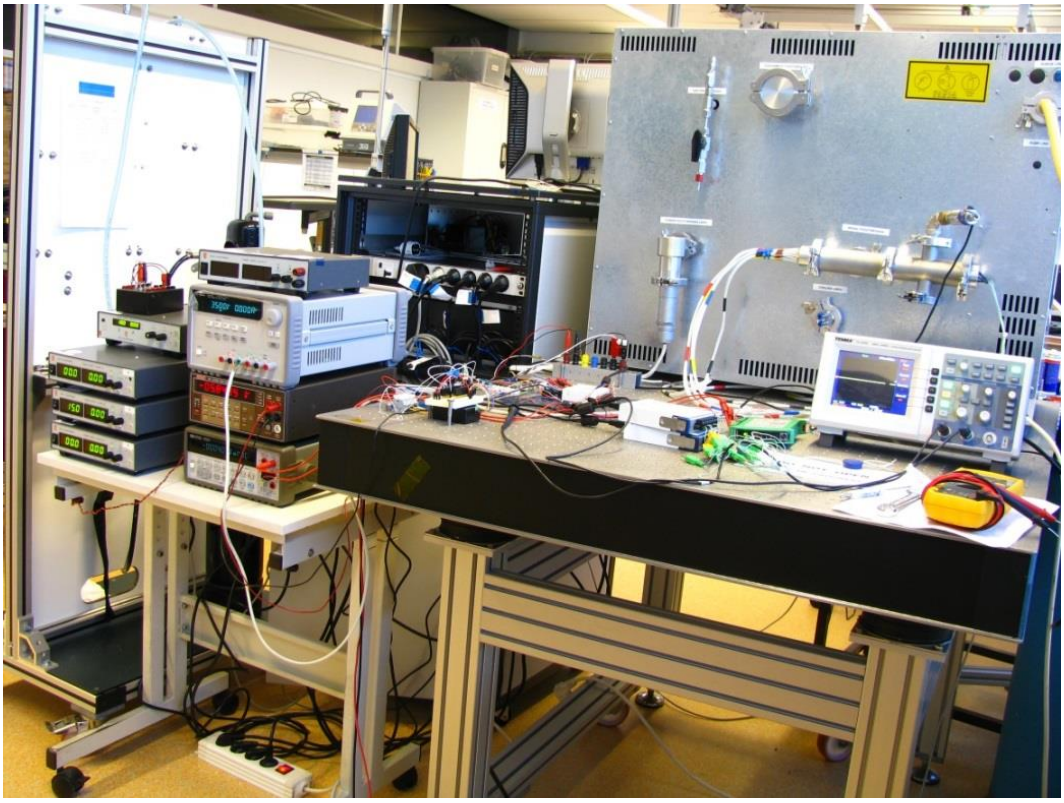

Figure 86: Complete Test Setup

7.7. LabVIEW Software

To control all the hardware and to log the data LabVIEW 2013 was used. Using LabVIEW a program was made that can control up to 4 ES030-5/10 power supplies, a HP 34401a digital multimeter, Mettler Toledo PB8001-S/FACT Scale, one multi-functional DAQ card such as the USB-6008 and up to 2 thermocouple DAQ cards such as the USB-9211A. While some of the components are optional, for the program to run at least a multi-functional DAQ card and the multimeter need to be connected. In the background, the program runs 2 blocks in parallel, one controlling all the power supplies and another controlling all the other components and logging the data. The program was made in such manner due to the fact that the power supply control loop is much slower than the rest of the components used in the test setup and if run coupled with the second block it makes precise data logging impossible. The user interface of the program is shown in Figure 87. The left side (block 1) is used for setting up everything and controlling all the components and the right side (block 2) is used for real time monitoring of different values. Next the different tabs of the LabVIEW program will be explained.

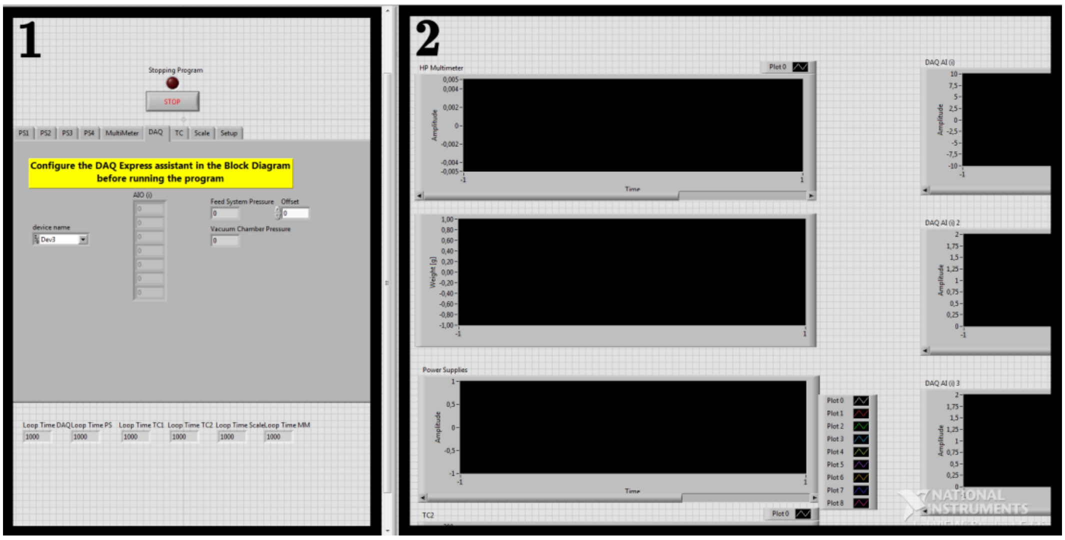

Figure 87: LabVIEW Program UI

7.7.1. Power Supply Tab

The user interface for the power supplies is shown in Figure 88 and it's identical in all 4 tabs. As it was stated previously, up to 4 power supplies can be connected and controlled at the same time. Block 1 in Figure 88 needs to set up for successful communication with the power supplies. The Com port needs to respond to the port connected to the power supply that needs to be controlled and the bit rate and channel to the hardware switches on the ES030-5/10 power supply being controlled. More information about setting up the ES030-5/10 power supplies for remote control can be found in [66]. Once that and all the other parameters have been set-up, the program waits until all the power supplies are enabled or disabled and all tabs are confirmed (Block 2 - Figure 88). When all tabs have been confirmed the program tries to establish contact with the power supply. If successful in Block 3 the light will light up green, and the maximum voltage and current supported by the power supply will be detected and the dials in block 4 will adjust accordingly. Block 4 is also used to control and monitor the voltage and current output. The dials are used for setting the voltage and current output and the digital displays show the actual current and voltage output.

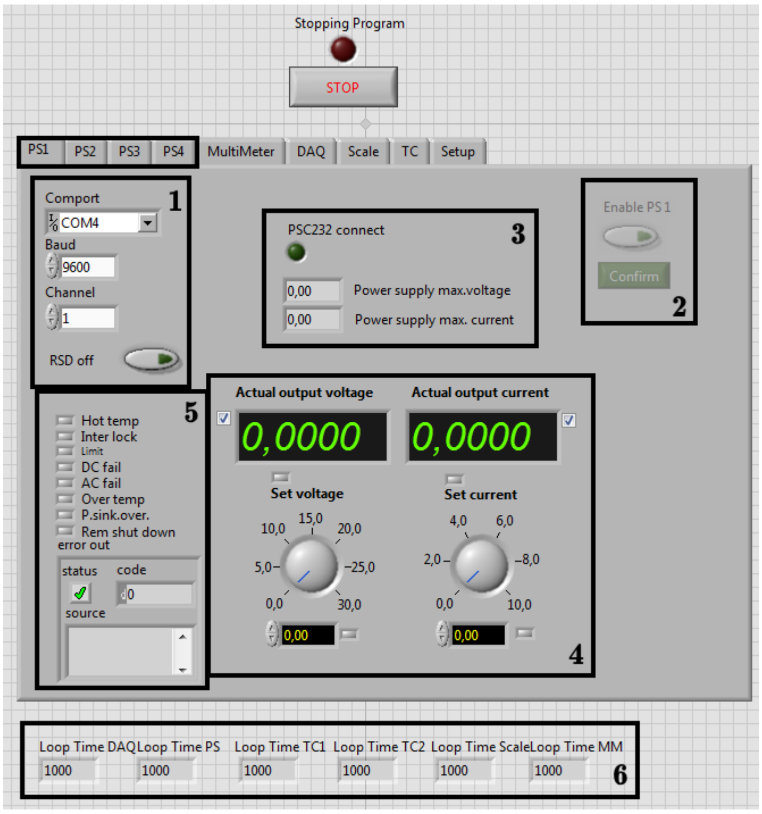

Figure 88: Power Supply Control UI

If the connection is unsuccessful an error message will appear in block 5. Furthermore block 5 is used as a debugging block and will report if any problems are detected with the power supply. Finally block 6 is used to monitor if all control block are in sync and the time (in milliseconds) it takes for one block to be executed. It was noticed due to the nature of the power supply drivers, the more power supplies used the longer the loop would take to run. Therefore it is recommended that only power supplies that have to be controlled on the fly (such as power supplies used to power the heaters) be controlled using the LabVIEW program.

7.7.2. Multimeter Tab

The next tab (Figure 89) is for setting up the HP 34401A multimeter. The multimeter runs in parallel with the scale, the multi-functional DAQ and the thermocouple DAQs and will not start running until confirming the scale tab. The settings in Block 1 need to be correctly setup before confirming as they will be read only once (except of the loop time).

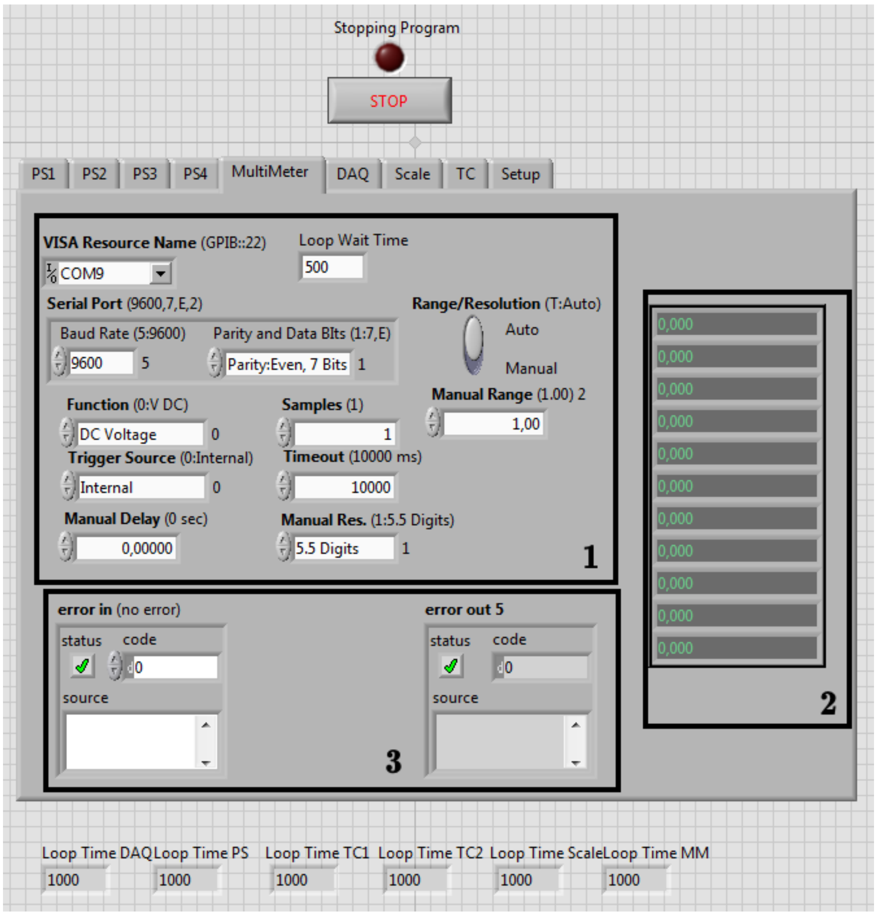

Figure 89: Multimeter Control UI

The VISA Resource Name should be set to the correct Com port where the multimeter is connected and the serial port settings need to be correspond to the settings set on the HP 34401A. The rest of the settings depend on the type of measurements that are desired and more information about them can be found in [67]. Note if auto resolution and scale is used the time between measurements is slower thus this is recommended to be used only if the measured values can have wide range. The loop time is the minimum time between measurements, as the maximum time is depended on the settings themselves. It is recommended that the loop times of the multimeter, DAQ cards and the scale be equal. In the array in block 2 the last measurement is shown and block 3 is used for debugging and to display error messages.

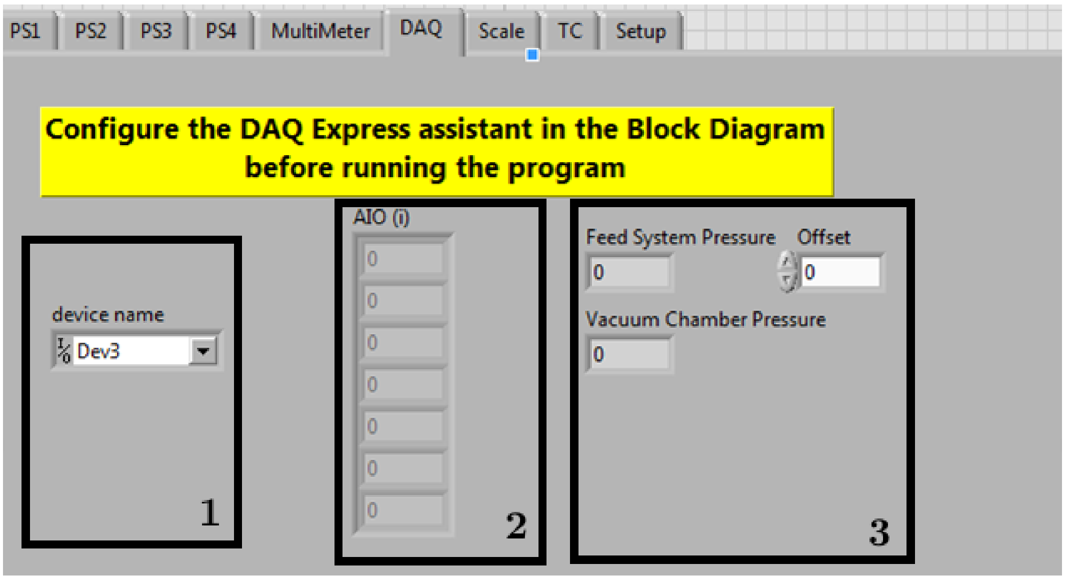

Figure 90: DAQ Card Tab

7.7.3. Multi-functional DAQ Card Tab

The multi – functional DAQ card is shown in Figure 90. The front end of this tab is basic since most of the setting up is done in the back end. If the same test setup is preserved the only setting that needs to be done is making sure if the device name (Box 1) is the actual multi – functional DAQ card used and connected and not another DAQ card (example the DAQ cards used for the thermocouples). In Box 2 the raw values will be shown of the voltage read at the connected analog inputs and in Box 3 the feed system and vacuum chamber pressure will be calculated using previously established equations.

If the previous test setup has been changed or the calibrated values of the sensors are not valid anymore the user needs to change values in the program. Box 2 in Figure 91 converts the voltage values of both pressure sensors to a pressure value from a calibration curve previously established. The current equations used are given in(4.3). Note that this is only for display purposes to ease operations and the values are saved in the raw output from the sensors (In the current setup that is Volts).

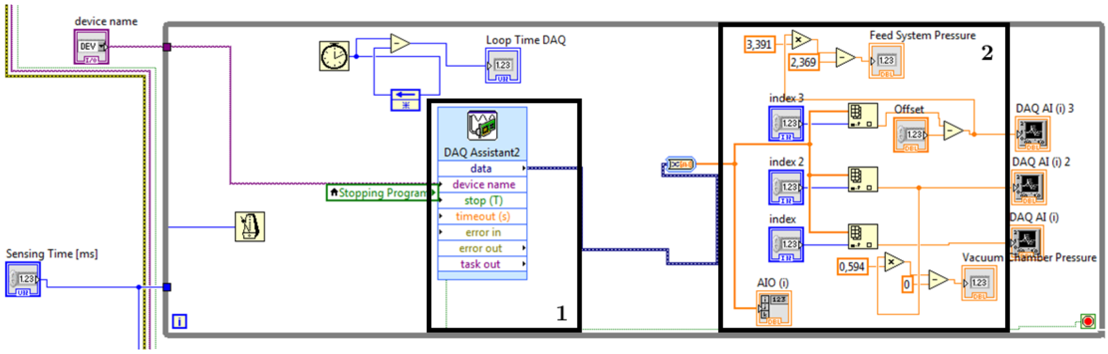

Figure 91: DAQ Card Program

$$
\begin{aligned}
P_{[bar]} &= V_{[volts]} \times A + B \\
P_{feed} &= 3.391 \times V - 2.369 \\
P_{vacuum} &= 0.594 \times V - 0
\end{aligned}
\tag{4.3}
$$

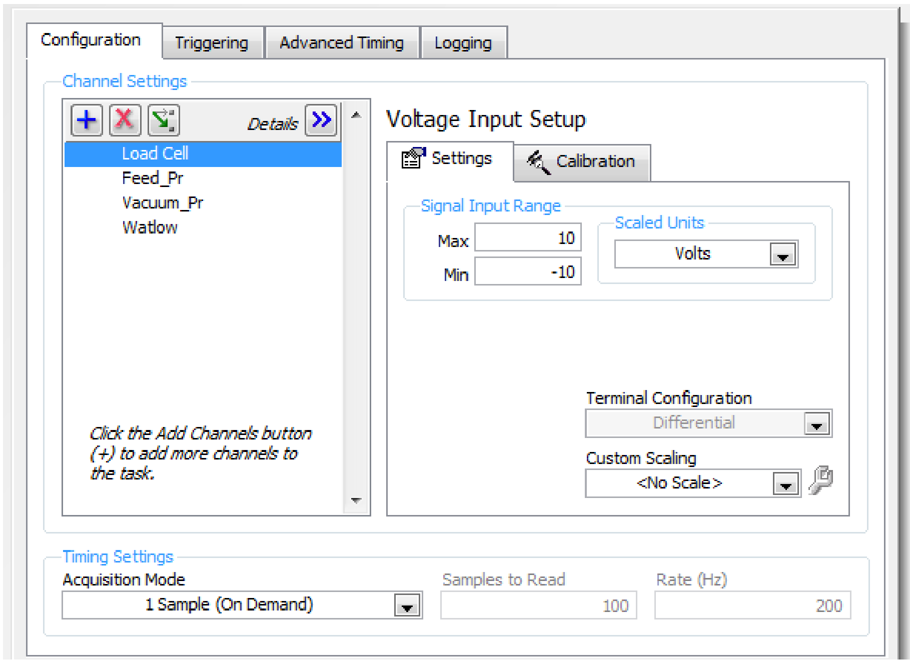

Figure 92: DAQ Assistant

Furthermore if the sensors are connected differently, or different sensors or DAQ card is used the DAQ Express Assistant needs to be activated again (Box 1) to complete the initial setup. Double clicking on the DAQ Assistant block will show a window as given in Figure 92 where every channel can be setup by giving it a name, type of measurement, range and acquisition model. Furthermore if unsure about how to connect the hardware or to double check if everything is connected correctly, the connection diagram can be used (Figure 93).

Depending on the channel and the type of measurement used the DAQ Assistant connection diagram will show which outputs of the DAQ card should be connected and in what manner. It is a very useful tool incorporated into LabVIEW.

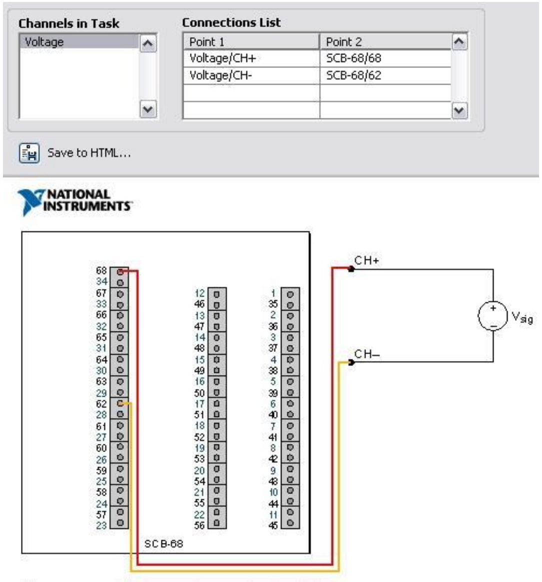

Figure 93: DAQ Assistant Connection Diagram

7.7.4. Mettler Toledo Scale Tab

The Scale tab is shown in Figure 94. Except for the power supplies all other tabs will wait for the scale tab to be confirmed before starting. This was done since if the scale is to be used it needs to do internal calibration and zeroing which takes about 30 [s] and could render otherwise the scale block out of sync with the rest of the blocks. If the scale is not being used in the current test setup then just by pressing confirm in Block 2, all other settings are ignored and the program continues. If the scale needs to be used, Block 1 needs to be set-up first such that it corresponds to the correct COM port where the Mettler Toledo scale is connected and the same port settings as set on the scale. For how to check the current settings of the serial port on the scale and set them as needed please refer to the manual [68]. Once the settings have been set the scale can be enabled and the choice needs to be confirmed in Block 2. When the choice has been confirmed the scale will undergo internal calibration and zeroing. Note that no mass should be placed before the internal calibration and zeroing has completed. After the initial setup the scale makes measurements in grams equal to the sensing time set for all the loops and this is displayed in Block 3. If zeroing is needed (because of putting some mass for example), the zero switch can be pressed and the scale will return zero on the next measurement and measure the change in mass from that zero point.

Due to the nature of the measurements and the potential high sensing rate (in the order of few hundred milliseconds) by default the program uses the SI command (send current net value regardless of balance stability [69]). This means that vibration, jolts or movements of the components or table where the scale is set can momentarily affect the measured mass as well. The program has a simple option of making a change if the stable weight (command S) or unstable weight (command SI) is required, namely in the program the value in Block 1 Figure 95 needs to be 0 for SI or 1 for S. The drivers had to be written from the ground up so if different commands needs to be sent or additional options are required please refer to [69] for all the available commands. With some understanding of LabVIEW, the current command block can be used as a baseline and with just changing the command send, in theory, new functionally can be added.

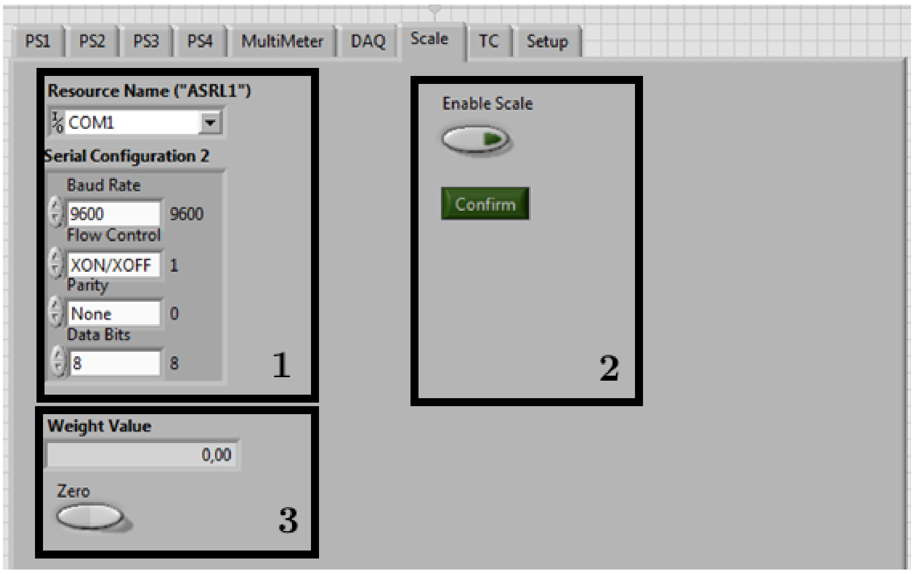

Figure 94: Scale Tab

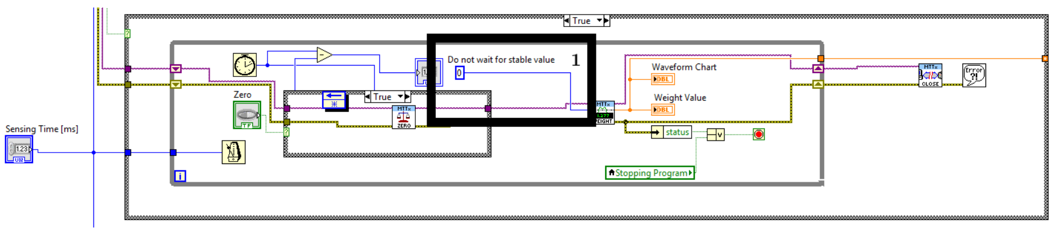

Figure 95: Scale LabVIEW Program

7.7.5. Thermocouple DAQ Cards Tab

The LabVIEW program has the capability to interface with up to 2 thermocouple DAQ cards. Using 2 NI USB-9211A cards, which are available at the MeetShop of TU Delft, up to 8 thermocouples can be logged at the same time which has been considered adequate for these tests. If more than 8 thermocouples are required, either the program needs to be expanded with more TC DAQ card block (which can be done fairly easy with just copying the current blocks) or a DAQ card with more TC terminals should be used. The TC DAQ Card tab is shown in Figure 96. As with the multi – functional DAQ card tab given in Section 7.7.3 the cards are configured using the DAQ Express Assistant. DAQ Assistant 3 corresponds to TC DAQ 1 and DAQ Assistant 4 corresponds to TC DAQ 2 (Figure 97). The default measurement type is on demand in Kelvin and K-Type thermocouples are measured. Once again using the DAQ assistants the type of thermocouples and measurements needs to be set if changed from the default. In the tab one must ensure if the device address corresponds to the actual address of the TC DAQ Card (Block 1 in Figure 96). In Block 2 the value of the thermocouples are displayed. If a TC is not connected or broken an abnormally high temperature value will be displayed. For example when set to K-type TC a value of 2358 [K] was displayed on an open port.

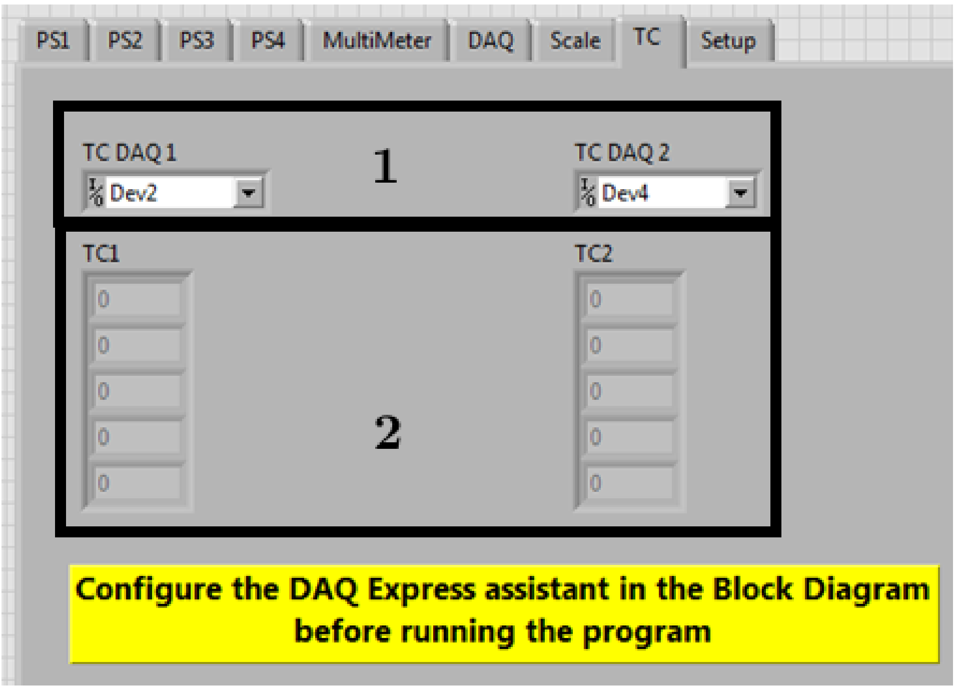

Figure 96: TC DAQ Card Tab

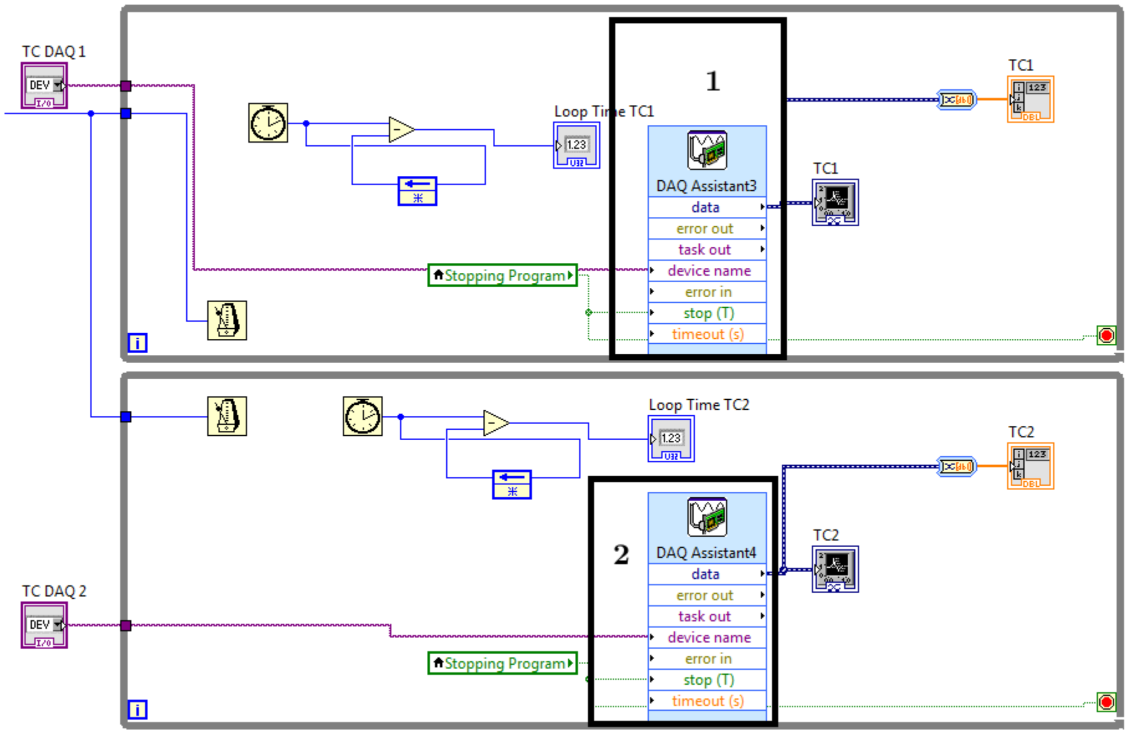

Figure 97: TC DAQ Card Program

7.7.6. Setup and Control Tab

The last tab in the LabVIEW program is used for setting up the data-logging and controlling the thruster and it is shown in Figure 98. In Block 1, the sensing time of every component and the logging time can be set. Note that this is the minimum sensing time and some components may take longer (depending on the settings). If synchronous measurements are to be guaranteed, the minimum sensing time should be set higher than the slowest components. The sensing time of all components is displayed in Block 3. Furthermore in Block 1, a test name can be assigned which will be displayed in the logged file and file path to specify where the file is to be saved. The saving of the data starts once the save data button is pressed and the saving data led lights up green. Once the saving starts the saved data points and the elapsed time is also shown in Block 1.

In Block 2 the valve and different power supplies can be controlled. The valve is controlled using the thrust switch and the thrust time. First the thrust time is set to the desired time the valve should be open and the thrust switch is toggled. The multi – functional DAQ Card the sends a signal to the circuit shown in Figure 80 which in turn turns on the spike and hold circuit and the valve is actuated. Obviously the spike and hold circuit needs to be powered separately as explained earlier in Section 7.6.1 for the valve to open. Sometimes there can be a difference of few milliseconds until the circuit reacts and close the valve therefore the actual elapsed time is also shown. While the valve is open the Thrusting led will be lit up green.

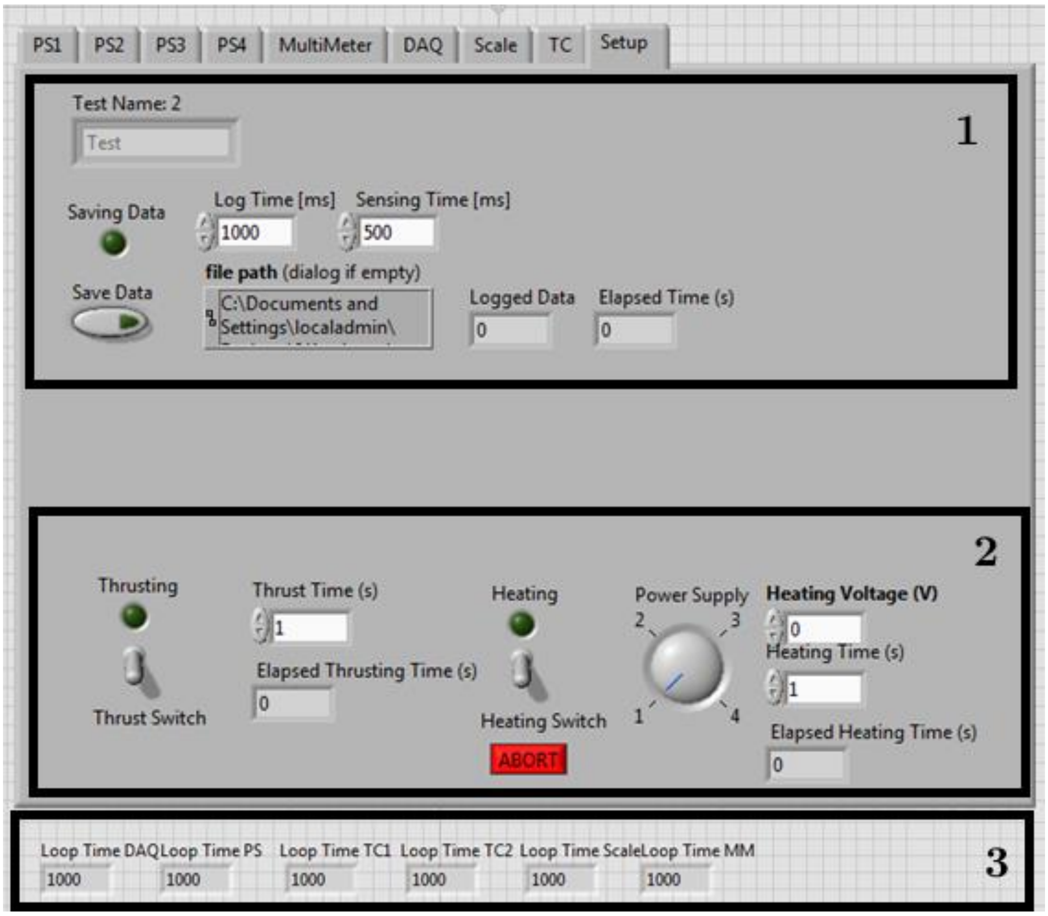

Figure 98: Setup and Control Tab

The heating of the thruster is also controlled in this tab by controlling the power supplies in Block 2. First the correct power supply needs to be chosen using the knob with 1 to 4 corresponding to power supply (PS) 1 to 4 respectively. Next the desired heating voltage is set and the heating time. When ready the heating is started by toggling the heating switch. As mentioned earlier the power supplies can have up to few seconds delay before receiving and acknowledging the command. When the power supply actually acknowledges the command and sets the desired voltage level, the heating led will lit up green and the elapsed heating timer will start counting. There can be difference between the desired and actual heating time by up to few seconds but this is not considered crucial for the testing since the heating time is normally in the order of few hundred seconds. Finally if the temperature is gets too high or for some reason the thrusting or heating needs to be aborted immediately there is an abort button that will close the valve and turn off the power supply straightaway.

Initially a control loop was also envisioned that would modulate the voltage level or the power supply on-off automatically as to achieve a desired temperature. However due to time constraints this was not possible to be incorporated in the current version of the LabVIEW program and therefore if the operator wants to maintain a certain temperature level for longer period of time, the power supply or voltage level will need to be changed manually.

8. Test Campaign

In this chapter the test plan and specific changes to the test setup are given for each planned test. For the test campaign of the EM thruster the following tests are planned:

- Components Test
    - Heater
    - Valve
- Feed System and Thruster Assembly and Inspection
- Propulsion System Test
    - Leak test
        - Feed System
        - Thruster
    - Mass Flow Test
    - Heating test
    - Calibration of thrust bench
    - Thrust test
    - Pressure drop test
    - Post inspection of the thruster

The engineering model of the propulsion system has two components that can be tested separately, namely the valve and the heaters. Testing the components separately will allow better characterizing them and checking if there are any differences between the specified and actual performance.

When all the components are tested the thruster and feed system need to be assembled and integrated and inspection should be made of the assembly. The first test to confirm a good assembly and integration is to have both the feed system and the thruster leak tested. Next the mass flow through the valve at different pressures is tested. This will useful to know later in the thrust test to know how much water has been injected in the chamber. Following the mass flow test is the heating test which will provide data on the temperature achieved in the chamber and heating and cooling time required using different mediums (empty, nitrogen gas or water) and at different power levels. Following logical flow of the different tests, the next test would be the pressure drop test in the chamber due to the porous media. However since the thruster needs to have a connector exchanged for this test, which may damage the thruster (and render the leak data generated earlier useless_ this test is left for last. Instead the thrust bench is first calibrated and then the thruster is tested for thrust levels at different pressures and power levels. When the thrust test is completed the pressure drop test is made as to have all the information available to calculate the efficiency of the nozzle. Finally a post testing inspection is made of the thruster.

8.1. Heater Testing

The heaters will be tested to verify if there are any deviations from the stated specifications, to check the heating and cooling time required and the temperature that can be achieved. They will be tested at 2 power levels, namely at their maximum power level and the power level at which they would be used in the satellite. The goal of this test is to gain experience with the testing equipment and find the set and actual voltage level and the resulting input power of the heaters. Furthermore a heating and cooling graph will be obtained which while not representable for when the heater will be incorporated in the thruster it will give first indication of the each heater performance.

8.1.1. Test Setup and Procedure

For this test since only temperature measurements where required, the RS-1316 was used in combination with DHTherm 1.6. The heaters where placed inside the vacuum chamber and tested in both ambient and vacuum conditions. The test was done in the following manner:

- Start logging every 2 seconds
- Log for 1 minute at ambient conditions, heater unpowered
- Turn on heater at desired power level for 10 minutes or when
- Turn of the power supply after 10 minutes and wait until the heater has reached < 30 [°C] or 10 minutes has passed (whatever comes first).

The test setup is shown in Figure 99. Due to the long wires from the power supply to the heater inside the heater chamber, a significant voltage drop was observed. Therefore a feedback loop was made as to monitor the set vs actual voltage. Furthermore due to the large currents of the Elstein heater at 12 [V] and the possibility of overheating the wires when in vacuum, the current had to be split by using to cables in parallel.

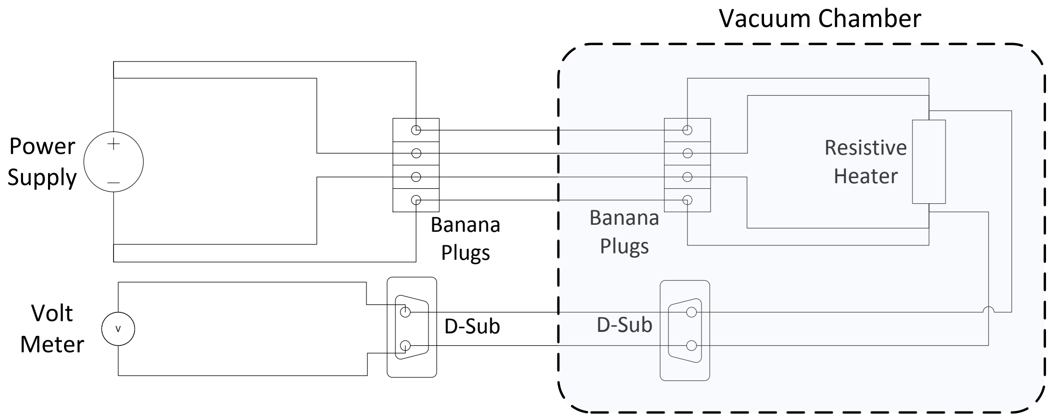

Figure 99: Heater Test Setup Schematic

8.1.2. Test Results and Deliverables

Two example test results are shown in Figure 100 and Figure 101. Since the Elstein is an IR heater, a lot more heat was lost in the environment and the heater itself achieved a lower temperature for the same power level. The Watlow heater on the other hand achieved much higher temperature but it is expected that the stay time of the water should be increased in the chamber to have this extra heat effectively transferred to it. The results are given in Table 34

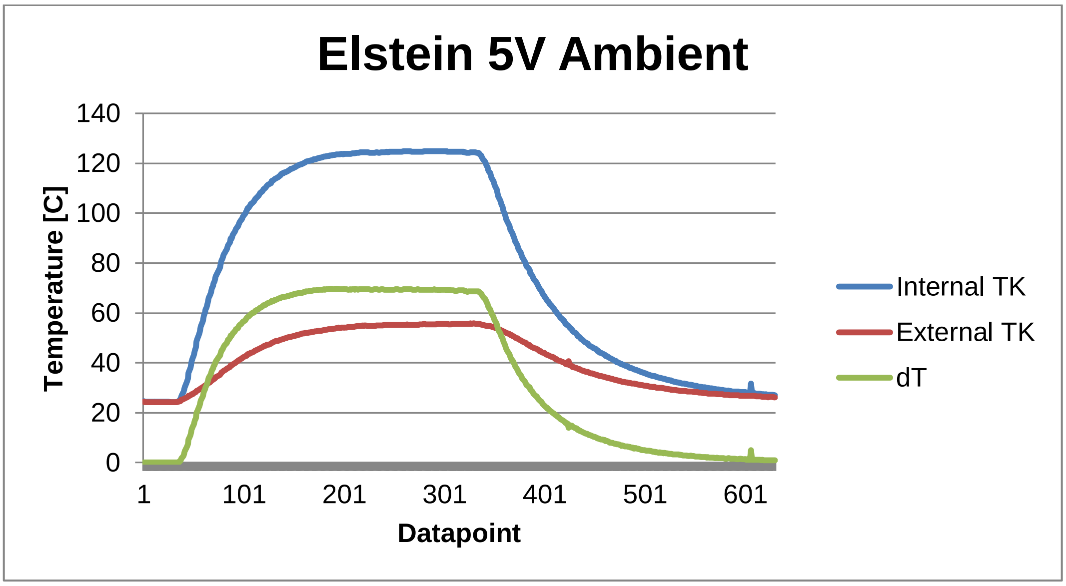

Figure 100: Example Elstein Test Data

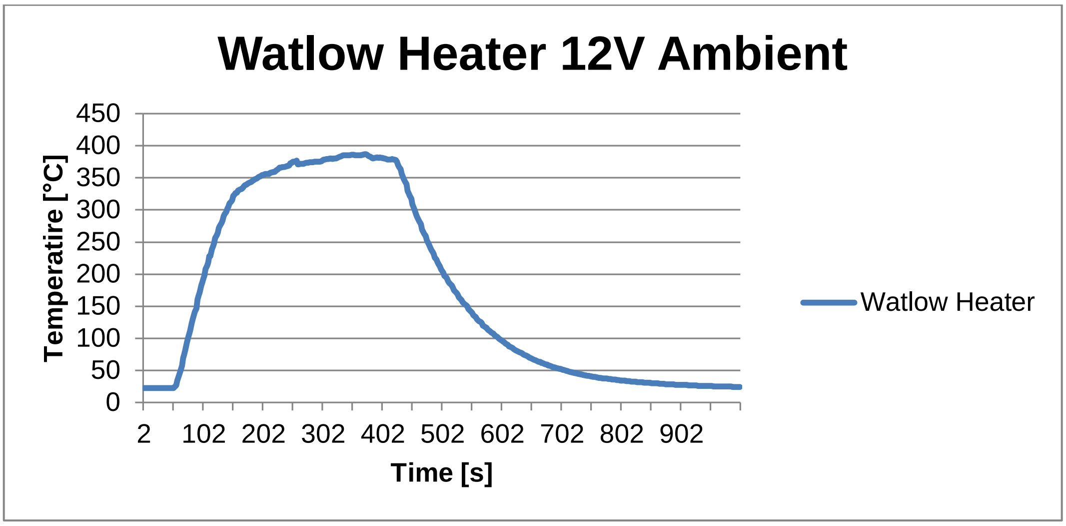

Figure 101: Example Watlow Test Data

Table 34: Heater Test Results

Heater	V_{set} [Vdc]	V_{read}[Vdc]	Power [W]
Watlow	12.2	12	7
Watlow	24.8	24	28
Elstein	5.6	5	8
Elstein	13.8	12	45

This test was deemed successful since the different power levels and voltage levels were determined for both heaters and the functionality of the test setup, thermocouple data loggers and DAQ Cards.

8.2. Valve Testing

The valve will be tested to check if it can hold pressures up to MEOP, the opening current, voltage spike and spike time required will be investigated at MEOP. The valve tested will be the INKX0514300AA4 which is the 24 [Vdc] version of the valve. The reason why this valve was chosen is that there are currently 2 in inventory, whereas only 1 INKX0514300AA5 is available and if the valve were to get damaged during testing there is a replacement. If the test setup and equipment prove to be benign the INKX0514300AA5 can easily be re-tested as to give an impression of what sort of requirements the flight model valve would impose to the EPS and electronics of the DelFFi satellite. The goal of this test is to determine spike time required to open the valve at MEOP and voltage levels for the spike and hold circuit. Furthermore it will validate that the TTL signal generator circuit and the LabView program are correctly made.

8.2.1. Test Setup and Procedure

For this test the Tenma 72-8395 was used. The probes have to be connected to both pins of the valve coil and the ground. The system is pressurized up to 8 [Bar] and then the spike time is increased until the valve opens reliability at least 3 times for a period of 1 [s]. The test setup is shown in Figure 102.

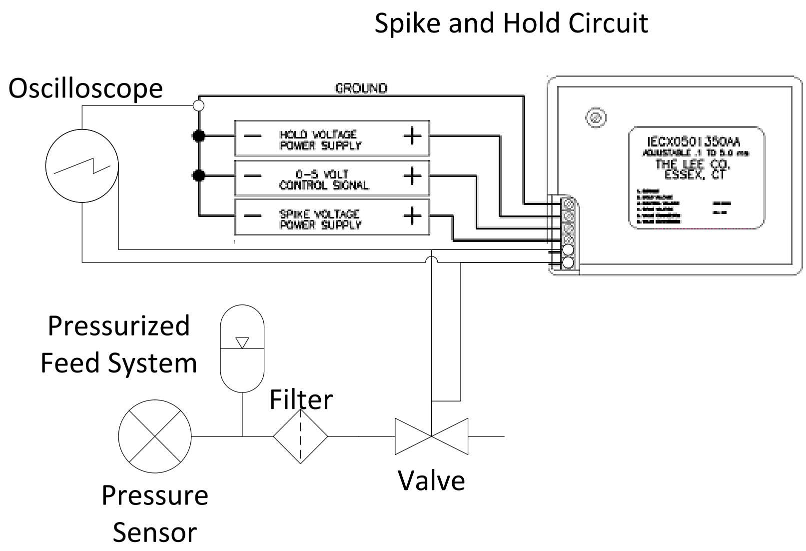

Figure 102: Valve Test Setup Schematic

8.2.2. Test Results and Deliverables

The results of a test performed at 8 [Bar] is given in Figure 103 and Figure 104 . It can be seen that the valve is powered for 0.6 [ms] at 24 [V] and then the valve remains open at 3.2 [V]. The minimum spike time for the valve to reliably open was found to be 0.3 [ms] but during testing a margin was added (safety factor of 2) to ensure that the valve will have enough power to open every time. The test was deemed successful because the minimum spike time was successfully determined and TTL signal generator circuit and the test setup was validated.

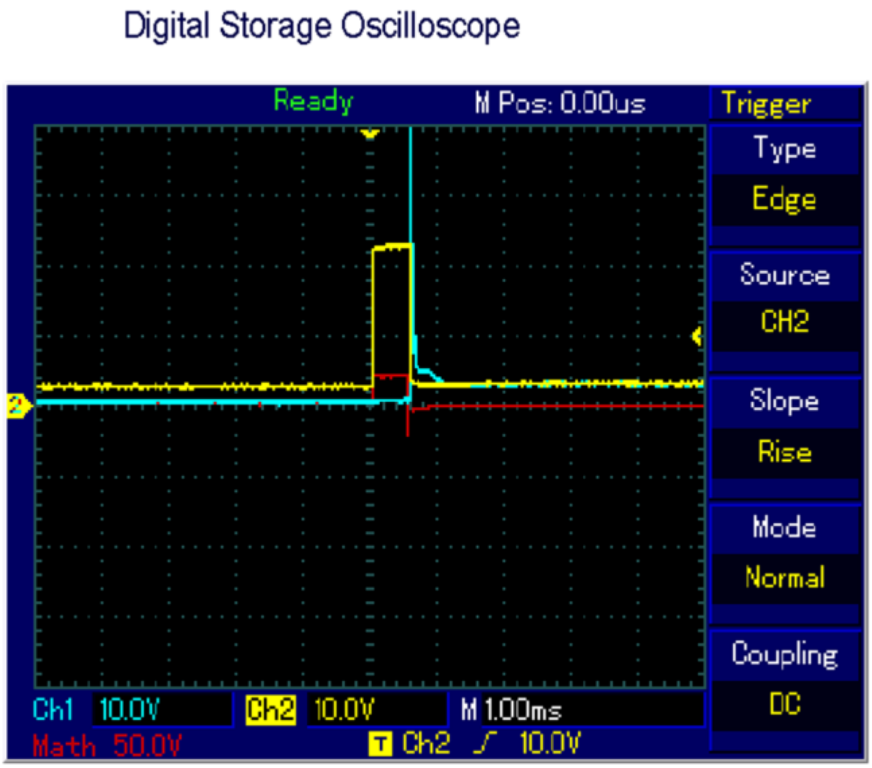

Figure 103: Oscilloscope Capture

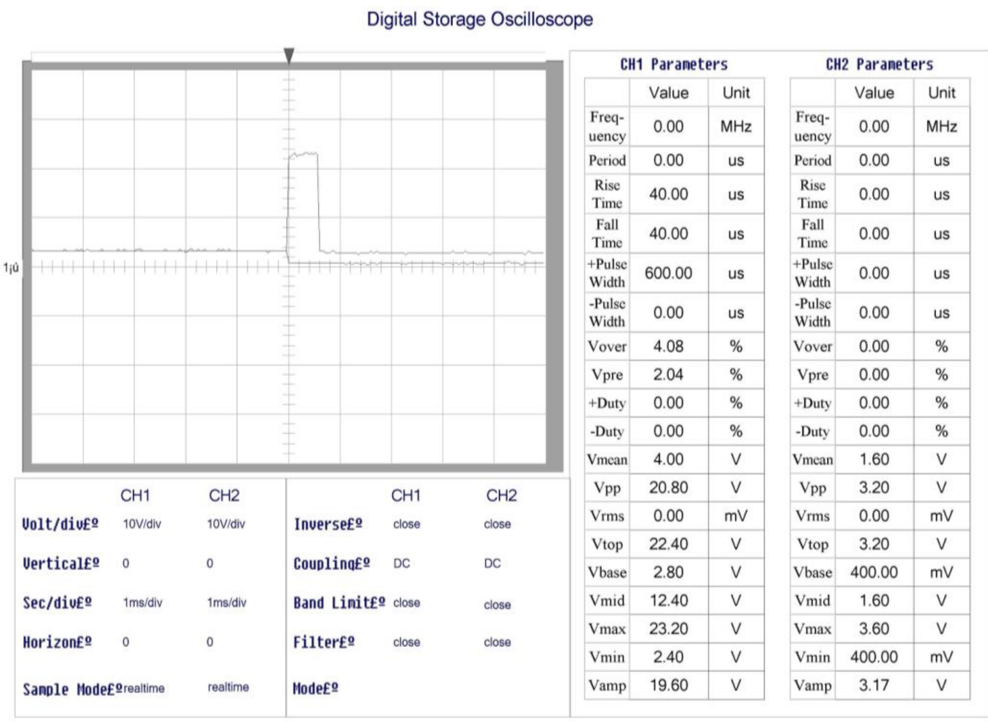

	CH1	CH2		CH1	CH2
Volt/div£º	10V/div	10V/div	Inverse£º	close	close
Vertical£º	0	0	Coupling£º	DC	DC
Sec/div£º	1ms/div	1ms/div	Band Limit£º	close	close
Horizon£º	0	0	Filter£º	close	close
Sample Mode£º	realtime	realtime	Mode£º		

CH1 Parameters

	Value	Unit
Frequency	0.00	MHz
Period	0.00	us
Rise Time	40.00	us
Fall Time	40.00	us
+Pulse Width	600.00	us
-Pulse Width	0.00	us
Vover	4.08	%
Vpre	2.04	%
+Duty	0.00	%
-Duty	0.00	%
Vmean	4.00	V
Vpp	20.80	V
Vrms	0.00	mV
Vtop	22.40	V
Vbase	2.80	V
Vmid	12.40	V
Vmax	23.20	V
Vmin	2.40	V
Vamp	19.60	V

CH2 Parameters

	Value	Unit
Frequency	0.00	MHz
Period	0.00	us
Rise Time	0.00	us
Fall Time	0.00	us
+Pulse Width	0.00	us
-Pulse Width	0.00	us
Vover	0.00	%
Vpre	0.00	%
+Duty	0.00	%
-Duty	0.00	%
Vmean	1.60	V
Vpp	3.20	V
Vrms	0.00	mV
Vtop	3.20	V
Vbase	400.00	mV
Vmid	1.60	V
Vmax	3.60	V
Vmin	400.00	mV
Vamp	3.17	V

Figure 104: Valve Test Results

8.3. Feed System and Thruster Assembly Inspection

With the components tested, next the feed system and thruster where assembled and inspected. Teflon tape was used on every thread except of the MINSTAC. The temperature sensor for the liquid was installed by the DEMO workshop due to the thread being not manufactured correctly. For the leak test a M2 screw was inserted into the threaded hole for the nozzle. After the leak test the nozzle was installed. Due to the small size, it was not possible to use Teflon tape but high temperature silicon rated up to 300 [°C] (Figure 105) was used to make sure the connection is leak tight. The nozzle was inspected under a microscope to ensure that the throat is clear from obstructions (Figure 106).

Figure 105: Bison High Temperature Silicone

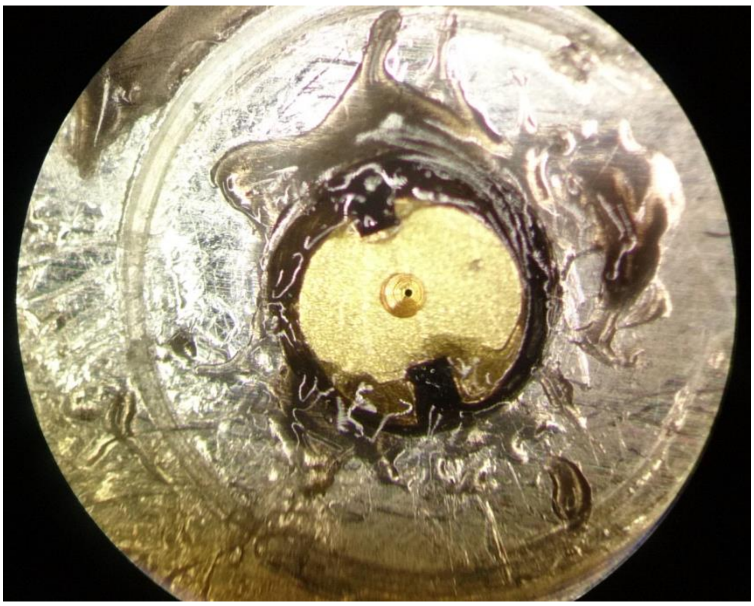

Figure 106: Nozzle Inspection

8.4. Leak Test

Next a Leak Test will be done to both the feed system and the thruster. The feed system will be tested using only nitrogen and after the initial identification of leaks will be tested inside the vacuum chamber. For convenience the leak test of the thruster was done in atmospheric conditions as it is easier to inspect it. It was decided to leave 1 [Bar] margin when testing the valve due to reports that the previous valve may have been damaged. When the thruster and the feed system are tested in ambient a caution will be made that instead of MEOP, they are pressurized at MEOP + 1 or 7 [Bar] as to have the same pressure difference as when used at MEOP in vacuum. Two leak rates will be investigated, namely gas leak rate and liquid leak rate with the latter being more important. For the gas leak rate the chamber is filled using nitrogen, and for the liquid leak rate the chamber is filled using demineralized water and pressurized with nitrogen.

The goal of this test is to determine the leak rate of both the feed system and the thruster. Ideally the leak rate of the feed system should be lower than the requirement of the valve given in Section 4.1.1 and the leak rate of the thruster should be an order of magnitude lower than the mass flow as calculated in Section 5.5. This is to ensure that the majority of the propellant will flow through the nozzle and not leak into the environment and thus render the thrust measurements unusable.

8.4.1. Test Setup and Procedure

The feed system was tested up to and including the valve. When the gas leak rate was tested the water filling branch was closed, the system was pressurized and the quick release connection disconnected. The valve was unpowered, thus closed and measurements were taken over the course of several hours. For the liquid leak rate the system was first filled with predetermined amount of water and then pressurized.

When measuring the thruster leak test, the thruster was completely shut by screwing a M2 screw in the threaded hole intended for the nozzle. The valve was removed from the feed system as to avoid being powered and open for an extended period of time. Again both gas leak rate and liquid leak rate where tested. The test setup is shown in Figure 107.

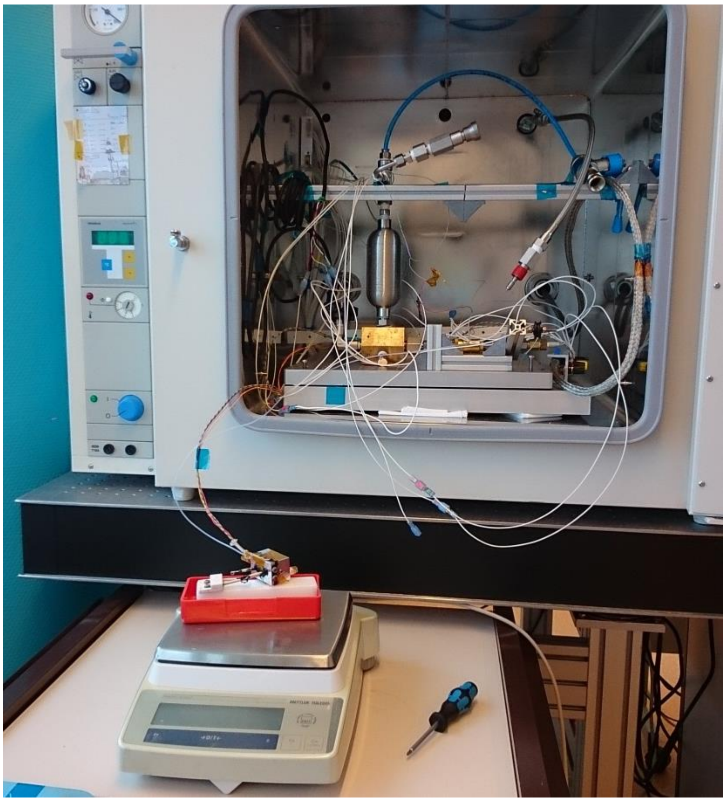

Figure 107: Leak Test - Test Setup

8.4.2. Test Results

The feed system was first tested in ambient pressure. After it was left overnight a pressure drop was detected in the system (Figure 108). Upon inspection this was due to a bad connection between the plug and the hexagon. This was fixed and in a later test done in vacuum where after setting the initial pressure to 6.34 [Bar] after 14 hours the total pressure drop was only 40 [mbar] down to 6.30 [Bar]. These results are shown in Figure 109.

The first test of the thruster was a complete failure. The thruster was not able to hold pressure even for few minutes and was leaking from the whole contact surface between the cap and the chamber. Therefore silicon was applied throughout the connection area with the thruster ending up looking as shown in Figure 110

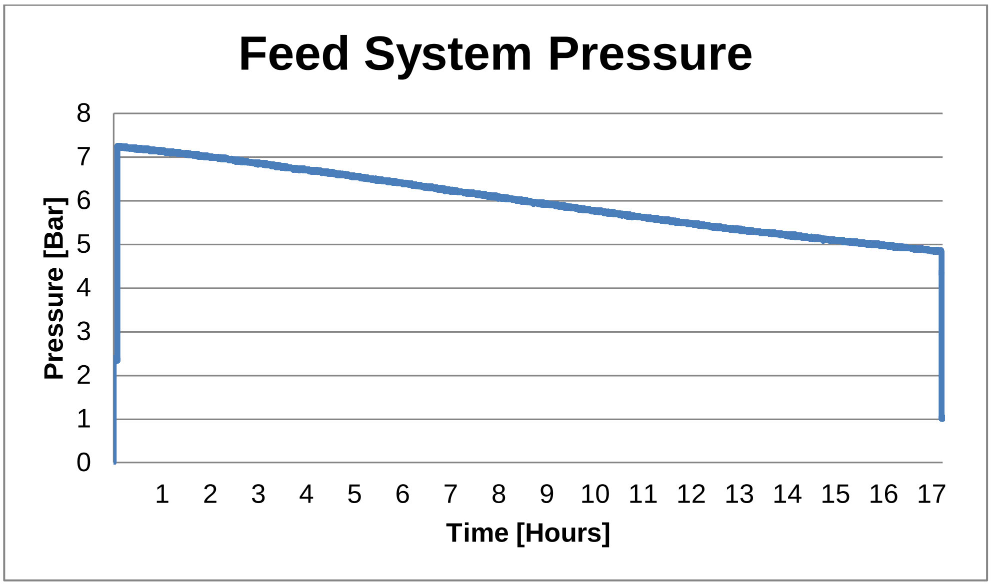

Figure 108: Feed System Leak Test 1

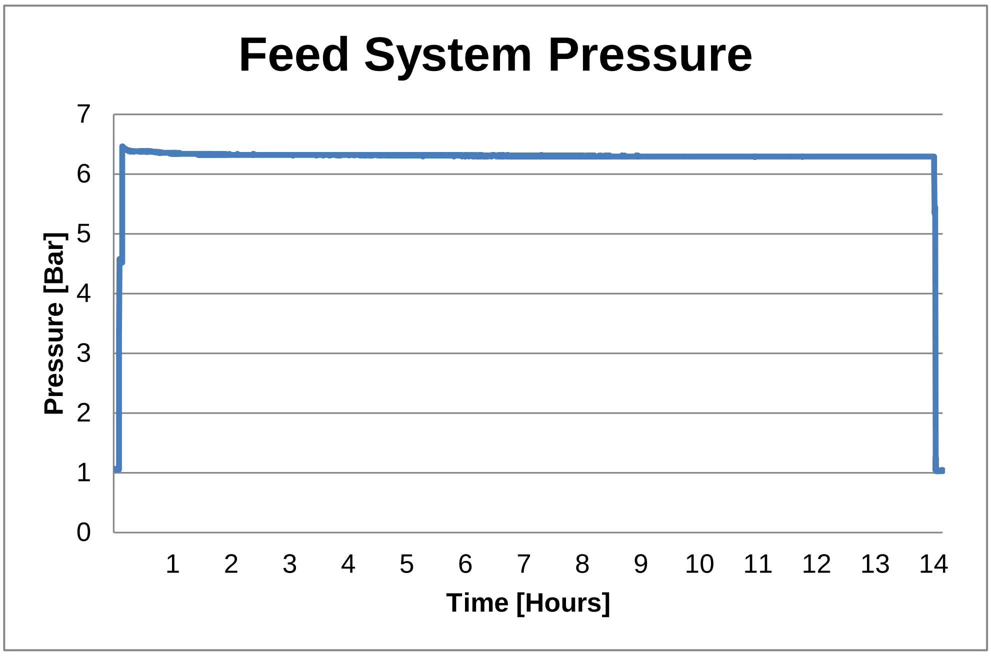

Figure 109: Feed System Leak Test 2

.

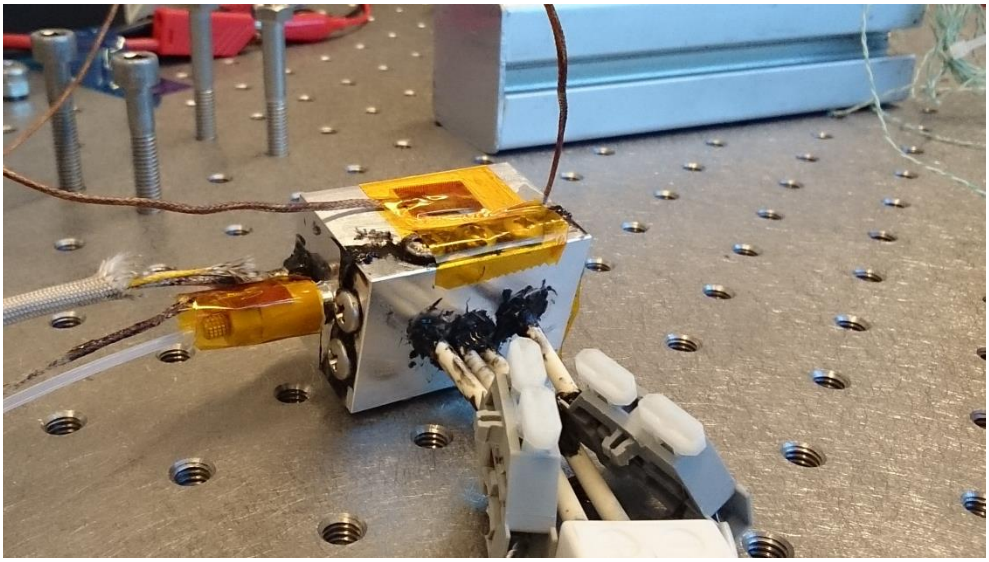

Figure 110: Thruster with silicon applied

Never the less there was still gas coming out from the leads of the Elstein heater. After several unsuccessful tries to stop the leak this test was abandoned and a water leak test was made. However the same happened again but at a much slower rate. Water was still dripping through the leads as it can be seen in Figure 111. The results from the test are given in Figure 112.

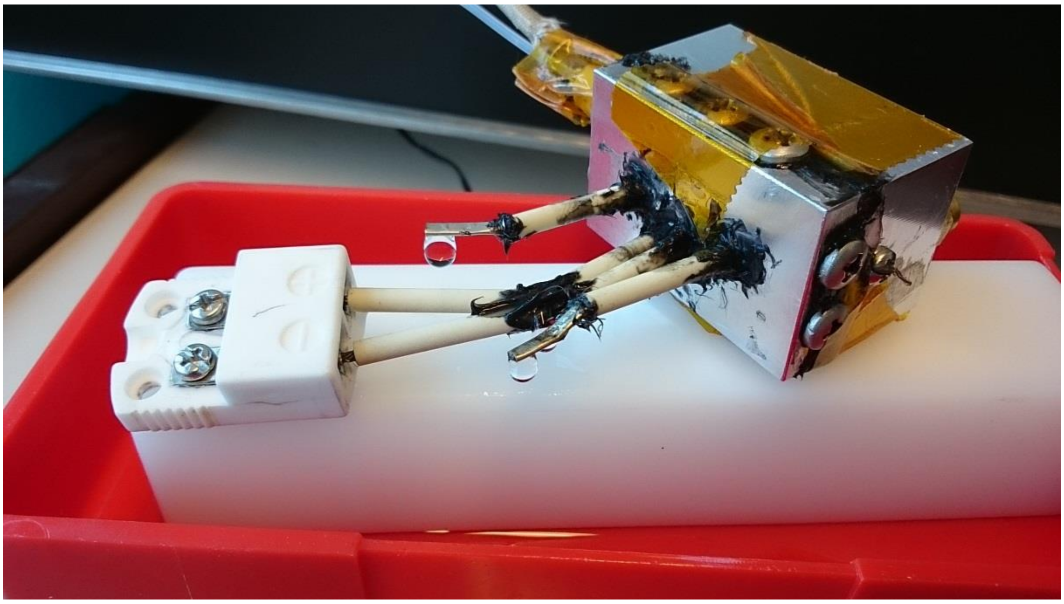

Figure 111: Thruster Leak Test

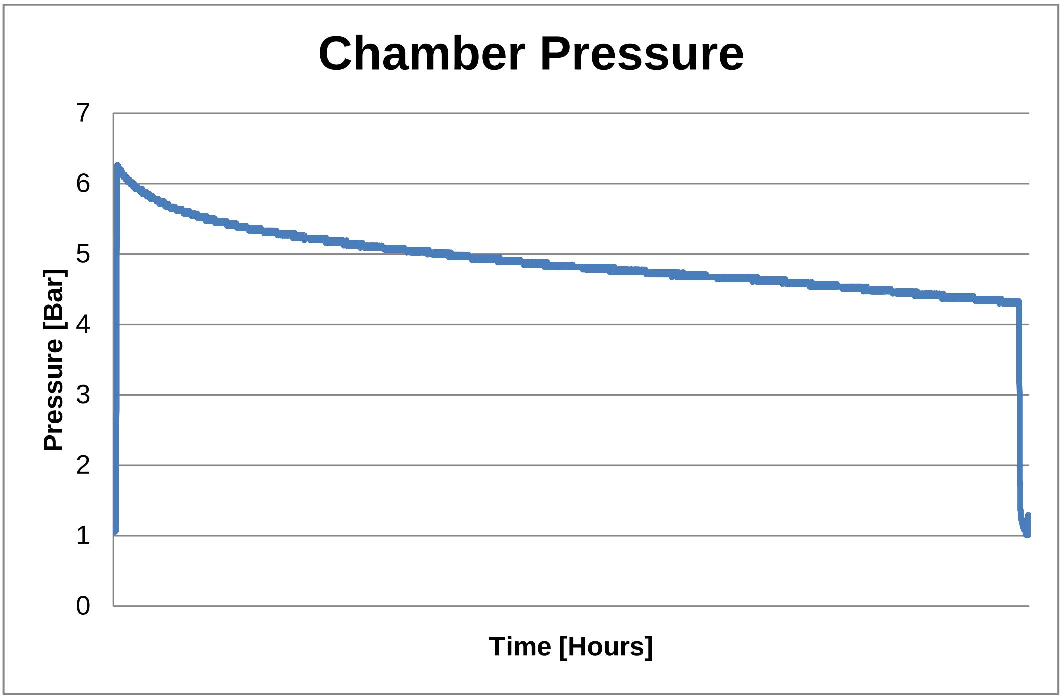

Figure 112: Thruster Leak Test Results

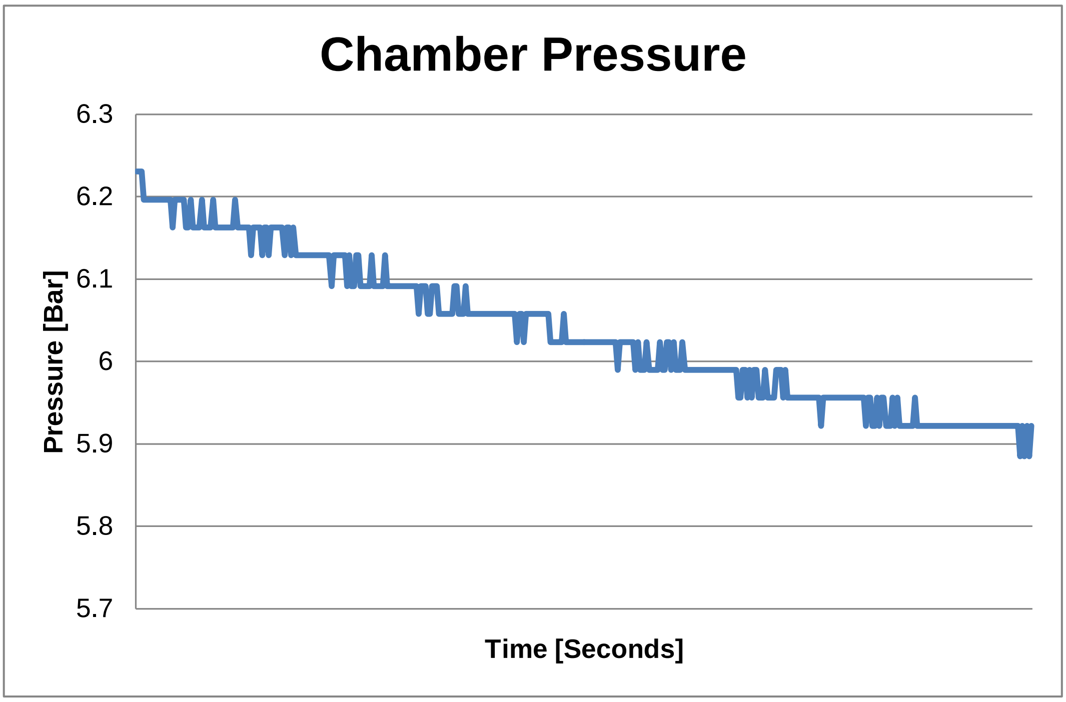

Figure 113: Thruster Leak Test Result Section

It is interesting to note the shape of the pressure drop when zoomed in. One can see that it looks like stairs which is due to the pressure overcoming the vicious forces of the water in the heater leads. Once again after many tries, the leak was not able to be mended and it was accepted the fact that thrust measurements may not be possible at all.

8.5. Heating Test

Due to the silicon used in the assembly of the thruster for improving the leak tightness, the structure temperature is limited to about 300 [°C]. To avoid complicated control loops and power modulation of the supplies the heating up phase will be controlled with timed pre-heating. In this test a series of heating up and cooling down will be made and temperature will be monitored on key components of the chamber, namely:

- Heater temperature
- Chamber temperature (using 2nd heater thermocouple)
- Wall temperature on 4 sides (temperature distribution)
- Temperature of the valve connector (limited due to PEEK nut)

The test will be done in vacuum due to the fact that a lot of heat will be lost in the air from convection. The test will be done interchangeably with both heaters as to characterize the heating up phase and the temperature distribution and power consumption of each heater.

8.5.1. Test Setup and procedure

In this section the test setup and procedure of the testing are outlined. The heaters where connected the same as given in Figure 99. The thermocouples where connected to different positions as given in Table 35. The setup is shown in Figure 114.

Table 35: Thermocouple Position

TC1	TC2	TC3	TC4	TC5	TC6	TC7	TC8
Thruster Top	Valve Connection	Watlow TK	Elstein TK	Thruster Bottom	Thruster Front	Side Watlow	Side Elstein

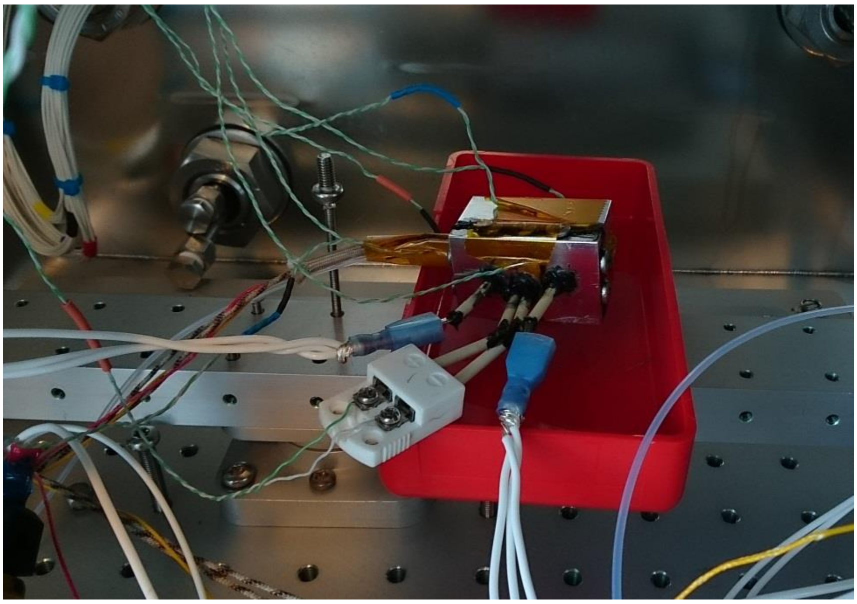

Figure 114: Heating Test - Test Setup

8.5.2. Test Results

In this section the test results are given. The temperatures reached by the heaters at different level are given in Table 36. With the temperature profile for the Watlow at 7 [W] and Elstein at 8.5 [W] given in Figure 115 and Figure 116 respectively. It can immediately be seen while the Watlow heater reaches much higher temperature the chamber heats up significantly less than when the Elstein heater is used. This is due to the fact that the Elstein ceramic heater releases more heat to the environment, however with the current chamber even with 10 [W] the desired temperature of 550 [K] cannot be reached. The Watlow heater exceeds this requirements but careful chamber design is needed to ensure that this heat is transferred to the fluid.

Table 36: Heater Test Results

Heater	Temperature [C]	Power [W]	Voltage [Vdc]
Watlow	303	7	12
Watlow	> 300	10	14.4
Watlow	> 300	30	24
Elstein	187	8.5	5
Elstein	214	10	5.5
Elstein	> 300	45	12

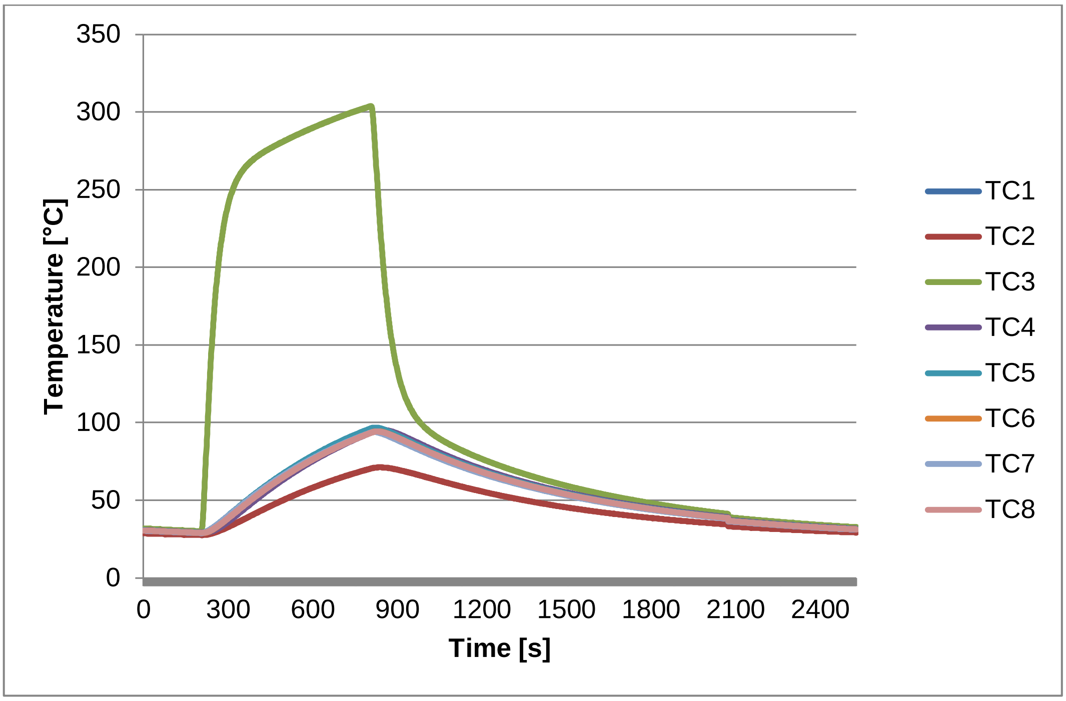

Figure 115: Watlow Heating Profile at 12 [Vdc]

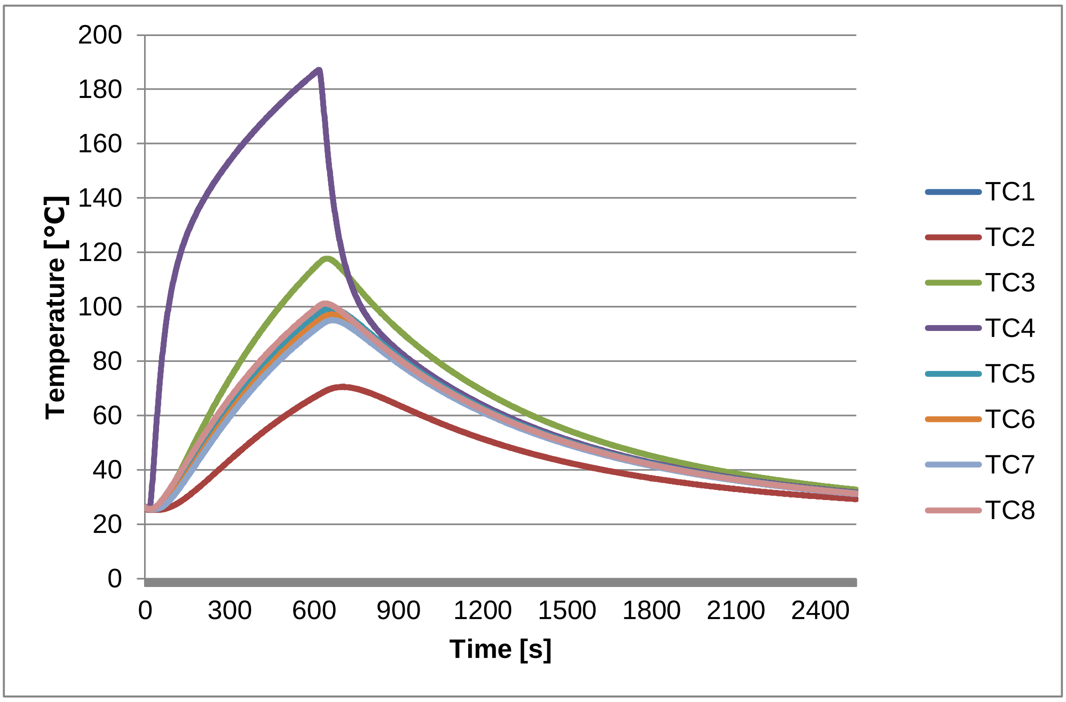

Figure 116: Elstein Heating Profile at 5 [Vdc]

8.6. Mass Flow Test

The Mass Flow Test is used to determine the flow through the valve at different pressures levels. The test will be done from 6 [Bar] to 2 [Bar] at 1 [Bar] steps to simulate 5 to 1 [Bar] in vacuum. The results from this stage can be used in a later stage of the testing to relate the necessary opening time of the valve to the thrusting time of the thruster. Given the similar size and dimensions of the VHS and IEP valves it is expected that this data can be correlated also for the flight thruster.

8.6.1. Test Setup and procedure

As it was said previously the test was done from 6 [Bar] to 2 [Bar] in 1 [Bar] steps. The valve was set to discharge the fluid in a tank that is placed on a scale. Three thrusts of 5 and 10 seconds each will be made and the average will be taken for the mass flow per second

8.6.2. Test Results

The results are summarized in Table 38 and an example test result is given in Figure 117. Given the calculated mass flow through the nozzle of 2.4 [mg/s] this means that opening the valve for 1 [s] at 6 [Bar] overpressure, enough propellant will go through the valve for the thruster to thrust for more than 500 [s]. Therefore pulsing or valve – thrusting circuit logic is highly recommended for the flight model. Furthermore it can be seen in Figure 118 that the mass flow is fairly linear w.r.t. to the pressure.

Table 37: Valve Mass Flow

Pressure [Bar]	Mass Flow [g/s]
6	1.29
5	1.09
4	0.91
3	0.68
2	.44

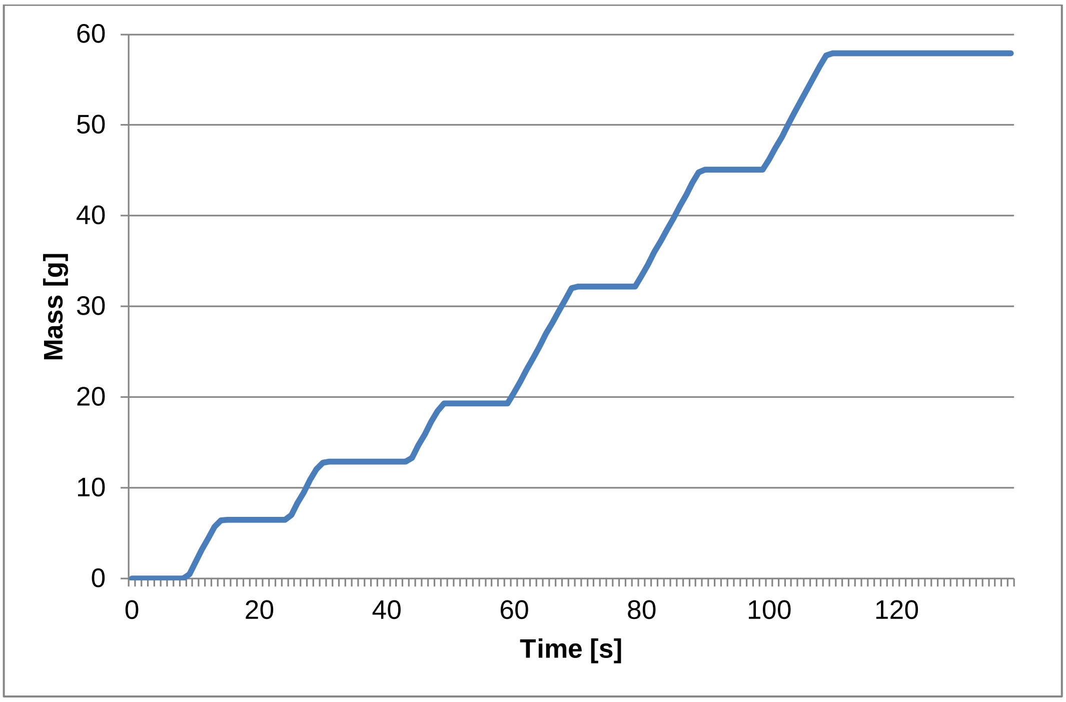

Figure 117: Valve Mass Flow at 6 [Bar]

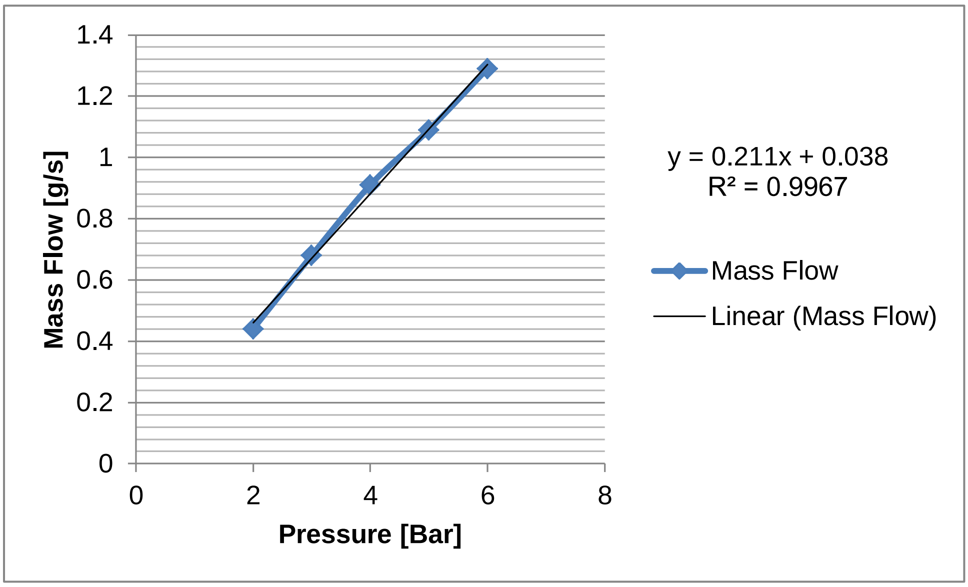

Figure 118: Mass Flow vs Pressure

8.7. Thrust bench calibration

While not directly related to the test campaign of the EM thruster, the calibration of the test bench will be used to verify the results obtained by Q. Bellini in a previous attempt and to get accustomed in using the thrust bench. Furthermore the results from the calibrations can be used later in the test campaign if successful thrust measurements are to be made.

Ideally multiple calibration runs should be made as to minimize the effect of differences of the test setup, pulley friction etc. however due to time constraints only one calibration run was made.

8.7.1. Test Setup and procedure

In this section the test setup and procedure of the testing are outlined. The trust bench was assembled the pulley was installed on the mounting plate. Next using spider silk rope a pulley system was attached to the chamber. It is important to keep the rotating arm as straight as possible as to avoid creating a moment of the load cell instead of pure tension / compression force. The setup is shown in Figure 119. Before calibrating, the thrust bench had to be leveled using a spirit.

The testing procedure is as follows. First of all the thrust bench at rest is defined. Next the pulley is attached and left for 60 [s] to stabilize to define the new zero and the amplifier was zeroed. Afterwards weights of 10, 20, 20, 50, 100, 200, 200 and 500 [mg] where added on the pulley for about 60 [s] each and then they were taken out in reverse order.

The load cell output will be monitored both directly with the HP Multimeter and with the NI DAQ card using the signal amplifier.

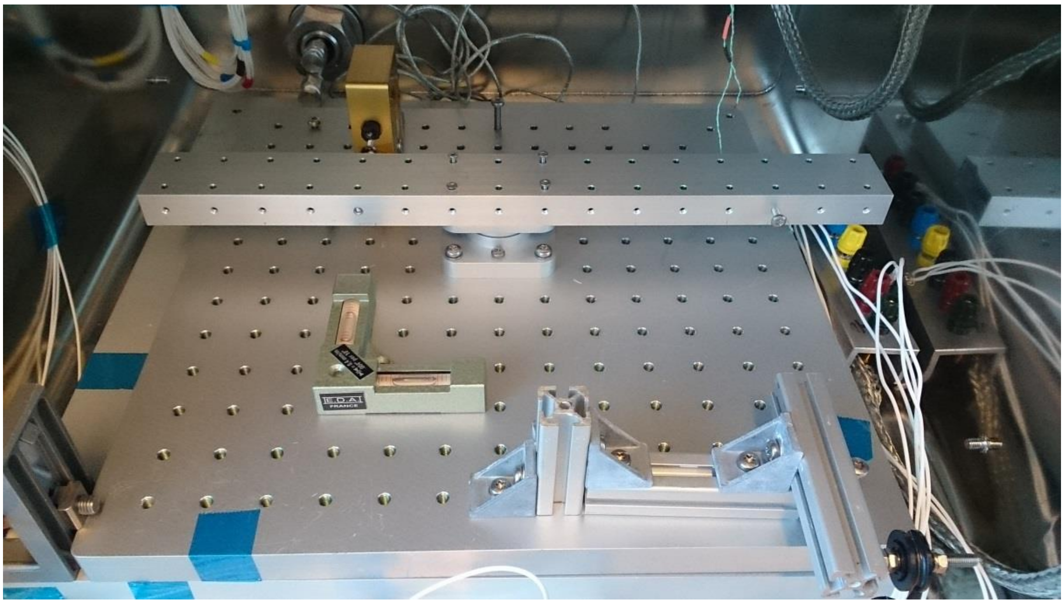

Figure 119: Thrust Bench Calibration Setup

8.7.2. Test Results

In this section the test results are given. The raw graph data is given in Figure 120 and the data is summarized in Table 38. Unfortunately due to a coding error in the program not enough significant digits where saved to make use of the data as logged by the HP Multimeter so only the output connected to the signal amplifier was available. Once this became apparent the code was fixed but the test setup has already been dismantled and thus re-calibrating was not possible.

As it can be seen from the graph and the tables the displacement and thus the output of the load cell is not the same when loading and unloading the load cell. Furthermore for mass changes lower than 100 [mg] the output change is not consistent. This can be due to both friction of the pulley or the arm bearing and the fact that 10 [mg] corresponds to only 1 [%] of the full scale load. Given that the expected thrust of the chamber if no leakage is present was between 0.5 and 2.5 [mN] it is uncertain if significant measurements could be made. The calibration line is given in Figure 121.

Table 38: Load Cell Calibration Data

Action	Time [s]	Output [mV]
Attach Pulley	70	6039.6
Zero Amplifier	190	97.6
Add 10 [mg]	270	99.9
Add 20 [mg]	330	155.6
Add 20 [mg]	390	183.0
Add 50 [mg]	455	248.9
Add 100 [mg]	522	362.6
Add 200 [mg]	580	608.5
Add 200 [mg]	640	812.8
Add 500 [mg]	715	1411.3
Remove 500 [mg]	800	612.6
Remove 200 [mg]	880	540.8
Pulley Stuck	960	-
Remove 200 [mg]	1024	241.3
Remove 100 [mg]	1110	22.6
Remove 50 [mg]	1210	-7.5
Remove 20 [mg]	1290	-71.9
Remove 20 [mg]	1360	-118.9
Remove 10 [mg]	1430	-105.3
Remove Pulley	1510	-2550.6

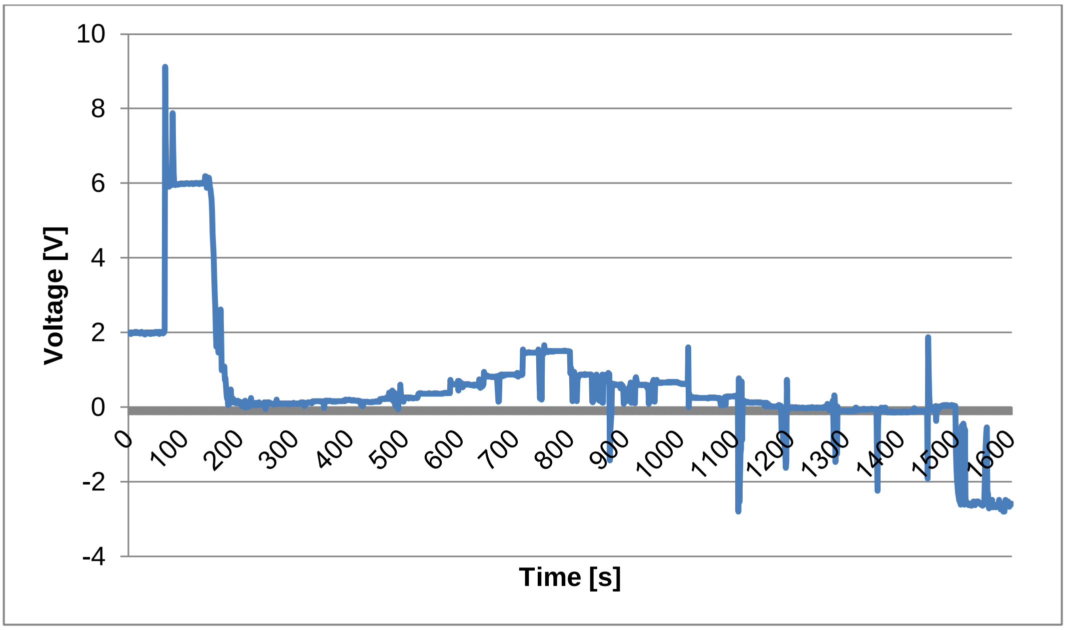

Figure 120: Load Calibration Raw Data

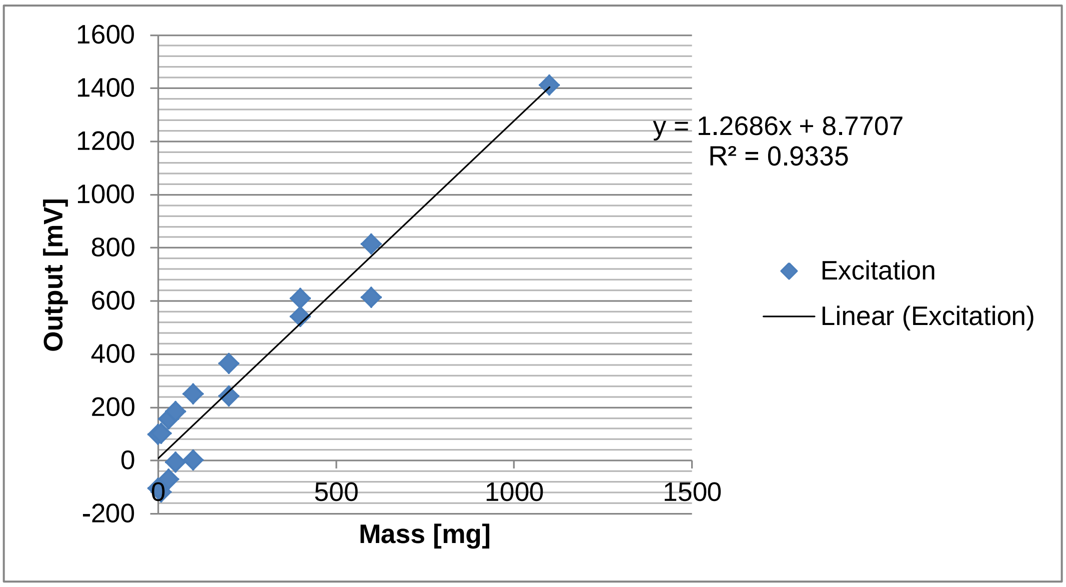

Figure 121: Load Cell Calibration Line

8.8. Thrust measurement

Following the calibration of the thrust bench a thrust measurement will be done. The thrust will be measured in vacuum and with the pressure port in the chamber closed. The thrust will be once again measured at pressures from 1 [Bar] to 5 [Bar] in 1 [Bar] steps.

Furthermore also blow-down mode to simulate conditions in space was envisioned but this was not done due to the high leak rate of the thruster. Temperature of the heater, chamber and walls will also be constantly measured and also the power used by the heaters.

8.8.1. Test Setup and Procedure

For the thrust measurement the same settings where kept on the signal amplifier as to have the previous calibration data obtained valid for analysis of the result. The test setup is given in Figure 122. As it can be seen a large number of wires and thermocouples run over the arm. This poses a concern as they may cause interference with the thrust measurement by not enabling the thrust arm to move freely.

As previously mentioned the planned procedure is to do thrust measurements at different pressure levels and at power level of 7 [W] for the Watlow and 8.5 [W] for the Elstein heater to simulate real world application. However if no thrust measurement is made the power level can be increased up to the maximum of each heater respectively or even both can be used together for maximum power.

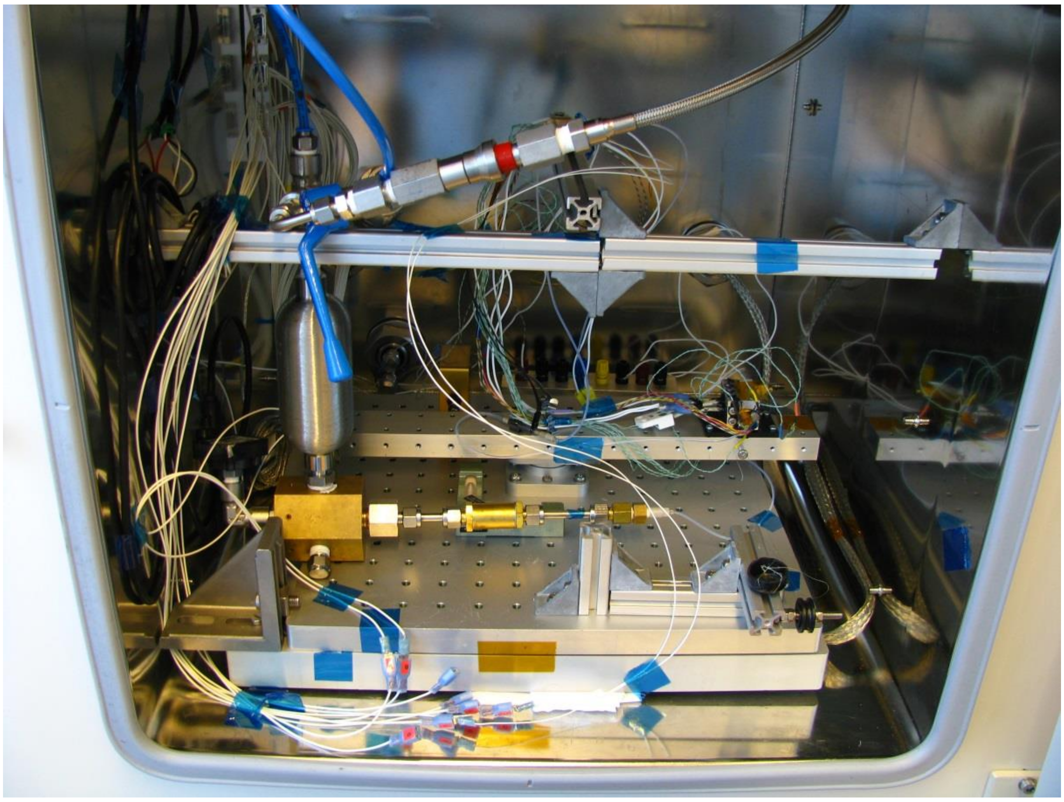

Figure 122: Thrust Measurement Test Setup

8.8.2. Test Results

Unfortunately after many different tries no conclusive results could be extrapolated from the test. Even when using both heaters at the same time, no change was observed in the load cell signal. Furthermore since as previously said the data from the HP Multimeter which was directly connected to the load cell was rendered useless only the data logged by the DAQ card and the signal amplifier was used which was prone to both time and temperature drift. This made analysis of the data simply impossible.

Furthermore water leaking of the thruster was observable on the chamber cold plate and fogging of the inside of the window as well which meant that water vapor was present inside (Figure 123). In addition there was water pumped out by the vacuum pump which lead to water condensation inside the pump and expelled in the clean room (Figure 124). The vacuum pump used is not rated to be used with water and does not include a water catching cup therefore for future testing is recommended to incorporate one before the pump itself.

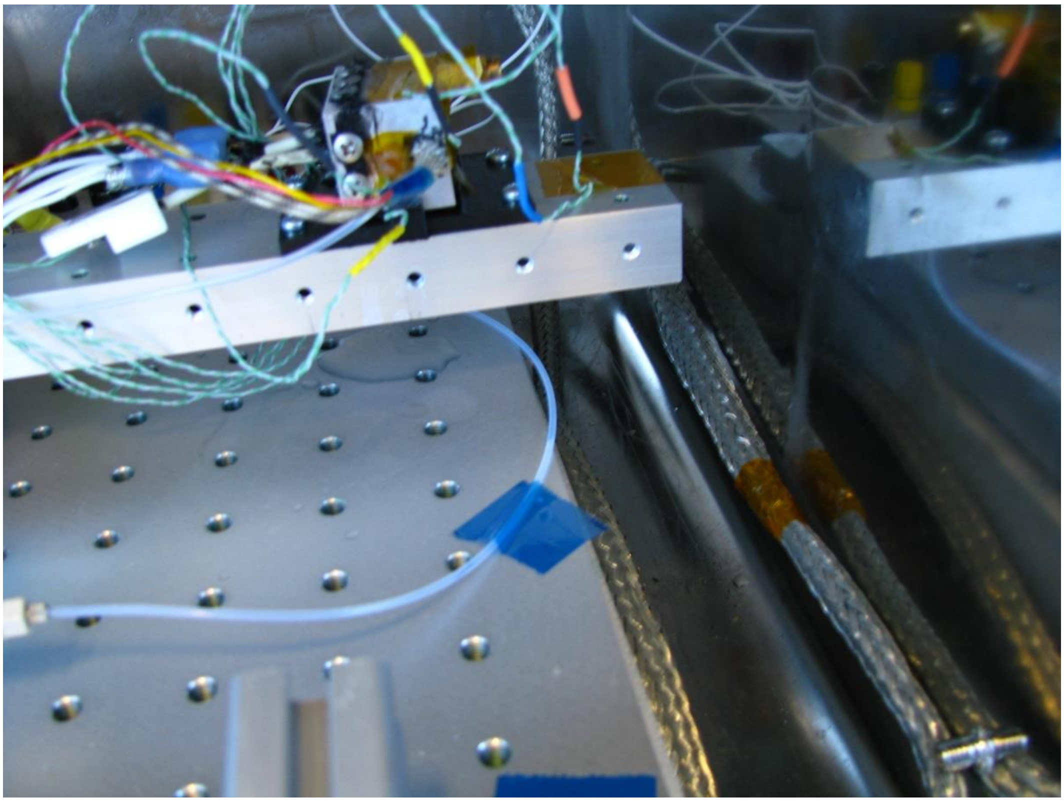

Figure 123: Thruster Leakage during Testing

Next the thruster was taken outside the chamber to be able to inspect it while in operation and to avoid damaging the vacuum pump. At full power of the heater definitely hot gas was observed coming out from the nozzle with minimal or no spitting but again no thrust measurement was made by the thrust bench. Finally during one of the high power test, chamber failure occurred due to quite possibly big pressure build up inside the chamber. Unfortunately no chamber pressure information was available however the pressure was definitely higher than the feed system pressure because reverse flow was observed when opening the valve.

Figure 124: Water Condensation inside the Vacuum Pump

8.9. Pressure Drop Test

This test is to determine the pressure of the chamber as a function of the pressure in the tank. The test was envisioned to be done in ambient with sufficient power to gasify the water or vacuum with a fixed power level. However due to the imminent clean room renovation there was not enough time for this test to be completed.

8.10. Post Test Inspection

After testing the thruster was inspected. Even though demineralized water was used significant mineral deposits were found on the thruster (Figure 125) and when inspecting the nozzle under the microscope it can be seen that the throat was also affected (Figure 126) and while not clogged the diameter has been significantly reduced. This could in theory also affect the lack of proper thrust measurements. The inside of the thruster and the heaters are shown in Figure 127 and Figure 128. As it can be seen there have been also significant mineral deposits and corrosion. This means that either the water used has in fact been normal tap water or due to mineral deposits on the feed system components which have not been cleaned properly.

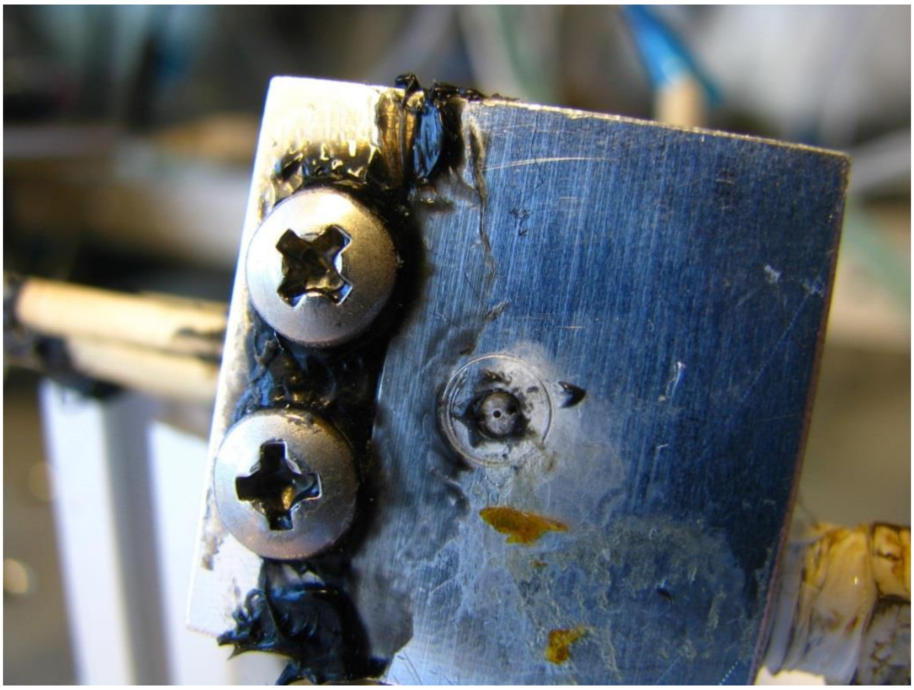

Figure 125: Thruster Post Testing Inspection

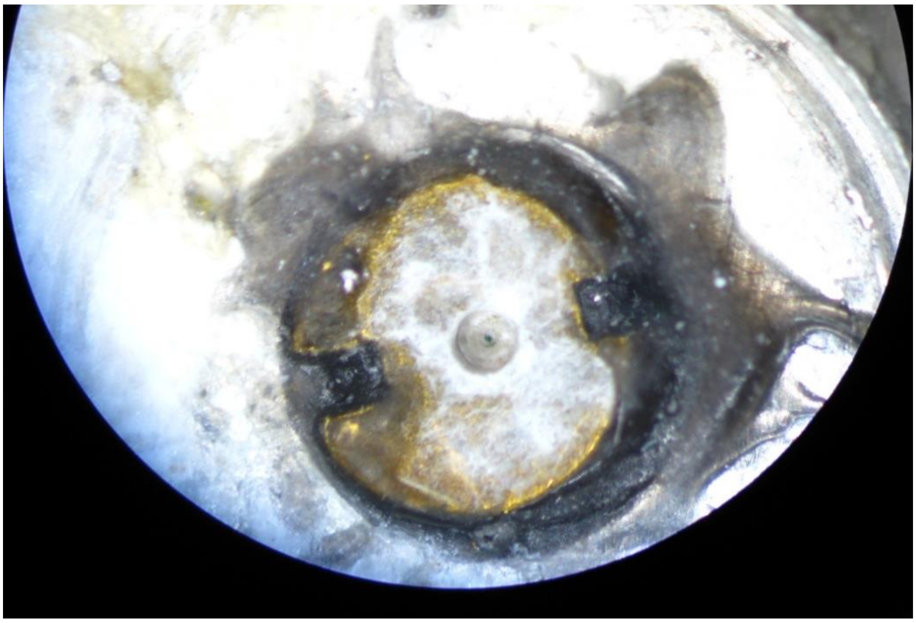

Figure 126: Nozzle Post Testing Inspection

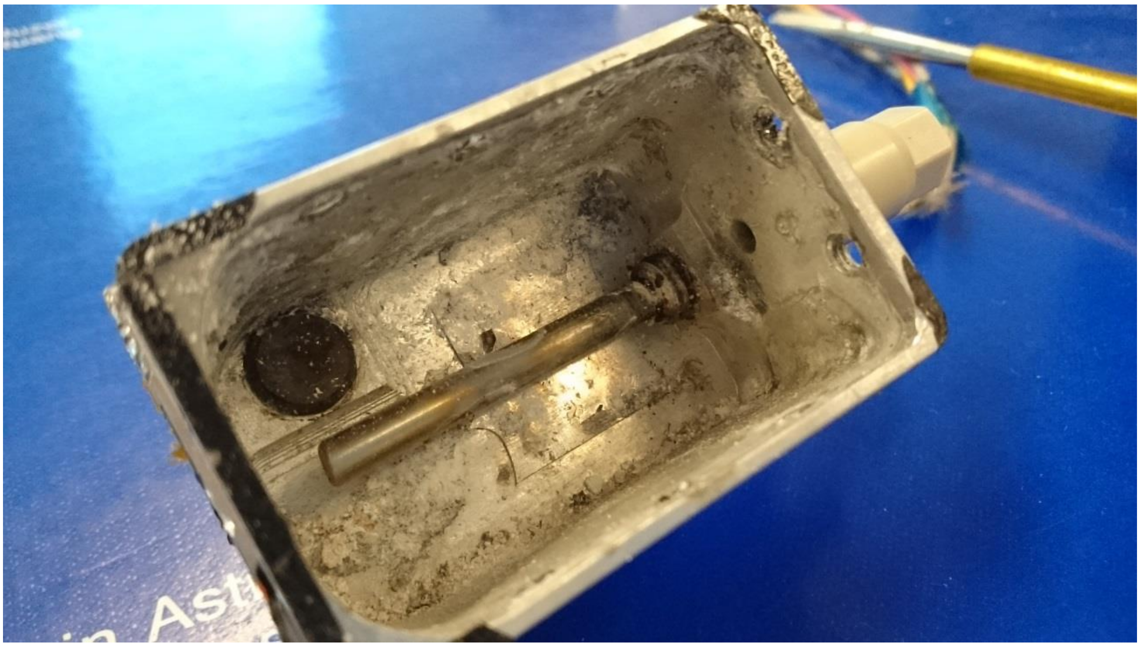

Figure 127: Post Testing Chamber Inspection

Figure 128: Post Testing Heater Inspection

9. Lessons Learned

With the testing campaign finished, in this chapter the results will be analyzed and the lessons learned will be given. First in Section 9.1 a block diagram of the electronics required for the propulsion system will be given. Next the results will be analyzed and a proposed thruster flight model design will be given in Section 9.2.

9.1. Electronic Circuit Engineering Model

The engineering model of the electronics needs to combine all the different blocks and components used during testing. The block diagram of the electronics needed is given in Figure 129. For the engineering and flight model of the propulsion system the voltage needs to be converted locally, thus the need for DC / DC converters locally on the PCB. Furthermore only one heater will be used in the final thruster. There are a large number of voltages monitored in the current diagram, which will be rather useful for the engineering model testing but if deemed necessary may be omitted of the flight model PCB. The requirements where previously given in Section 1.3.

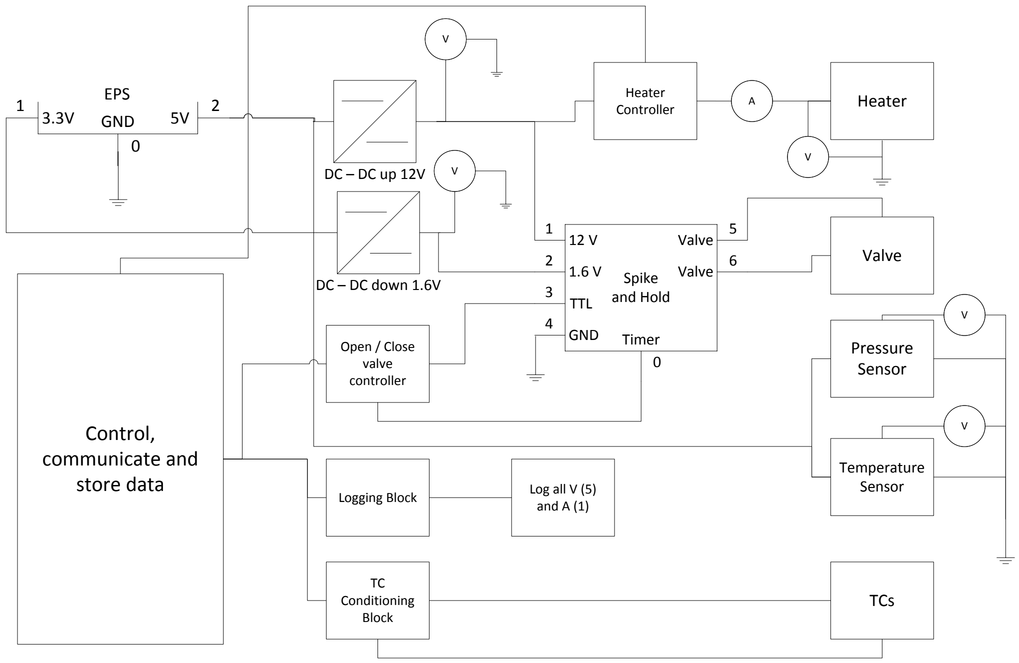

Figure 129: Electronics Block Diagram

9.2. Result Analysis

Looking at Chapter 8 it can be clearly seen that the testing was far from a complete success. It was not possible to sanitize the leakage from the Elstein heater and the thrust measurement was inconclusive even after many different attempts. This could have been avoided if 2 separate chambers where made for both heaters. Furthermore due to both time constraints and not being able to measure thrust and thus to have a meaningful comparison, the effect of the different porous media was not investigated Finally with the impending clean room renovation and the fact that another student also needed the testing facilities there was no time to complete the chamber pressure test and thus the pressure drop caused by the porous media and feed system is currently unknown.

Never the less a lot of experience was gained from the testing and some rather important conclusions can be drawn. Furthermore a general test setup and LabView program was made that can be used not only for propulsion system testing but also other systems. A completely different system was tested using the same setup and program by another student after only a brief introduction to the setup and the program. Still there are some improvements that can be incorporated in the program with the main one being a temperature control loop that will maintain a target temperature and a thrust to valve open time loop that using the information about the mass flow thru the valve at different temperatures can extrapolate the required opening time to match the desired thrust time.

Regarding the heaters, it was concluded that the Elstein heater is very difficult to integrate and to make a leak tight connection with the thruster is nearly impossible. The Watlow heater achieves higher temperature but radiates less heat thus stay time and contact area with the water needs to be maximized. In the next design to improve the connection, in addition to thread, a flange should also be welded and a high temperature silicon O-ring can be used to ensure leak tight assembly. It is also recommended that temperature control loop with variable voltage output (or to demonstrate real flight operation on / off cycling of the heater) is added for reduced power consumption when a temperature is reached and better control and repeatability of tests.

Regarding the valve the VHS valves have proved to be reliable and usable in the system therefore the IEP valve should be ordered ASAP due to the long lead time. Due to the order of magnitude of difference between the mass flow through the valve and the nozzle pulsing or really short valve openings times are needed. Otherwise as it was observed pressure will build up and the structural integrity of the chamber may come in question (long opening times lead to the chamber acting like a water cooker / boiler).

The proposed design for the flight model using the Watlow heater and the IEP valve is given in Figure 130. Given the simple cylindrical shape it is expected that this chamber will be cheap to be produced and thus more can be made as to test different porous materials. The thruster and the valve are to be welded together and this can also be done with the heater and the chamber as well. The chamber should be made out of steel as to have material compatibility with the piping from the IEP valve and also for heater when welding. Steal also has lower heat capacity than aluminum thus the heating efficiency of the thruster should increase. Finally the same nozzle can be used as made for the engineering model.

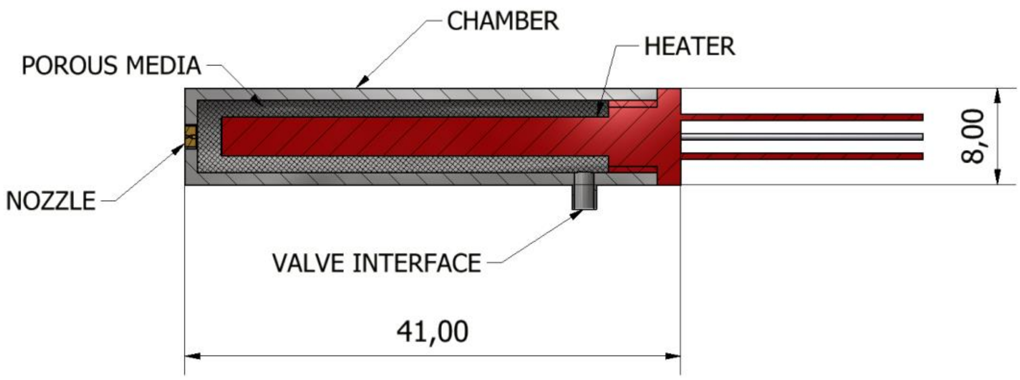

Figure 130: Proposed FM Thruster Design (Concept)

Regarding the test equipment there is a concern that the TB-50m is not able to measure these thrust levels reliably because even though water vapor flow was observed during testing, nothing was measured by the load cell. This can either be due to the large number of stiff wires that prevented rotation of the arm of the thrust bench or the thrust levels being too low for the test bench to register them. Furthermore it is recommended that the whole system is purged and cleaned before the next use. Mineral residue was observed on the nozzle throat and exit even thou demineralized water was being used during testing. Due to the small throat diameter this can lead to clogging of the nozzle.

10. Conclusions & Recommendations

The format and size specifications of the CubeSat platform require highly miniaturized subsystems, one of the most challenging ones being the propulsion system. The importance of a miniaturized propulsion system becomes even more apparent when taken into consideration that most, if not all, of the CubeSats launched to date, due to budget constraints, have been piggybacking their launches into space and therefore they may end up in a non-optimal orbit. Having a propulsion system onboard the spacecraft would allow the operator to control the satellite velocity which could be used for orbit control and maintenance and attitude control. The aim of this thesis was to design a thruster that will satisfy the design criteria following from the DelFFi satellites requirements. In this chapter the conclusions and recommendations from this research project are given. Additional recommendations regarding the project management are given in Appendix A.

10.1. Conclusions

In Chapter 2, a number of Commercial-Off-The-Shelf (COTS) systems have been investigated to find suitable candidates that fulfil these minimum requirements. However, it has been concluded that currently no existing system fulfills completely the main requirements and that a new propulsion system needs to be designed. A system trade – off was made in Chapter 3 and a water resistojet pressurized by Nitrogen was chosen as the winning concept.

Next with the thruster requirements set the design phase commenced in Chapter 5. It was decided to procure a Commercial off the Shelf (COTS) valve, porous media and two different heaters. Furthermore since an EM model was being made and due to budget constrains it was decided that instead of two separate chambers, one chamber to house both heaters. Finally 3 different nozzle types where investigated using CFD and Ansys Fluent and based on different criteria a winning design was chosen. Both the chamber and the nozzle where produced by DEMO. The resulting thruster design has the specifications summarized in Table 39.

Due to the lack of a feed system, one had to be designed and made which was described in Chapter 6. Furthermore a general test setup and program was made that it can be used for testing different systems. It can communicate with different equipment and allows remote valve control, monitoring pressure and temperature sensors and log data. The same program and similar setup was also used later by another student to test the DelFFi Thermal Subsystem.

Table 39: Expected EM Thruster Specification

Parameter	Value	Unit
Thrust	2.7 – 0.6	[mN]
Pressure	7 – 1	[bar]
Target Temperature	550	[K]
Exhaust velocity	1100	[m/s]
Specific Impulse	112	[s]
Propellant Mass	50	[g]
ΔV	15.4	[m/s]
Mass Flow	2.4 – 0.3	[mg/s]
Mass	< 48	[g]
Power Consumption	< 9.5	[W]

With the design setup finished the testing phase could start. The test plan and results are presented in Chapter 8. Due to the time spent on designing, refining and tweaking the test setup and the LabVIEW program and the scheduled renovation of the clean room not all planned tests where completed.

During the testing, the heaters and valve where characterized. It was found that the heaters satisfy the power requirement but the Elstein heater does not achieve the target temperature. The valve was found to need a minimum spike time of 0.3 [ms] and have much higher mass flow rate resulting in filling up the chamber with water. Next a leak test was performed. While the feed system had no significant leaks the thruster did. After numerous tries sanitation of the leak was not successful and it was attributed to the Elstein heater. Therefore it was concluded that he Elstein heater is very difficult to integrate and to make a leak tight connection with the thruster is nearly impossible. The Watlow heater achieves higher temperature but radiates less heat thus stay time and contact area with the water needs to be maximized. It was decided the Watlow heater to be used for the FM. However during the thrust testing no useful data was acquired. Since the thrust was not measured the performance of the thruster could not be verified. Never the less a lot of experience was gained from the testing and some rather important conclusions where drawn. Furthermore a general test setup and LabVIEW program was made that can be used not only for propulsion system testing but also other systems. A completely different system was tested using the same setup and program by another student after only a brief introduction to the setup and the program.

10.2. Recommendations

In the next design to improve the connection between the Watlow heater and the chamber, in addition to thread, a flange should also be welded and a high temperature silicon O-ring can be used to ensure leak tight assembly. It is also recommended that temperature control loop with variable voltage output (or to demonstrate real flight operation on / off cycling of the heater) is added for reduced power consumption when a temperature is reached and better control and repeatability of tests. Regarding the valve the VHS valves have proved to be reliable and usable in the system therefore the IEP valve should be ordered ASAP due to the long lead time. Due to the order of magnitude of difference between the mass flow through the valve and the nozzle pulsing or really short valve openings times are needed. Otherwise as it was observed pressure will build up and the structural integrity of the chamber may come in question (long opening times lead to the chamber acting like a water cooker / boiler).

Regarding the test equipment there is a concern that the TB-50m is not able to measure these thrust levels because even though water vapor flow was observed during testing, nothing was measured by the load cell. This can either be due to the large number of stiff wires that prevented rotation of the arm of the thrust bench or the thrust levels being too low for the test bench to register them. Therefore the TB-5m should be used for testing the FM. Furthermore it is recommended that the whole system is purged and cleaned before the next use. Mineral residue was observed on the nozzle and chamber even thou demineralized water was being used during testing. Due to the small throat diameter this can lead to clogging of the nozzle.

Bibliography

[1] A. Marinan, A. Nicholas and K. Cahoy, "Ad Hoc CubeSat Constellations: Secondary Launch Coverage and Distribution," Massachusetts Institute of Technology, Cambridge, USA, 2013.

[2] D. Selva and D. Krejci, "A survey and assessment of the capabilities of Cubesats for Earth observation," *Acta Astronautica,* pp. 51 - 67, 9 December 2011.

[3] A. J. Mannucci, J. Dickson, C. Duncan and K. H. , "GNSS Geospace Constellation (GGC): A Cubesat Space Weather Mission Concept," Jet Propulsion Laboratory, California Institute Of Technology, 2010.

[4] L. David, "Cubesats: Tiny Spacecraft, Huge Payoffs," Space.comn, 08 September 2004. [Online]. Available: http://www.space.com/308-cubesats-tiny-spacecraft-huge-payoffs.html. [Accessed 11 December 2013].

[5] NASA, "CubeSat Launch Initiative (CSLI)," 18 November 2013. [Online]. Available: http://www.nasa.gov/directorates/heo/home/CubeSats_initiative.html. [Accessed 11 December 2013].

[6] R. Villanueva, "Boeing Successfully Completes CubeSat Mission," Boeing, 16 August 2007. [Online]. Available: http://boeing.mediaroom.com/2007-08-16-Boeing-Successfully-Completes-CubeSat-Mission-to-Advance-Nano-Satellite-Technology. [Accessed 11 December 2013].

[7] C. Scharleman, M. Tajmar, I.Vasiljevich, N. Buldrini, D. Krejci and B. Seifert, "Propulsion for Nanosatellites," 2011.

[8] B. Zandbergen, "Micropropulsion Systems for Cubesats," Delft University of Technology, Delft, 2013.

[9] M. V. Fernández, "Mission analysis of QB50, a nanosatellite intended to study the lower thermosphere," University of Liège, 2011.

[10] A. Cervone, "Propulsion System Requirements for the Delffi Satellites," Delft University of Technology, Delft, May 2013.

[11] F. Singarayar, "System Requirements and Recommendations," von Karman Institute for Fluid Dynamics, February 2013.

[12] J. C. Mankins, "TECHNOLOGY READINESS LEVELS - A White Paper," NASA,

April 6, 1995.

[13] I. Krusharev, "Literature Study: Micro - Thruster Design and Development," Delft University of Technology, Delft, December 2013.

[14] J. Mueller, "Survey of propulsion Technologies applicable to Cubesats," 2010.

[15] J. M. Cardin, "A Cold Gas Micro-Propulsion System for CubeSats," VACCO Industries, 2003.

[16] A. Migliaccio, "Vacuum Testing of a Micropropulsion System Based on Solid Propellant Cool Gas Generators," in *61st International Astronautical Congress*, Prague, 2010.

[17] Clyde Space Ltd., "CubeSat uPulse Plasma Thruster," 2011.

[18] D. Schmuland, C. Carpenter, R. Masse and J. Overly, "New Insights Into Additive Manufacturing Processes: Enabling Low-Cost, High-Impulse Propulsion Systems," in *27th Annual AIAA/USU Conference on Small Satellites*, 2013.

[19] L. Paritsky, V. Ethier, T. Moser, J. Slostad and R. Hoyt, "Development of a CubeSat Water Electrolysis Propulsion System - HYDROS," in *27th AIAA/USU Conference on Small Satellites*, 2013.

[20] F. T. Nardini, "Advanced Cold Gas Propulsion System," TNO, Rijswijk, 2011.

[21] S. Ciarali, M. Coletti and S. B. Gabriel, "µ-PPTs diagnostics: a high accuracy impulsive thrust balance," in *The 33rd International Electric Propulsion Conference*, The George Washington University, USA, 2013.

[22] Clyde Space, "CubeSat Pulse Plasma Thruster," Clyde Space, 2013. [Online]. Available: http://www.clyde-space.com/cubesat_shop/propulsion/303_cubesat-pulse-plasma-thruster. [Accessed 20 September 2013].

[23] A. D. Ketsdever and M. M. Micci, Micropropulsion for Small Spacecraft, American Institute of Aeronautics and Astronautics.

[24] F. La Torre, "Gas Flow in Miniaturized Nozzles for Micro - Thrusters," Delft University of Technology, Delft, Netherlands, 2011.

[25] B. Zandbergen, "Thermal Rocket Propulsion," Delft University of Technology, Delft, 2010.

[26] T. V. Mathew, "Design of a MEMS Micro-Resistojet," Delft, June 2011.

[27] F. Valente, Development and verification of test set up for microthrusters testing, Delft: Delft University of Technology, 2009.

[28] I.Krusharev, "Literature Study: Micro - Thruster Development," Delft University of Technology, Delft, 2013.

[29] ANSYS, "Ansys 14.5 Help System," 2013.

[30] K. K. .. Quintao, "Design Optimization of Nozzle Shapes for Maximum Uniformity of Ex it Flow," Florida International University, 2012.

[31] G. Eggenspieler, "Turbulence Modeling," ANSYS, 2013.

[32] J. Tu, G. H. Yeoh and C. Liu, Computational Fluid Dynamics: A Practical Approach, Butterworth-Heinemann, 2007.

[33] Stanford University, Simulation of Turbulent Flows, 2011.

[34] I. Krusharev, "Literature Study: Micro - Thruster Design and Development," Delft Unviersity of Technology, December 2013.

[35] CustomPartNet, "Machining," 2013. [Online]. Available: http://www.custompartnet.com/wu/machining. [Accessed 21 November 2013].

[36] E. C. Jameson, Electrical Discharge Machining, SME, January 2001.

[37] CustomPartNet, "Additive Fabrication," 2013. [Online]. Available: http://www.custompartnet.com/wu/additive-fabrication. [Accessed 22 November 2013].

[38] R. Bijster, "Microthruster Characterization Using Thrust Benches," Delft University of Technology, March 2013.

[39] S. Janssens, "Desing of a Micro Propulsion Test Bench," Delft University of Technology, 2009.

[40] D. Perez-Grande, "Design and Development of a nano-propulsion," Delft University of Technology, Delft, Netherlands, 2010.

[41] A. Cervone, B. Zandbergen, J. Guo and E. Gill, "Application of an Advanced Micro-Propulsion System to the DelFFi Formation Flying Demonstration Within the QB50 Mission," in *IAC-12-C4.6.2*, Naples, Italy, 2012.

[42] National Institute of Standards and Technology, "Thermophysical Properties of Fluid Systems," 2011. [Online]. Available: http://webbook.nist.gov/chemistry/fluid/. [Accessed September 2013].

[43] R. Humble, G. Henry and W. Larson, Space propulsion analysis and design, McGraw-Hill, 1995.

[44] J. Guo, "Phase B Study on Formation Flight Within QB50," Delft University of

Technology, April 2013.

[45] C. Schuurblers, "T3uPS Qualification Model Design Documentation," TNO, Delft, 2009.

[46] J. Bouwmeester, "Interface Control Document T3uPS," TNO, Rijswijk, May 2011.

[47] The Lee Company, "Micro-Dispensing Application Development Kit - IKTX0322000A C," 2007.

[48] The Lee Company, *Electro-Fluidic Systems Handbook,* Westbrook, Connecticut 06498-0424 U.S.A., 2013.

[49] L. Oehen, "Electronic Design PCB v1," TNO, 2009.

[50] Minnesota Rubber and QMR Plastics, Elastomers and Thermoplastics Engineering Design Guide, 2013.

[51] Parker Hannifin Corporation, Parker O-Ring Handbook, 2007.

[52] Texas Instruments, "xx555 Precision Timers," Dallas, Texas 75265, September 2014.

[53] R. Ferreira, "Development and Testing of a Water Microresistojet," Delft University of Technology, Delft, September 2008.

[54] T. J. Lawrence, "Research into Resistojet Rockets for Small Satellite Applications," University of Surrey, 1998.

[55] R. v. d. Boom, "Recemat Metaalschuim," 2009.

[56] R. Hoole, "Resistojet Demonstration Model," TU Delft, October 1990.

[57] Elstein, "MSH Ceramic Infrared Radiators," 2011.

[58] P. Bula, "HotRod Cartrdige Heaters," HotSet, 2013.

[59] Watlow, "Cartrdidge Heaters," 2013.

[60] D. K. Huze and D. H. Huang, Design of Liquid Propellant Rocket Engines, National Aeronautics and Space Admnistration, 1967.

[61] R. L. Bayt, "Analysis, fabrication and testing of a MEMS based micropropulsion System," Massachusetts Institue of Technology, Cambridge, 1999.

[62] R. L. Bayt and K. S. Breuer, "Viscous Effects In Supersonic Mems-Fabricated Micronozzles," in *3rd ASME Microfluids Symposium*, Anaheim, CA, November 1998.

[63] W. F. Louisos and D. Hitt, "Heat Transfer & Viscous Effects in 2D & 3D Micro-Nozzles," in *37th AIAA Fluid Dynamics Conference*, Miami, Florida, 2007.

[64] R. Poyck, "Design, manufacturing and characterisation of a water fed CubeSat micro-

resistojet," Delft University of Technology, Delft, 2014.

[65] RS, "RS-1316 Instruction Manual".

[66] Delta Elektronika, "ES 300 Series DC Power Supplies," 2015.

[67] Agilent Technologies, "Agilent 34401A User Guide," 2001.

[68] Mettler Toledo GmbH, "Operating Instructions B-S Line of Balances," Switzerland .

[69] Mettler Toledo, "Standard Interface Command Set - Reference Manual," Switzerland, 2003.

[70] J. R. .. W. J. Larson, Space Mission Analysis and Design, Microcosm Press and Kluwer Academic Publishers, 2005.

[71] M. S. P. E. T. L. Vadim Zakirov, "Specifics of Small Satellite Propulsion: Part 1," 2001.

[72] M. J. T. Morris, "Study of an electrostatic micropropulsion system for nanosatellites," *Canadian Aeronautics and Space Journal,* 2011.

[73] K. Sathiyanathan, "YUsend-1 Solid Propellant Microthruster Design, Fabrication and Testing," 2010.

[74] C. T. Ryan Pahl, "Design, Test, and Validation of a Refrigerant-Based Cold-Gas Propulsion System for Small Satellites," 2010.

[75] P. Rangsten, "MEMS Micropropulsion Components for Small Spacecraft," NanoSpace AB, 2011.

[76] P. Rangsten, "Advanced MEMS Components in Closed-loop Micro Propulsion Applications," NanoSpace AB, 2012.

[77] J. Mueller, "Thruster options for Microspacecraft; A Review and Evaluation of State of," Jet Propulsion Laboratory, Pasadena, 2000.

[78] G. Moore, "3D Printing and MEMS Propulsion for the RAMPART 2U CUBESAT," 2010.

[79] M. Mihailovic, "MEMS Silicon-Based Resistojet Micro-Thruster For Attitude Control Of Nano-Satellites," Delft University of Technology, Delft, 2011.

[80] P. M. Matthew Dushku, "Additively Manufactured Propulsion System," 2012.

[81] T. V. Mathew, "A Silicon-Based Mems Resistojet For Propelling Cubesats," Delft University of Technology, Delft, 2011.

[82] R. M. C. S. Derek Schmuland, "Hydrazine Propulsion Module for CubeSats," in *Small Satellite Conference*, 2011.

[83] C. Clark, "An Off-the-shelf Electric Propulsion System for CubeSats," 2011.

[84] T. S. Chris Biddy, "Monopropellant Micropropulsion System for CubeSats," Stellar Exploration Inc., 2009.

[85] R. Munakata, "CubeSat Design Specifications," California Polytechnic State University, August 2008.

[86] A. Cervone, B. Zandbergen, J. Guo and E. Gill, "Application Of An Advanced Micro-Propulsion System To The Delffi Formation Flying Demonstration Within The QB50 Mission," in *IAC-12-C4.6.2*, Naples, Italy, 2012.

[87] M. M. Micci and A. D. Ketsdever, Micropropulsion for Small Spacecraft, Progress in Astronautics and Aeronautics Volume 187, June 2000.

[88] NanoSpace, "MEMS Flow Control Valve," March 2011.

[89] P. Galambos, J. Lantz, M. S. Baker, J. McClain, G. R. Bogart and R. J. Simonson, "Active MEMS Valves for Flow Control in a High-Pressure Micro-Gas-Analyzer," *Journal Of Microelectromechanical Systems,* vol. 20, no. 5, October 2011.

[90] C. Baker, M.-A. Schwab, R. Moseley, R. Syms and E. Yeatman, "Monolithic Mems Vacuum Valves For Miniature Chemical Preconcentrators," Microsaic Systems Ltd., April 2010.

[91] Committee of Experts on the Transport of Dangerous Goods and on the globally Harmonized System of Classifications and Labelling of Chemicals, "Model Regulations on the Transport of Dangerous Goods," United Nations, Geneva, 2006.

[92] B. J. McBride and S. Gordon, "Computer Program for Calculation of Complex Chemical Equilibrium Compositions and Applications - User Manual and Program Description," NASA, Cleveland, Ohio, June 1996.

[93] A. Ponomarenko, "Rocket Propulsion Analysis User Manual," Cologne, Germany, 2013.

[94] R. H. Todd, Manufacturing Processes Reference Guide, Idustrial Press, 1994.

[95] Ceradyne, "Ceramic Injection Modeling," 2013. [Online]. Available: http://www.ceradyne.com/products/medical/ceramic-injection-molding.aspx. [Accessed 20 November 2013].

[96] CustomPartNet, "Injection Molding," 2013. [Online]. Available: http://www.custompartnet.com/wu/InjectionMolding. [Accessed 20 November 2013].

[97] CustomPartNet, "Metal Injection Molding," 2013. [Online]. Available:

http://www.custompartnet.com/wu/metal-injection-molding. [Accessed 20 November 2013].

[98] W. H. Cubberly and R. Bakerjian, Tool and Manufacturing Engineers Handbook, Society of Manufacturing Engineers, 1989.

[99] Elektroform, "Micro Structures," 2013. [Online]. Available: http://www.elektroform.eu/content.php?nav_id=141. [Accessed 4 December 2013].

[100] G. K. Fedder, "MEMS Fabrication," Department of Electrical and Computer Engineering, Carnegie Mellon University, Pittsburgh, 2003.

[101] MNX, "What is MEMS Technology?," 2013. [Online]. Available: https://www.memsnet.org/about/what-is.html. [Accessed 18 November 2013].

[102] MEMSnet, "Fabricating MEMS and Nanotechnology," MEMS and Nanotechnology Echange (MNX), 2013. [Online]. Available: https://www.memsnet.org/about/fabrication.html. [Accessed 18 November 2013].

[103] M. Sargento, "Electroforming Schematic," 02 June 2008. [Online]. Available: http://upload.wikimedia.org/wikipedia/commons/7/7b/Eformschematic.svg. [Accessed 20 November 2013].

[104] P. Sundaramoorthy, E. Gill, C. Verhoeven and J. Bouwmeester, "Two CubeSats with Micro-Propulsion in the QB50 Satellite Network," 2010.

[105] MINCO, "Flexible Heater Design Guide," 2007.

[106] Nexthermal, "Nexthermal Coil Heaters," 2012.

[107] Rotfil, "Ultramax: High Power-Density Cartridge Heaters," 2006.

Appendix

Appendix A: Project Planning and Management

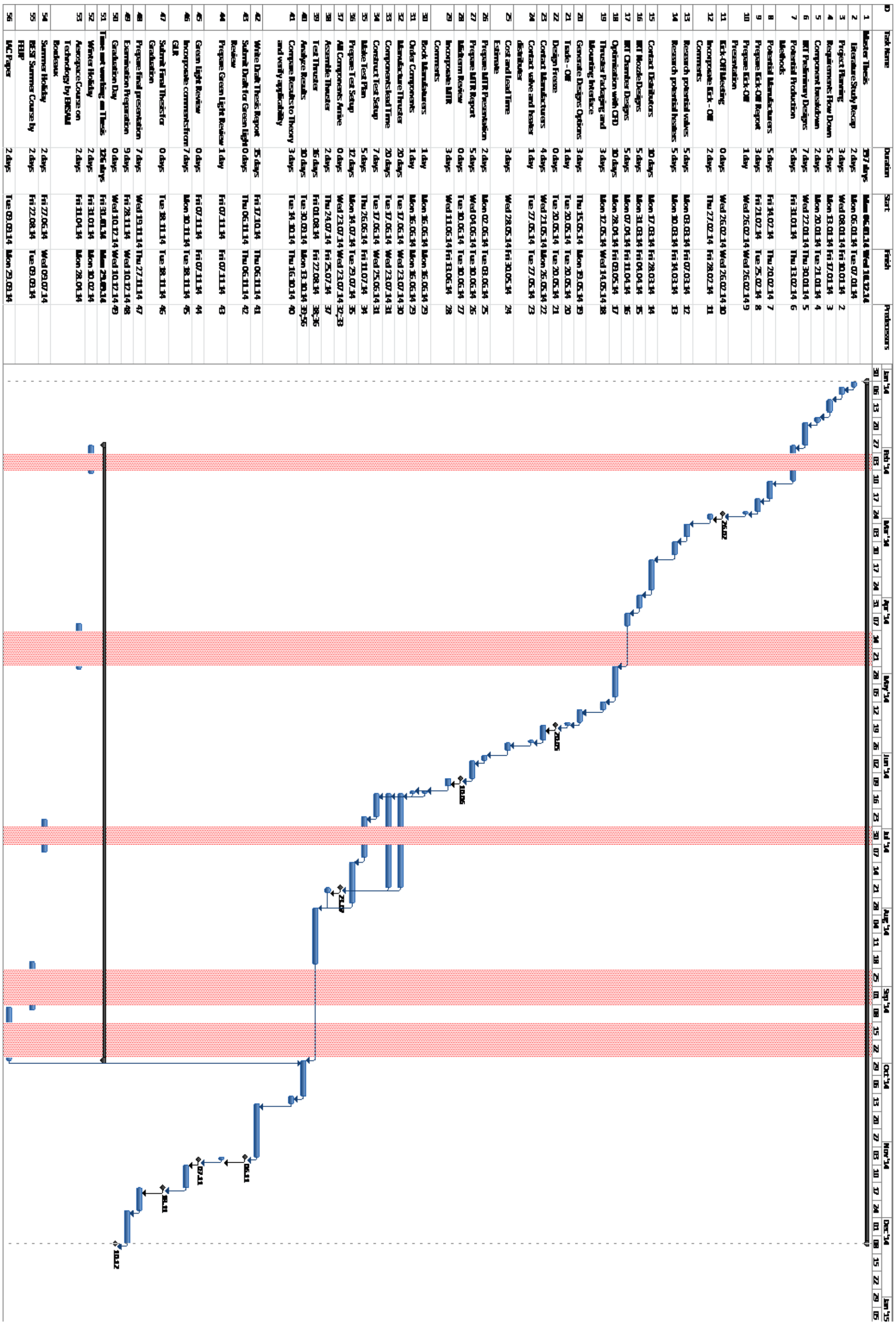

Since it is outside of the scope of the thesis in the appendix I would like to reflect shortly in what should be done in my opinion in order to improve project knowledge transfer and project management:

- Introductory course to LabVIEW (maybe even as an elective / practical)
    - I have had experience but other students have not and I have been asked to show LabVIEW to few students.
- Encourage students to make more general test setups, labview programs and connections and keep clear overview of the components used such that they can be used by others and time is not wasted "re-inventing" the wheel
    - Spent few days going to every different Swagelok part
    - Spent 2-3 weeks preparing the chamber and all test setup even though similar things have been done in the past
    - A student with a completely different project has been able to use my test setup and program
- Better overview of components, tools and apparatus in the chair and inventory should be kept in the future not just boxes of parts
    - Can avoid ordering double parts as now the SSE chair has 3 valves and 2 spike and hold circuits or about 800 euros wasted
- Workshops about the clean room and the gear available there (oscilloscope, ni card available, microscope, power supplies etc.)
- Enable students when needed to install programs and change settings so they don't have to resort to "creative" workarounds bypassing the user restrictions such as:
    - Installing newest version of LabView
    - Installing DHThermo
    - Adding internet connection to the Clean Room pc because its blocked by ICT
    - Finding old COM PCI addon cards in piles of hardware to extend the connection capabilities of the clean room PC
    - All this leads to wasted time and effort to things other than the thesis itself
- Remove 150 pages limit
    - Arbitrary number, not taking into account the circumstances, thesis length and scope. Should be phrased as a guideline or recommendation

- Thesis topics involving hardware development rarely seem feasible in 7 months. Students either need much more time or no hardware is delivered at the end of the 7 month period
- Support staff such as Nuno Santos is highly appreciated and ideally more should be available

Appendix B: Technical Drawings

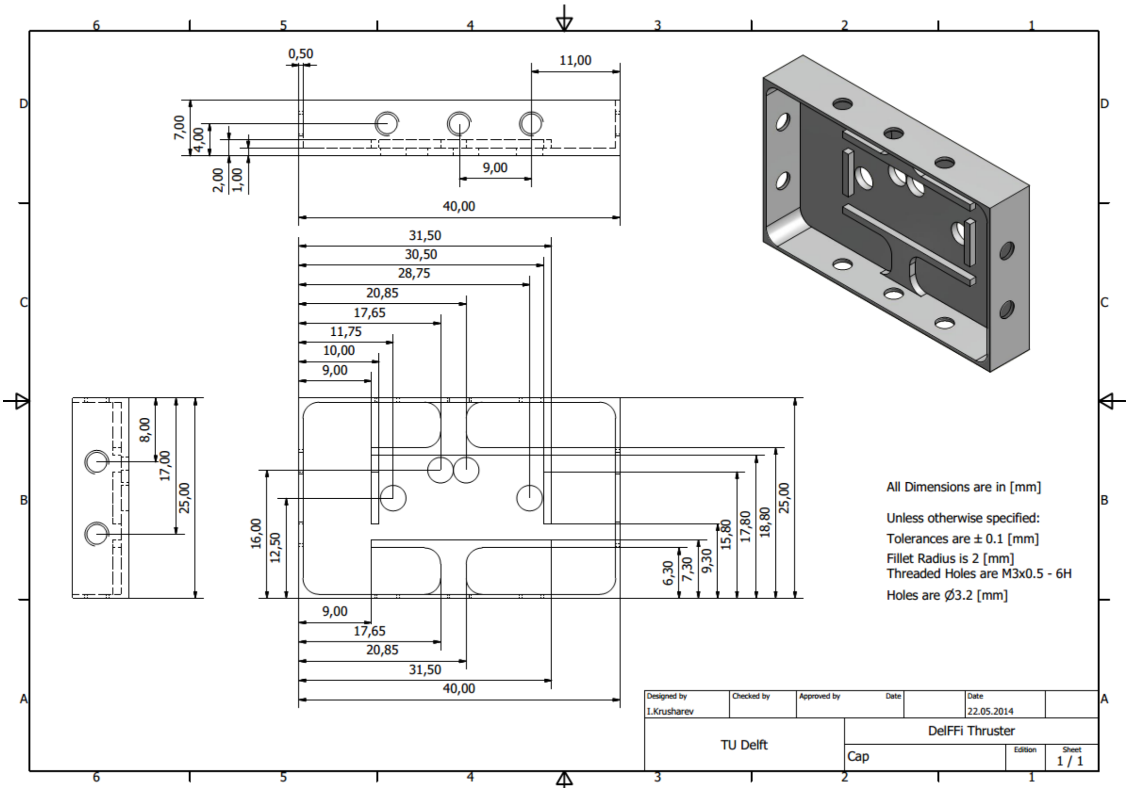

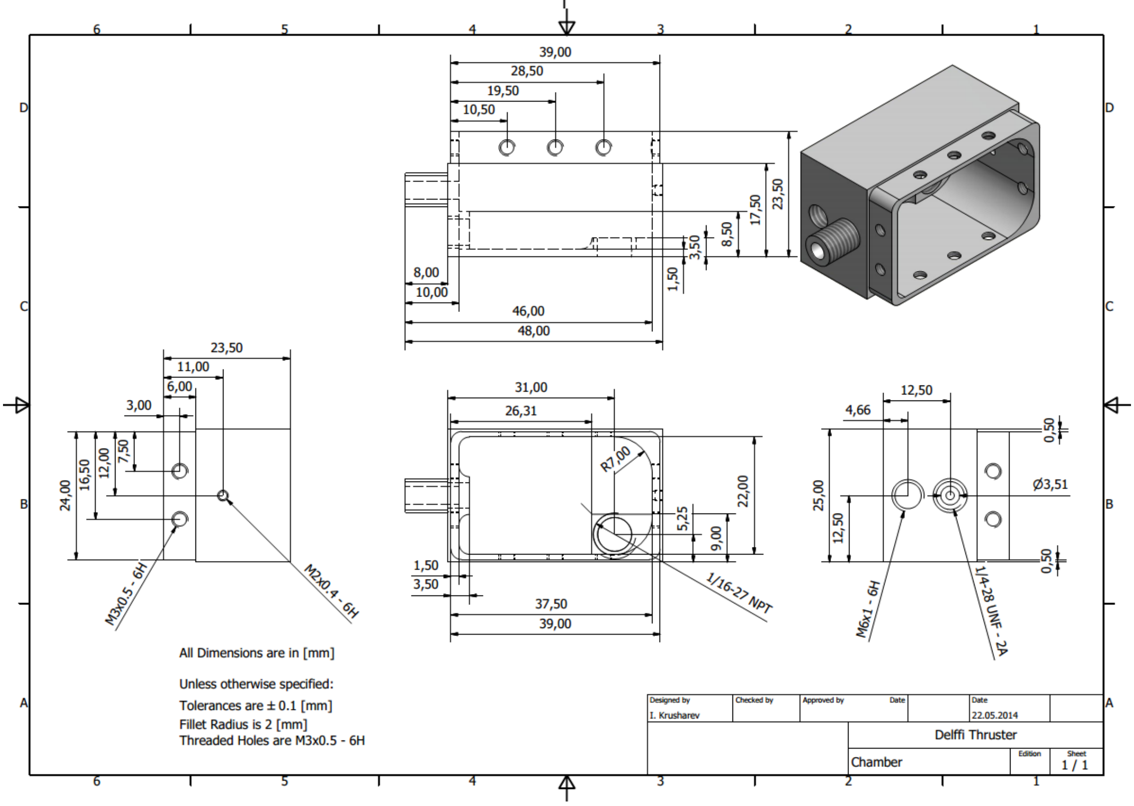

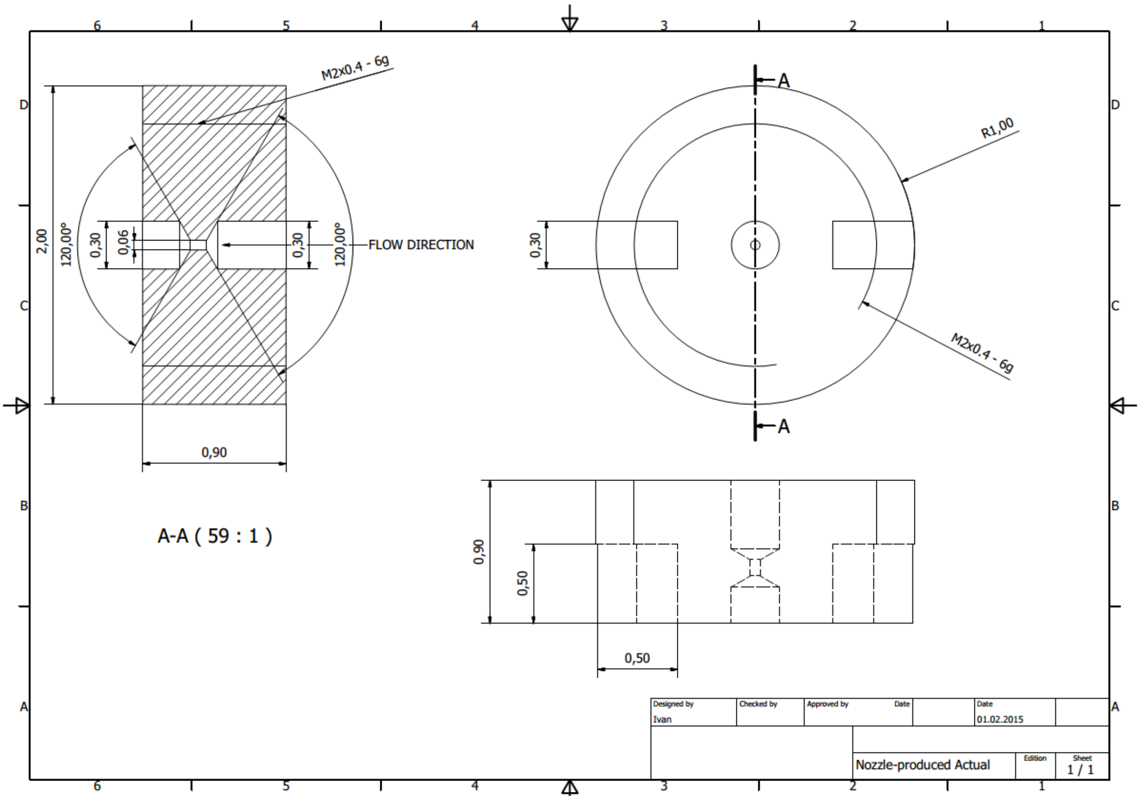

M2x0.4 - 6g
2,00
120,00°
0,30
0,06
0,30
120,00°
FLOW DIRECTION
0,90
A-A (59 : 1)
A
A
R1,00
M2x0.4 - 6g
0,30
0,90
0,50
0,50
Designed by
Ivan
Checked by
Approved by
Date
Date
01.02.2015
Nozzle-produced Actual
Edition
Sheet
1 / 1

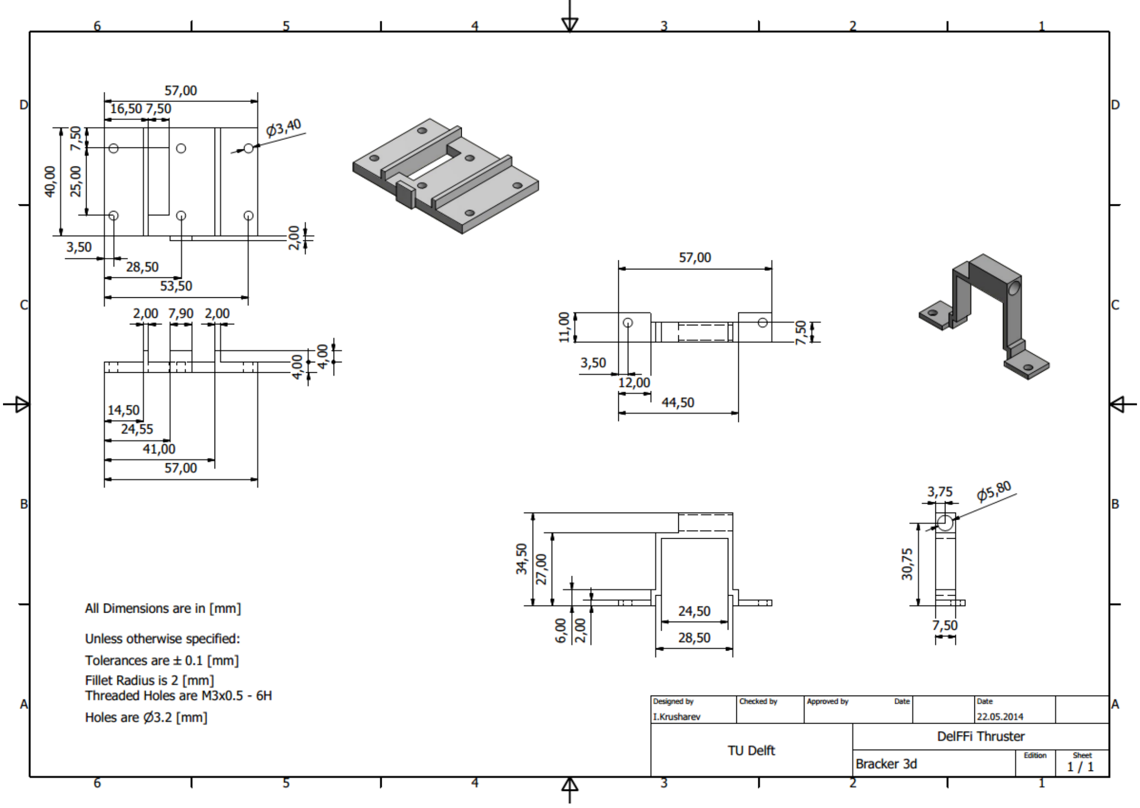

57,00
16,50 7,50
Ø3,40
40,00
25,00
7,50
2,00
3,50
28,50
53,50
2,00 7,90 2,00
4,00
4,00
14,50
24,55
41,00
57,00
57,00
11,00
7,50
3,50
12,00
44,50
3,75
Ø5,80
30,75
7,50
34,50
27,00
6,00
2,00
24,50
28,50
All Dimensions are in [mm]
Unless otherwise specified:
Tolerances are ± 0.1 [mm]
Fillet Radius is 2 [mm]
Threaded Holes are M3x0.5 - 6H
Holes are Ø3.2 [mm]
Designed by
I.Krusharev
Checked by
Approved by
Date
Date
22.05.2014
TU Delft
DelFFi Thruster
Bracker 3d
Edition
Sheet
1 / 1

Appendix C: Quotations and Invoices

denisdeploeg

Quotation

Ship to:	
TU Delft	
2628 CD Delft	

Customer #:	:	132111
Quote #:	:	21451141
Quote Date	:	12-06-14
Your reference:	:	You RFQ
Payment term	:	Betaling binnen 30 dagen netto
Delivery:	:	Af Valkenburg met GLS

Dear Mister Krusharev,

We thank you for your enquiry and we have pleasure in quoting you against our terms of sales and delivery as follows:

Item	Description	Lead time	Quantity	Unit Price	Total
TUTC3216910D	Tubing w/2 fittings 062 minstac	1-2 weken	1	€ 79,49	€ 79,49
TMZA3202010Z	062 Minstac Fitting End Kit	1-2 weken	1	€ 717,67	€ 717,67

E info@ddp.nl T +31 (0)43 8200 250 F +31 (0)43 8200 251 I www.ddp.nl
Geneldestraat 33 6301 HC Valkenburg a/d Geul (NL) Postbus 66 6300 AB Valkenburg a/d Geul (NL)
BTW NL006436912B01 KVK 14623620 ABN AMRO 58.46.92.552 BIC ABNANL2A IBAN NL62ABNA0584692552

Offerte

Verzendadres	Overige gegevens
TU Delft 2628 CD Delft	Debiteurennummer : 132111 Offertenummer : 21451147 Offertedatum : 23-06-14 Klantreferentie : Uw aanvraag 20.06.14 Betalingsconditie : Betaling binnen 30 dagen netto Levering : TNT

Dear Mister Krusharev,

Wij danken u voor uw aanvraag en bieden u conform onze leverings- en betalingsvoorwaarden als volgt aan:

Artikel	Omschrijving	Levertijd	Aantal	Prijs Netto /Stuk
TMDA3212950Z	062 Min.Boss to 1/4-28 Flat Bottom	1-2 weken	1	€ 24,54
TMDA3204950Z	Lee Adapter	1-2 weken	1	€ 17,38

E info@ddp.nl T +31 (0)43 8200 250 F +31 (0)43 8200 251 I www.ddp.nl
Geneidestraat 33 6301 HC Valkenburg a/d Geul (NL) Postbus 66 6300 AB Valkenburg a/d Geul (NL)
BTW NL006436912B01 KVK 14623620 ABN AMRO 58.46.92.552 BIC ABNANL2A IBAN NL62ABNA0584692552

Quotation

Ship to:	
TU Delft	Customer #: : 132111
2628 CD Delft	Quote #: : 21451112
	Quote Date : 20-03-14
	:
	Payment term : Betaling binnen 30 dagen netto
	Delivery: : Af Valkenburg met GLS

Dear Mister Krusharev,

We thank you for your enquiry and we have pleasure in quoting you against our terms of sales and delivery as follows:

Item	Description	Lead time	Quantity	Unit Price	Total
IKTX0322000A	VHS Starter Kit	2-4 weeks	1	€ 685,00	€ 685,00
INMX0350000A	12 Micron filter	4-5 weeks	1	€ 48,00	€ 48,00

E info@ddp.nl T +31 (0)43 8200 250 F +31 (0)43 8200 251 I www.ddp.nl
Geneidestraat 33 6301 HC Valkenburg a/d Geul (NL) Postbus 66 6300 AB Valkenburg a/d Geul (NL)
BTW NL006436912B01 KVK 14623620 ABN AMRO 58.46.92.552 BIC ABNANL2A IBAN NL62ABNA0584692552

KURVAL

TU Delft
Mr. Ivan Krusharev

Mekelweg 2
2628 CD DELFT

Nieuw Vennep, April 2, 2014

Concerns: quotation 201480164

Dear Mr. Krusharev,

We hereby quote the following heaters, according to our FME Sales conditions:

Item 1 - 3 pcs. Watlow Firerod cartridge heater as specified below:

- Watlowcode	C1A-9602
- diameter	Ø 1/8" (0.122" +/- 0.002")
- length	1" (+/- 2%)
- voltage	24V
- wattage	30W

Price each € 36,70

Item 2 - 3 pcs. Watlow Firerod cartridge heater as specified below:

- Watlowcode	C1J-9769
- diameter	Ø 1/8" (0.122" +/- 0.002")
- length	1-1/2" (+/- 2%)
- voltage	24V
- wattage	30W
- thermocouple	Cal. "K" (location C)
- leads	40" solid f/glass lds. (max. temp 250°C)

Price each € 73,55

Item 3 - 3 pcs. Watlow Firerod cartridge heater as specified below:

- Watlowcode	C1A-9602
- diameter	Ø 1/8" (0.122" +/- 0.002")
- length	1-1/2" (+/- 2%)
- voltage	24V
- wattage	30W
- leads	40" crimped on high temp. fiberglas lds. (max. 450°C)

Price each € 37,35

Kurval BV | Haverstraat 145, 2153 GD Nieuw Vennep, Postbus 212, 2150 AE Nieuw Vennep | T +31 (0)252 67 60 80, F +31 (0)252 67 61 04, info@kurval.nl, www.kurval.nl | ABN AMRO BIC ABNANL2A, IBAN NL82ABNA0547010699, KBC België BIC KREDBEBB, IBAN BE12730140271692 | KvK 34053362, BTW NL006056672B01

RE: Inquiry about Elstein MSH/20 and T-MSH/20

Willem Westhoek <WWesthoek@wilmod.nl> Wed, Feb 26, 2014 at 9:43 AM
To: "I.Krusharev@student.tudelft.nl" <I.Krusharev@student.tudelft.nl>

Industrieweg 10 Postbus 40 T 079 346 19 19 E info@wilmod.nl
2712 LB Zoetermeer 2700 AA Zoetermeer F 079 346 19 11 I www.wilmod.nl

Dear Ivan,

Hereby I can offer you:

Elstein Ceramic Heater
MSH/20
Price EUR 23,88 each

Delivery time: 4 pieces ca. 1 week, provided that unsold

Elstein Ceramic Heater
T-MSH/20
Price EUR 44,75 each
Delivery time: 15 pieces ca. 1 week, provided that unsold

Price: excluding VAT, ex. work
Delivery time: see above
(You can pick up the heater in Zoetermeer)
Payment: within 30 days after delivery
Price validity: 1 month from date

If you have any questions regarding this offer please do not hesitate to contact us.

Trusting to have made you a suitable offer we look forward to hearing from you.

Kind regards,

Willem Westhoek

Wilmod Heating & Systems